AD-A077 851 DAYTON UNIV OH RESEARCH INST F/G 20/4
DEVELOPMENT OF STABILITY METHODS FOR APPLICATION TO NONLINEAR A--ETC(U)
JUL 79 R F TAYLOR AFOSR-78-3487
UNCLASSIFIED UDR-TR-79-64 AFFDL-TR-79-3114 NL

1 OF 2
AD A077851

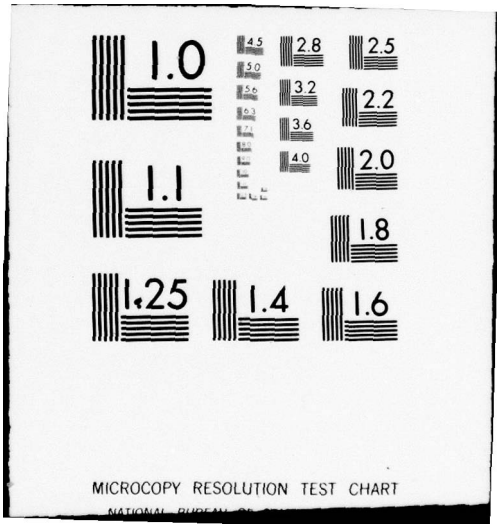
1.0
1.1
1.25
1.4
1.6
1.8
2.0
2.2
2.5
2.8
3.2
3.6
4.0
4.5
5.0
5.6
6.3
7.1
8.0
9.0
10.0
MICROCOPY RESOLUTION TEST CHART

AFFDL-TR-79-3114

DEVELOPMENT OF STABILITY METHODS FOR APPLICATION TO NONLINEAR AEROELASTIC OPTIMIZATION

R. F. Taylor

University of Dayton
Dayton, Ohio 45469

July 1979

TECHNICAL REPORT AFFDL-TR-79-3114
FINAL REPORT FOR PERIOD JANUARY 1978- JUNE 1979

Approved for public release; distribution unlimited.

Air Force Flight Dynamics Laboratory
Air Force Wright Aeronautical Laboratories
Air Force Systems Command
Wright Patterson Air Force Base, Ohio 45433

NOTICE

When Government drawings, specifications, or other data are used for any purpose other than in connection with a definitely related Government procurement operation, the United States Government thereby incurs no responsibility nor any obligation whatsoever; and the fact that the government may have formulated, furnished, or in any way supplied the said drawings, specifications, or other data, is not to be regarded by implication or otherwise as in any manner licensing the holder or any other person or corporation, or conveying any rights or permission to manufacture, use, or sell any patented invention that may in any way be related thereto.

This report has been reviewed by the Information Office, (ASD/OIP) and is releasable to the National Technical Information Office (NTIS). At NTIS, it will be available to the general public, including foreign nations.

This technical report has been reviewed and is approved for publication.

JAMES J. OLSEN
Actg Ch, Analysis and Optimization Branch
Structures and Dynamics Division

FOR THE COMMANDER

Copies of this report should not be returned unless return is required by security considerations, contractural obligations, or notice on a specific document.

AIR FORCE/56780/19 November 1979 — 150

UNCLASSIFIED

SECURITY CLASSIFICATION OF THIS PAGE (When Data Entered)

REPORT DOCUMENTATION PAGE

READ INSTRUCTIONS BEFORE COMPLETING FORM

1. REPORT NUMBER: AFFDL-TR-79-3114	2. GOVT ACCESSION NO.
3. RECIPIENT'S CATALOG NUMBER	
4. TITLE (and Subtitle): Development of Stability Methods for Application to Nonlinear Aeroelastic Optimization	5. TYPE OF REPORT & PERIOD COVERED: FINAL REPORT, January 1978 – June 1979
6. PERFORMING ORG. REPORT NUMBER: UDR-TR-79-64	
7. AUTHOR(s): R. F. Taylor	8. CONTRACT OR GRANT NUMBER(s): AFOSR-78-3487
9. PERFORMING ORGANIZATION NAME AND ADDRESS: University of Dayton Research Institute, 300 College Park Avenue, Dayton, OH 45469	10. PROGRAM ELEMENT, PROJECT, TASK AREA & WORK UNIT NUMBERS: 2307N513
11. CONTROLLING OFFICE NAME AND ADDRESS: Air Force Flight Dynamics Laboratory (FBR), Wright-Patterson AFB, OH 45433	12. REPORT DATE: July 1979 13. NUMBER OF PAGES: 189
14. MONITORING AGENCY NAME & ADDRESS (if different from Controlling Office)	15. SECURITY CLASS. (of this report): Unclassified 15a. DECLASSIFICATION/DOWNGRADING SCHEDULE

16. DISTRIBUTION STATEMENT (of this Report)

Approved for public release; distribution unlimited

61102F

17. DISTRIBUTION STATEMENT (of the abstract entered in Block 20, if different from Report)

18. SUPPLEMENTARY NOTES

19. KEY WORDS (Continue on reverse side if necessary and identify by block number)

Aeroelasticity	Nonconservative Forces	Nonlinear Systems
Transonic Flow	Follower Load	Limit Cycle
Flutter	Nonlinear Oscillation	
Divergence	Optimization	

20. ABSTRACT (Continue on reverse side if necessary and identify by block number)

An approximate procedure is developed which determines efficiently and accurately the amplitude-dependent stability of nonlinear systems. This new procedure, which is referred to as the 'method of imposed disturbances,' is shown to be especially applicable to studies of the sensitivity of nonlinear aeroelastic systems to changes in design variables. Emphasis is placed on airfoil and panel flutter instabilities in aerodynamically nonlinear flow.

DD FORM 1 JAN 73 1473 EDITION OF 1 NOV 65 IS OBSOLETE

UNCLASSIFIED

SECURITY CLASSIFICATION OF THIS PAGE (When Data Entered)

105 400

To develop the theory, a modified form of the van der Pol oscillator equation and of the Lewis servomechanism equation are studied. Based on the principle of conservation of energy in a limit cycle, approximate closed-form expressions are developed which relate the loading and the limit amplitude to system design variables. Results are compared to solutions obtained by numerical integration.

The method is also applied to nonlinear transonic flutter and divergence of a two-dimensional airfoil. Airloads are predicted using an existing small-disturbance computer code, LTRAN2, which determines structural loads due to airflow containing moving shock waves. Amplitude-dependent transonic airfoil divergence and unstable limit cycle flutter are predicted for a NACA 64A006 airfoil elastically restrained in pitch.

A nonlinear two-degree-of-freedom follower load problem is studied to demonstrate the applicability of the method of imposed disturbances to a multiple-degree-of-freedom system examined is a sandwich panel in nonlinear hypersonic flow, for which the rate of change of limit amplitude with respect to structural design variables is studied.

FOREWORD

This report is a reproduction of a dissertation submitted to the University of Dayton, in partial fulfillment of the requirements for the Degree of Doctor of Philosophy. The research reported herein was carried out under the supervision of Dr. Fred K. Bogner, Associate Professor of Mechanical Engineering. Funding was provided by the Air Force Office of Scientific Research under Grant 78-3487. The research was administered by Dr. James J. Olsen and Dr. V. B. Venkayya of the Structures and Dynamics Division, Air Force Flight Dynamics Laboratory, Wright-Patterson Air Force Base, Ohio.

The author wishes to acknowledge the valuable direction provided by his Dissertation Advisor, Dr. Bogner, and the most helpful comments and suggestions given by Dr. Olsen. Dr. W. F. Ballhaus of NASA-Ames and Dr. P. M. Goorjian of Informatics Corporation are also thanked for providing important software support.

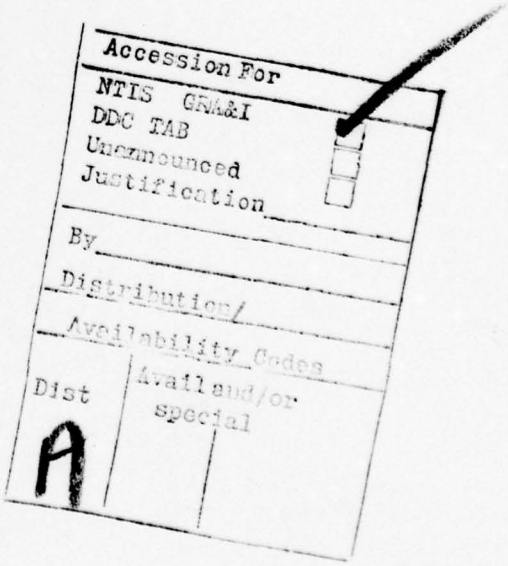

TABLE OF CONTENTS

LIST OF ILLUSTRATIONS

LIST OF ILLUSTRATIONS (Continued)

LIST OF ILLUSTRATIONS (Continued)

LIST OF ILLUSTRATIONS (Continued)

LIST OF ILLUSTRATIONS (Concluded)

LIST OF TABLES

NOMENCLATURE

a_i	- Fourier cosine coefficients
$a(t)$	- slowly varying amplitude
c	- chord of airfoil
f	- nonlinear right hand side of equation of motion
g	- airfoil damping parameter
$\vec{h}$	- design variables
k_1, k_2	- viscoelastic foundation parameters
k_c	- reduced frequency based on chord
ℓ	- characteristic dimension of structure
m	- panel mass per unit area
p	- static load parameter
q_i	- generalized coordinates in Galerkin solution
t	- time
w	- panel deflection
x	- dependent variable in nonlinear oscillator studies
$\vec{x}$	- generalized coordinate vector
$\vec{x}_0$	- initial conditions on generalized coordinates

NOMENCLATURE (Continued)

A	- amplitude parameter
A_1, A_2, A_3	- nondimensionalized parameters in airfoil pitch flutter equation
$\underset{\sim}{C}$	- generalized damping matrix
C_K	- nondimensional airfoil pitch spring constant
C_L	- lift coefficient
C_m	- aerodynamic moment coefficient
$C_{m\alpha}$	- slope of aerodynamic moment coefficient curve
C_P^*	- critical pressure coefficient
C_{PL}	- pressure coefficient distribution on lower surface of airfoil
C_{PU}	- pressure coefficient distribution on upper surface of airfoil
D	- panel bending stiffness
$\underset{\sim}{G}$	- generalized geometric stiffness
I	- airfoil pitch inertia
$\underset{\sim}{K}$	- generalized stiffness matrix
K_α	- torsional spring constant
$\underset{\sim}{M}$	- generalized mass matrix
M_e	- elastic restoring moment on pitching airfoil
M_0	- static aerodynamic moment
M_∞	- free-stream Mach number
N	- total numer of terms in a series
N_P	- total number of design variables

P	- panel compressive edge load
P_L	- pressure on lower surface of airfoil
P_U	- pressure on upper surface of airfoil
T	- period of steady-state oscillations
V_∞	- free-stream velocity
W^{NC}	- total nonconservative work done by system undergoing steady-state oscillations
$\vec{X}$	- imposed dusturbance vector during steady-state oscillations
α	- unsteady airfoil angle of attack
α_0	- steady airfoil angle of attack
ζ	- damping factor
κ	- ratio of specific heats for air
λ	- dynamic load parameter
μ	- small parameter in nonlinear equation
ξ	- nondimensionalized coordinate
ξ_c	- center of pressure location on airfoil
ξ_o	- pitch axis location on airfoil
ρ_∞	- free stream air density
τ	- nondimensionalized time
$\phi(t)$	- slowly varying phase angle
ω	- frequency of limit cycle oscillation
ω_1	- natural frequency of single degree-of-freedom system

Λ	- value of dynamic load parameter during steady-state oscillation
T	- period of motion
$\vec{\Psi}$	- normalized imposed disturbance vector
Ω	- frequency of state-state oscillations
$\dot{(\ )}$	- time derivative of ( )
$(\ )_{,i}$	- partial derivative of ( ) with respect to i^{th} variable
$\vec{(\ )}$	- vector
$\underset{\sim}{(\ )}$	- matrix

SECTION I

INTRODUCTION

There is considerable current interest in the effect of nonlinear, nonconservative loadings on the stability of elastic structural components. In particular, a new class of nonlinear, nonconservative problems has been introduced into the field of aeroelasticity with the development of efficient computational methods for unsteady transonic flow. Nonlinear transonic flutter calculations pose a new and challenging problem for the aeroelastician from both an aeroelastic analysis and an optimization standpoint.

In this chapter some background material is given on the nature of aeroelastic instabilities. This is followed by a statement of the research objectives. The background information points out some of the analytical difficulties introduced into flutter calculations by nonlinear transonic aerodynamics. Research objectives are defined which are designed to address not only transonic nonlinearities, but other types of nonlinearities as well. A summary statement concludes this chapter by giving a concise statement of the research developments and applications.

1.1 BACKGROUND

Aeroelasticity can be defined as the study of the effect of aerodynamic forces on a deformable body. In general, these forces will be nonconservative and contain both dissipative and circulatory terms. Under certain critical flow conditions, the deformable body may undergo large oscillatory deformations which can lead to structural failure due to material yielding or cyclic fatigue.

It is the problem of the aeroelastician to assure that the structure or structural component is free from failure when subjected to the service flow conditions. If a candidate design is not free from failure, an appropriate design change must be made to provide for safety with minimum loss in structural utility. The traditional design changes are the rearrangement of structural stiffness and mass with total mass taken as the measure of structural utility.

In his classic text on aeroelasticity, Y. C. Fung[1] distinguishes between dynamic response problems and dynamic instability problems. The former are characterized mathematically as systems of nonhomogeneous equations together with prescribed initial conditions. Dynamic instability problems involving nonconservative airloads, i.e., flutter, are characterized by systems of homogeneous equations. Flutter instability occurs when an airflow parameter is

exceeded as determined from the solution of an eigenvalue problem.

For aircraft flying in speed regimes other than transonic, flutter calculations are routinely formulated. The situation in the transonic range is quite different; however, since the governing aerodynamic equations are nonlinear and are quite difficult to solve. Moving shock waves are very often present[2] which implies that a nonlinear mixed hyperbolic-elliptic initial boundary value problem must be solved to determine the unsteady airloads.

One of the most important features of transonic flow from the aeroelastician's viewpoint is that the airloads are not related to structural deformation in a linear manner. Dynamic instability cannot be determined in general by solving an eigenvalue problem. The problem takes on some characteristics of a dynamic response calculation in that initial conditions must now be taken into account.

The transonic flow environment has long presented the designer with a number of critical problems. Recent flutter model tests on supercritical wings[3] have shown that catastropic flutter occurs at the lowest flight speed in the transonic Mach number range. It is in this aerodynamically nonlinear range that the structural designer's problem is the most complex and at the same time the most

important. Lifting surfaces and skin panels must be made free from instability with minimum added weight.

To date, consideration of unsteady aerodynamics in structural optimization has been limited to linear formulations of both the structural and the aeroelastic equations. A number of approaches to pressure calculations based on finite difference and finite element solutions of the nonlinear small-disturbance velocity-potential equation have recently been developed, but flutter calculations have been restricted to two-dimensional airfoil models having no more than three-degrees-of-freedom. In spite of the fact that transonic flutter computations are still in an early stage of development, it is appropriate to give consideration to the establishment of optimal design methods for transonic problems.

All nonlinear transonic flutter studies to date have relied heavily on a time history approach; i.e., numerical integration of the equations of motion. This procedure has been shown to be quite time consuming and to be subject to numerical instability. It can be sometimes difficult to distinguish the numerical instability from a real physical instability.

The method developed herein provides an efficient and easy way to implement an alternative to the time history procedure. It also has applicability to stability problems other than those induced by airflow. In addition, the

method is useful in the optimization of system design variables.

1.2 RESEARCH OBJECTIVES

The amplitude of disturbance to which a nonlinear aeroelastic system is subjected can greatly affect its stability. Time history solutions can be used to assess stability, but this approach can become expensive when applied to design optimization studies. A time history solution would need to be obtained at possibly a large number of steps in the optimization process. For optimization purposes, approximate methods from the theory of nonlinear oscillations are attractive, but their range of applicability has not been well defined for use by the aeroelastician. Furthermore, these methods have generally been applied to only single degree-of-freedom systems. Clearly, further analytical developments are needed in this area.

Therefore, it is the objective of this research to develop an efficient stability assessment procedure for systems subjected to nonlinear, nonconservative loadings. Such a stability assessment procedure is needed to solve aerodynamically nonlinear flutter and divergence problems. Although the primary need for the procedure is in transonic flutter studies, it is also an objective of this work to apply the method to other nonlinear, nonconserative problems of interest in analytical mechanics.

The computational objective is to provide an easy to implement stability assessment procedure which is of sufficient efficiency that it can be applied to nonlinear aeroelastic optimization problems. The end product of this research is an approach to the problem of determining the effect of system design variable changes on amplitude dependent instability. To date, no method has been developed which addresses this important design and analysis problem.

1.3 SUMMARY

The method of imposed disturbances is developed and applied to the problem of predicting amplitude dependent instabilities in nonlinear systems. For classical one-degree-of-freedom systems such as the van der Pol equation or the Lewis servomechanism equation, the load-amplitude stability predictions agree very closely with numerical integration.

A NACA 64A006 airfoil pitching in unsteady transonic flow is studied to determine the system damping required to prevent flutter. The trends predicted by numerical integration and the imposed disturbances method agree quite well over a wide range of pitch angle amplitudes. The LTRAN2 transonic aerodynamics code is used to predict the airload distributions, and it is shown in the case of increasing steady angles of attack, that center of pressure shifts can dramatically affect divergence. Airfoil divergence occurs

when the air speed dependent aerodynamic moment exceeds the elastic restoring moment. The critical air speed at which this occurs is the "divergence speed," and the statically unstable airfoil is said to be "torsionally divergent."[1]

Application of the method of imposed disturbances to a follower load problem is made to demonstrate the accuracy of the method for multiple degree-of-freedom systems. Again, the accuracy is quite good compared to other methods.

An important static subcase of the method is demonstrated in application to a panel in nonlinear hypersonic flow. A static instability is predicted by the method and compared with Kutta-Merson numerical integration. It is shown that the method is over three orders of magnitude faster than numerical integration and is thus ideally suited for nonlinear aeroelastic optimization studies which require a capability for rapid reanalysis.

SECTION II

REVIEW OF THE LITERATURE

Research in aeroelastic optimization involves an interplay of a number of broad technical areas. A complete review of the literature in any single participating discipline would be quite voluminous. However, the literature which is relevant to the extension of optimization procedures to nonlinear aeroelasticity is relatively small, and it is this subset which is reviewed. Since the research needed for this work grew out of work in linear aeroelastic optimization, the first subsection below gives a broad survey of work in this area. This is followed by reviews of unsteady transonic aerodynamics and nonlinear aeroelastic stability.

?.1 AEROELASTIC OPTIMIZATION

The following survey is not intended to provide an exhaustive review of aeroelastic optimization. The excellent paper by Stroud[4] gives a very complete survey of work done on lifting surfaces. Some of the more theoretical work on panel flutter optimization is detailed by Taylor.[5] However, it is the intent here to cite work which has found either significant application or which has provided

fundamental theoretical insight into minimum weight design with aeroelastic constraints. Reference is made to the paper by Lansing, Lerner and Taylor[6] as a detailed survey of recent engineering applications of aeroelastic design methods. The overall area of structural optimization since about 1900 is surveyed in References 7 through 10.

The term aeroelastic optimization is used herein to mean the minimum weight design of a lifting surface or skin panel subject to lower bound requirements on critical flutter velocity. Several other constraints are of interest in aeroelasticity such as requirements on natural frequencies and static divergence velocity. The review given mainly deals with work done on flutter constraints, since this is the area of prime concern in nonlinear and transonic aeroelasticity. Work relating to frequency constraints is discussed in so far as it can be related to flutter requirements.

The early work in aeroelastic optimization by Turner,[11] MacDonough,[12] and Head[13] deals with redistributing stiffness to achieve a condition which is indirectly related to flutter velocity. For example, the MacDonough condition is one of uniform strain energy density under the inertia loading associated with either a wing bending or torsional mode. It is necessary, however, to know beforehand the frequency requirements needed to prevent flutter. Head[13] stresses the importance of the uniformity

of strain energy density in the fundamental torsional mode as the key to flutter prevention with minimum weight.

The 1968 paper by Ashley and McIntosh[14] marks the beginning of recent work on aeroelastic optimization of continuous systems. All known results on optimal design of continuous aeroelastic systems are collected together and it is shown what functionals are uniform in minimum weight structures. Constraints include fixed longitudinal and torsional frequencies, torsional and chordwise wing divergence speeds, torsional wing flutter and sandwich panel flutter requirements. Although the sandwich panel flutter optimization is discussed at length, no numerical results are presented in this paper.

The work by Turner[15] lays the foundation for the finite element approach to aeroelastic optimization. The classical Lagrange multiplier technique is used to enforce the linear algebraic flutter equation constraints. A Newton-Raphson method is used to satisfy the nonlinear optimality equation. Results are given for a three element cantilever wing and for a segmented sandwich panel. The aerodynamic theories used are incompressible strip theory for the wing, and piston theory for the panel problem. Numerical results for the panel verify the theoretical prediction that the optimal panel thickness distribution is symmetrical about its midpoint.

The groundwork for continuous aeroelastic optimization laid by Ashley and McIntosh is further developed by Weisshaar.[16] Solutions to one-dimensional linear structural problems are obtained by the transition matrix procedure adapted from the theory of optimal control. For the first time, quite detailed information is shown on the minimum weight design of a sandwich panel in supersonic flow. Weisshaar also develops a basis for discrete element optimization via control theory methodology.[17] McIntosh[18] gives quite a complete survey of control theory methods as applied to structural optimization problems.

Optimization of discrete structures by numerical search techniques is further extended by Rudisill and Bhatia.[19] The key to their development is the derivation of expressions for partial derivatives of the flutter velocity with respect to the member sizes in the finite element structural model. A search strategy is employed based on flutter velocity gradient information. The method is shown to be quite computationally efficient and capable of being used in conjunction with important strength requirements.

It is interesting to note the variety of design sensitivity methods, such as the Rudisill-Bhatia flutter derivatives, that can be used in structural dynamics and aeroelasticity. In his doctoral dissertation, van de Vooren[20] applies perturbation theory to determine changes

in flutter eigenvalues when small changes in wing mass and stiffness are made. Cross and Albano[21] further develop the perturbation method and present a working procedure for rapidly analyzing a large number of wing store configurations for flutter clearance. Fox and Kapoor[22] compute frequency and mode shape derivatives for the generalized algebraic eigenvalue problem with symmetric matrices. Rogers,[23] Rudisill,[24] and Rudisill and Chu[25] extend this to more general systems which are not self-adjoint. Simpson[26] studies the case of derivatives of equal eigenvalues which is applicable to the design of systems subjected to nonconservative loads of the circulatory type. Both perturbation and derivative methods significantly reduce the cost of reanalysis when a large number of small changes must be made to a linear system.

Stroud, Dexter, and Stein[27] develop a computer code which considers both flutter and strength in a simultaneous manner. A plate model of a delta wing is studied, and design variables consist of coefficients in an assumed polynomial skin thickness distribution. Move directions for flutter resizing are generated by finite difference approximations to flutter derivatives. The overall flutter-strength resizing is accomplished by an interior penalty function mathematical programming technique. Similar work on multiple constraints is reported by Fox, Muira, and Rao[28] who treat flutter, deflection, and

natural frequency constraints in a simultaneous manner. The work is also notable since a combined weight-drag objective function is minimized.

In his doctoral dissertation, Gwin[29] describes the development of a mathematical programming approach to flutter optimization based on the method of feasible directions. For the first time, three-dimensional aerodynamic theories (doublet-lattice and Mach-box) are used to determine the flutter characteristics. It is shown that flutter velocity derivative information can be obtained from the rate of change of complex eigenvalues associated with critical points on the velocity-damping diagram. Using this flutter derivative information, Gwin efficiently obtains minimum weight designs of several complex finite element lifting surface models. Reference 30 gives further details of the results.

Parallel to the mathematical programming methods development are procedures based on an energy related optimality criterion. One of the most successful studies is that by Siegel[31] in which the B-1 wing structure is resized to meet a flutter requirement. Material is added to the areas of maximum strain energy density in the flutter mode. This is an important advance over the very early flutter optimization studies which concentrate on just a single free vibration mode. Using the Turner wing model

of Reference 15, Bogner[32] verifies the efficiency and utility of the strain energy procedure.

The flutter optimality condition of Wilkinson, et al.[33] requires uniform flutter velocity derivatives of the Rudisill-Bhatia form. An extensive evaluation of the mathematical programming and energy based optimality procedures is also presented. The result of the effort, a general purpose computer code FASTOP (Flutter And Strength Optimization Program), capable of combining strength and aeroelastic optimization, is now available to the aerospace community. A number of significant detailed applications of this code are given in Reference 34. It is important to note that only linear aerodynamic and structural theories are included in the code. The developments reported herein are designed to lay groundwork for new computer codes in this area.

In order to extend minimum weight design procedures to include complex multiple constraints and nonlinear effects, it is necessary to maintain and develop further a firm theoretical base for both the mathematical programming and optimality criteria approaches. The important work of Prager and Taylor[35] provides background for Plaut's excellent development[36] on design for specified critical loads. Reference 36 provides a most complete mathematical development of optimality for minimum weight design in the presence of circulatory, gyroscopic, and dissipative forces. The

doctoral dissertations of Segenreich, Johnson, and Rizzi[37] are also prime examples of contributions which have added in a fundamental way to an understanding of how mathematical programming and/or optimality criteria can be used in the presence of complex static and dynamic constraints.

In a recent paper by McIntosh and Ashley,[38] some comparisons are made between mathematical programming and optimality approaches. Based on a numerical test case, the authors conclude that the optimality approaches may indeed be better suited for incorporation into general design procedures than certain mathematical programming approaches. The McIntosh and Ashley formulation allows for the incorporation of an "aerodynamic memory" effect. This formulation could be very useful in the development of a practical aeroelastic design capability which includes the effect of aerodynamic gust loadings.

The above survey shows that there has been no work done to date in transonic aeroelastic optimization, or indeed in any area of design optimization where the system is undergoing nonlinear motions. The next section deals with the status of unsteady transonic aerodynamics methods which are applicable to nonlinear flutter problems.

2.2 UNSTEADY TRANSONIC AERODYNAMICS

In a recent survey of the literature, Borland[39] gives an extensive review of work relating to unsteady transonic flowfield determination. A comprehensive reference list

shows that over 200 papers and reports are available in the open literature dealing with this subject. The publications can be classified as to solution method, geometry, time dependence, and type of equations solved. Of the publications reviewed by Borland, only five are listed in the comprehensive reference list as dealing specifically with flutter. All five of the transonic flutter studies are shown to be experimental in nature. Out of a total of 171 theoretical publications, only six report data on unsteady pressure distributions which are an essential ingredient in transonic flutter calculations. Thus, although there is much available literature on "unsteady transonic flow," only a fraction of the literature deals with methods directly applicable to aeroelastic calculations.

McCroskey[40] makes the following categorization of unsteady transonic flow formulations in order of increasing complexity:

(1) linear potential theory,

(2) local linearizations,

(3) unsteady linearization of small disturbance equations,

(4) nonlinear small disturbance equations

(5) nonlinear Euler equations, and

(6) Navier-Stokes equations.

Of these formulations, the nonlinear small disturbance methods have achieved a high degree of development and can be used to solve aeroelastic stability problems while maintaining the nonlinear nature of the problem. It is essential to use nonlinear aerodynamic theory to look for the onset of amplitude dependent flutter and divergence. Tijdeman[2] shows essentially the same scheme to categorize the analytical formulations. It appears that by far the most used computational method of solution is finite differences. In all six areas noted above, much work is reported in the literature which makes use of this procedure.

The monograph by Landahl[41] gives a brief but straightforward derivation of the basic transonic potential flow equation. The order of magnitude analysis needed to arrive at the various potential flow approximations is presented by numerous investigators including Olsen.[42,43] For an introduction to the method of finite differences, the texts by Ames[44], and Richtmyer and Morton[45] are particularly useful and present much material relating to the solution of nonlinear flow problems.

The alternating-direction implicit finite difference algorithm is used by Ballhaus and Goorjian[46,47] to solve the low-frequency, small disturbance potential flow equations. A computer code, LTRAN2, is now available which can predict the shock wave motions on an oscillating

airfoil or an airfoil with an oscillating flap. The analytical results agree qualitatively with other recent experimental work of Tidjeman[48] and the numerical solutions of Magnus and Yoshihara[49] who solved the Eulerian equations with an explicit finite difference algorithm. Ballhaus and Goorjian report that a solution for one cycle of unsteady motion can be obtained in eight seconds on the CDC 7600 computer, compared to 1500 seconds for the Magnus-Yoshihara procedure.

In November of 1978 a conference entitled "Transonic Unsteady Aerodynamics for Aeroelastic Applications" was held at Columbus, Ohio, under the sponsorship of the Air Force Flight Dynamics Laboratory. Papers presented at that conference show that much work has been done to predict accurately the effect of a moving shock wave on the pressure distribution at the surface of an oscillating airfoil. It appears that three-dimensional aeroelastic analyses will soon be feasible on some of the larger digital computers. A full-scale aeroelastic optimization capability does not appear possible in the near future using the analysis methodologies that have been proposed to date.

2.3 NONLINEAR AEROELASTIC STABILITY

In this subsection the area of nonlinear aeroelasticity is reviewed. Publications cited deal primarily with either structural or aerodynamic nonlinearity. By

far the most analytical work has been done in the structural area. This type of nonlinearity originates usually in control system linkage mechanisms or from the in-plane tensile stresses in panels. The analytical work that considers aerodynamic nonlinearity deals mainly with hypersonic, transonic, or vortex shedding phenomena. Chapter 10 of the text by Bisplinghoff and Ashley[50] gives an excellent introduction to some of the more classical methods used in the analysis of nonlinear systems.

In the paper by Woolston, Runyan, and Andrews,[51] nonlinear flutter calculations are performed on a typical airfoil section which has pitch and plunge degrees of freedom. Structural nonlinearities considered are due to free-play, cubic stiffness, and hysteresis effects in the restraining springs. Numerical results from an analog computer are presented which indicate that stability is highly dependent upon the magnitude of the initial displacements. The introduction of free play into the torsional spring causes the nonlinear flutter speed to be lower than the speed predicted without it. The ratio of the nonlinear flutter speed to the linear speed decreases with increasing initial pitch displacement. A similar trend is noted in the case of a cubic variation in pitch spring stiffness. When hysteresis is added to the wing control surface system, the linear flutter speed results seem to provide a good lower bound on the nonlinear case.

A number of instances of limited amplitude flutter are shown. In these situations, flutter could contribute significantly to fatigue failure of the system.

The "principle of harmonic linearization" of Kryloff and Bogoliuboff[52] is applied in the paper by Shen and Hsu[53] to the flutter problem of Reference 51. By balancing the fundamental harmonic, flutter velocity versus amplitude trends are shown which demonstrate the utility of this procedure. Woolston and Andrews[54] point out that direct integration of the nonlinear aeroelastic equations gives flutter velocity as a function of the amplitude of the initial conditions of the system. On the other hand, the Kryloff and Bogoliuboff method gives velocity as a function of the limit cycle or long term amplitude of the system. Shen[55] elaborates further on the harmonic linearization method and shows that the long term amplitude results of Reference 53 are not directly comparable to those of Woolston, Runyan, and Andrews.

Transient and nonlinear aeroelastic effects are considered by Brunelle[56], and an approximate method is developed to handle systems with one or two degrees of freedom. Brunelle points out that the Kryloff-Bogoliuboff solution assumes that only weak nonlinearity

and small damping are present. He then shows how to solve the van der Pol equation starting with an assumed solution which contains an exponential time function to account for strong nonlinearities. In the two-degree-of-freedom case, the Brunelle method becomes quite lengthy. Results for the van der Pol equation agree quite well with numerical integration and indicate that this approximate method can predict accurately the limit cycle behavior of the can der Pol equation with strong nonlinearity. No numerical results were given for the two-degree-of-freedom system.

Nonlinear aeroelastic response of panels is discussed at length by Dowell in Chapter 3 of his monograph.[57] The basic technique of modal expansion is presented and applied to skin panels where in-plane stretching is the source of the nonlinearity. The effects of static pressure differential, in-plane loading, and curvature on flutter dynamic pressure are presented. In References 58 and 59, Dowell also discusses direct numerical integration of the nonlinear panel flutter equations from a given set of initial conditions.

Perturbation and harmonic balance methods are applied by Kuo, Morino, and Dugundji[60] to large deflection panel flutter problems. Results agree well with those obtained

by the direct integration method. It is shown that structural damping can have a destabilizing effect on flutter at high mass-air ratios. Both the perturbation method and the harmonic balance method are shown to require only about four percent of the computing time needed for numerical integration.

The direct method of Liapunov[61] has been studied by a number of investigators including Parks,[62] George,[63] and Dimantha and Roorda.[64] As applied to panel flutter, Parks shows that the Liapunov method can lead to highly conservative bounds on critical dynamic pressure. Such results can be highly dependent on the form of the Liapunov functional that is constructed. The work of Diamantha and Roorda deals with this problem, and they show how to construct functionals for some simple nonconservative systems. The power of the Liapunov method lies in the fact that stability "in the large" can be determined. The problem of constructing appropriate functionals for complex nonlinear systems such as those encountered in aeroelasticity remains an area of current research.

On a practical engineering level, the effect of structural nonlinearities on flutter behavior is of continued interest to the aircraft designer. The recent papers by Breitbach,[65] Laurenson and Trn,[66] and Sensburg and Schoen[67] show that there is continuing concern within the

aerospace industry over effects of free play and nonlinear stiffness on missile and aircraft control surface flutter boundaries. Approximate analytical tools are being built around the method of harmonic balance, and experimental models are being used to check the accuracy of the analyses.

Work in the area of aerodynamically nonlinear flutter appears to be quite limited. Eastep and McIntosh[68,69] investigate the stability of a flat panel in nonlinear hypersonic flow. Both numerical integration and the Dimantha-Roorda[64] energy considerations lead to the conclusion that a panel can become unstable in hypersonic flow if the energy input of the initial disturbance is sufficiently large.

Instabilities of a nonlinear aerodynamic nature can also involve separated flow around an oscillating airfoil. At relatively low subsonic speeds, a complex interaction involving the fluctuating lift due to vortex shedding and an elastic structure can occur. This "vortex-induced vibration" is self-excited and self-limited. A precise modeling of the flow environment would require solving the full Navier-Stokes equations, but some investigators such as Hartlen and Currie[70] have proposed an attractive alternative. In their study, use is made of experimental lift data for a long circular cylinder in low-speed flow to derive a nonlinear lift-oscillator model of the

aerodynamic environment. The governing equations for the system can be shown to be equivalent to the van der Pol oscillator. Approximate solutions are obtained based on the approximate method given by Minorsky.[71] Agreement with experiment is quite good; however, other investigators such as McCroskey[40] have criticized the lift-oscillator model on the grounds that it is not derived from the fundamental principles of fluid mechanics.

A related aerodynamically nonlinear problem, stall flutter, is investigated by Dugundji and Chopra.[72] In this primarily experimental study, the stability of two-dimensional wings is investigated at high angles of attack in subsonic flow. Nonlinear divergence is shown to occur at angles of attack above about 10 degrees. In the case of bending-torsion flutter, limit cycle behavior is shown at torsional amplitudes as great as 40 degrees. The onset of this coupled mode flutter can be predicted with reasonable accuracy using linear aerodynamic theory.

In the transonic speed range, a single degree-of-freedom instability known as "aileron buzz" has been known to occur. This phenomenon results from a separated flow condition and is very difficult to predict analytically. As early as 1946, these unstable aileron oscillations were of concern to the aeroelastician. Smilg[73] presents a practical engineering approach to the problem and reports

in detail on the effect that various airfoil and aileron parameters have on the oscillations. As a result of this investigation and also a later paper by Smilg,[74] the importance of single degree-of-freedom aeroelastic stability considerations is well established.

Within the last two years, several important transonic flutter studies have been completed which incorporate state-of-the-art unsteady transonic aerodynamic methods. Ballhaus and Goorjian[47] present flutter results of a NACA 64A006 airfoil pitching in transonic flow. The LTRAN2 code[46] is coupled with a simple numerical integration procedure to solve the structural and aerodynamic equations. Rizzetta[75-77] also investigates the use of numerical integration. The equations of motion for a three-degree-of-freedom airfoil-aileron system are coupled with LTRAN2 aerodynamic lift and moment calculations and integrated simultaneously. Rizzetta shows that the Adams-Moulton implicit predictor-corrector method[78] has superior numerical stability compared to other procedures tried, such as the Euler-Cauchy and the Milne three-point implicit schemes. A number of amplitude dependent flutter cases are shown which indicate the essential nonlinear character of the transonic flutter problem.

The work by Yang, Striz, and Guruswamy[79,80] represents a comprehensive study of the effect of various structural and aerodynamic parameters on the flutter behavior of two-dimensional airfoils in transonic flow. The results of Reference 79 indicate that relaxation[81] and indicial[47] aerodynamic methods give comparable flutter solutions in the low transonic Mach number range. In Reference 80, a direct integration method is coupled with the LTRAN2 code, to compute time-history flutter solutions. Results for a NACA 64A006 airfoil agree quite well with those of Ballhaus and Goorjian.[47] Time-history solutions and the indicial and relaxation methods give significantly different estimates of aerodynamic coefficients. Reference 80 states that the differences are due to the time linearization assumption of the indicial and relaxation methods.

Qualitative results on the influence of shock wave motion on typical-section wing flutter are presented by Ashley.[82] Shock parameters considered are displacement amplitude, phase lag behind quasi-steady behavior, steady strength, and chordwise position. The effect of the shock is shown to be generally destabilizing for single-degree-of-freedom pitching motion. For bending-torsion cases the shock can be either stabilizing or destabilizing, depending on the system parameters. Qualitative results such as Ashley's should provide insight into the basic transonic

flutter mechanism which will be of great use in further analytical work.

SECTION III

THEORETICAL DEVELOPMENT

The "method of imposed disturbances" is derived based on the concept of conservation of energy in a limit cycle.[83] For certain problems, nonlinear instability occurs at zero frequency and the method takes the form of a set of generalized force balance equations. The limitations of the Kryloff-Bogoliuboff method are shown in the first subsection below. This is followed by a general formulation of the method of imposed disturbances. It is shown how the method is easily used in conjunction with sophisticated aerodynamic calculations. As an alternative to the cumbersome time history approach to nonlinear flutter calculations, the method is highly efficient and gives clear physical insight into the nature of the instability.

3.1 LIMITATIONS OF THE KRYLOFF-BOGOLIUBOFF METHOD

The literature survey shows that the harmonic balance method due to Kryloff and Bogoliuboff (K-B method) is currently being applied to obtain approximate solutions to nonlinear flutter problems. In what follows, two simple examples will be studied to point out the utility and also the limitations of this approach. The discussion of the

method follows that of Minorsky[84] and the original Kryloff-Bogoliuboff reference.[52]

3.1.1 Basic Considerations

Consider a differential equation for a single degree-of-freedom dynamic system which has the form

$$\ddot{x} + 2\zeta\omega_1\dot{x} + \omega_1^2 x = \mu f(x,\dot{x}) \tag{3.1}$$

where f is in general a nonlinear function of the displacement, x, and the velocity, $\dot{x}$. The quantities ω_1 and ζ are the undamped natural frequency and damping factor, respectively. The nonlinear terms are scaled by the small parameter μ. Equation (3.1) can be written as a pair of first order equations

$$\frac{d\dot{x}}{dt} = -F(x,\dot{x}) \tag{3.2a}$$

$$\frac{dx}{dt} = \dot{x} \tag{3.2b}$$

where

$$F(x,\dot{x}) = 2\zeta\omega_1\dot{x} + \omega_1^2 x - \mu f(x,\dot{x}) \tag{3.3}$$

Division of (3.2a) by (3.2b) gives

$$\frac{dy}{dx} = \frac{Q(x,y)}{P(x,y)} \tag{3.4}$$

where $y = \dot{x}$

$$Q(x,y) = -F(x,y) \tag{3.5}$$

and,

$$P(x,y) = y \tag{3.6}$$

If x and y are considered to be points in a plane, i.e., the phase plane, then it can be shown[84] that Equation (3.4) has only one integral curve passing through each regular point of the plane. A point in the phase plane is regular if P and Q do not both vanish; otherwise, the point is said to be singular.[84] A limit cycle, C, is a special solution of Equation (3.2) with the following properties: (1) it is a closed trajectory, and (2) all other solutions, C', either approach C as $t \to \infty$ or as $t \to -\infty$. If C' approaches C as $t \to \infty$, then C is a stable limit cycle, and in the case that C' approaches C as $t \to -\infty$ the limit cycle is said to be unstable. Not all nonlinear systems exhibit limit cycle behavior; however, the phenomenon does occur in many instances which are of practical concern in analytical mechanics. Typical limit cycle behavior in the phase plane is shown in Figure 1. Stable limit cycle behavior is exhibited in Figure 1a, since both representative trajectories converge toward the same closed curve. Just the opposite is true in Figure 1b as both curves diverge away from the closed path, C. Trajectories which start exactly on the unstable limit cycle will continue indefinitely on this path. The unstable limit cycles are difficult to calculate numerically since a small accumulation of error will deflect the trajectory either to the origin or to some unbounded path.

$$\ddot{x} + 2\zeta\omega_1\dot{x} + \omega_1^2 x = \mu f(x,\dot{x})$$

C: limit cycle
C': solution trajectories
o: solution starting point

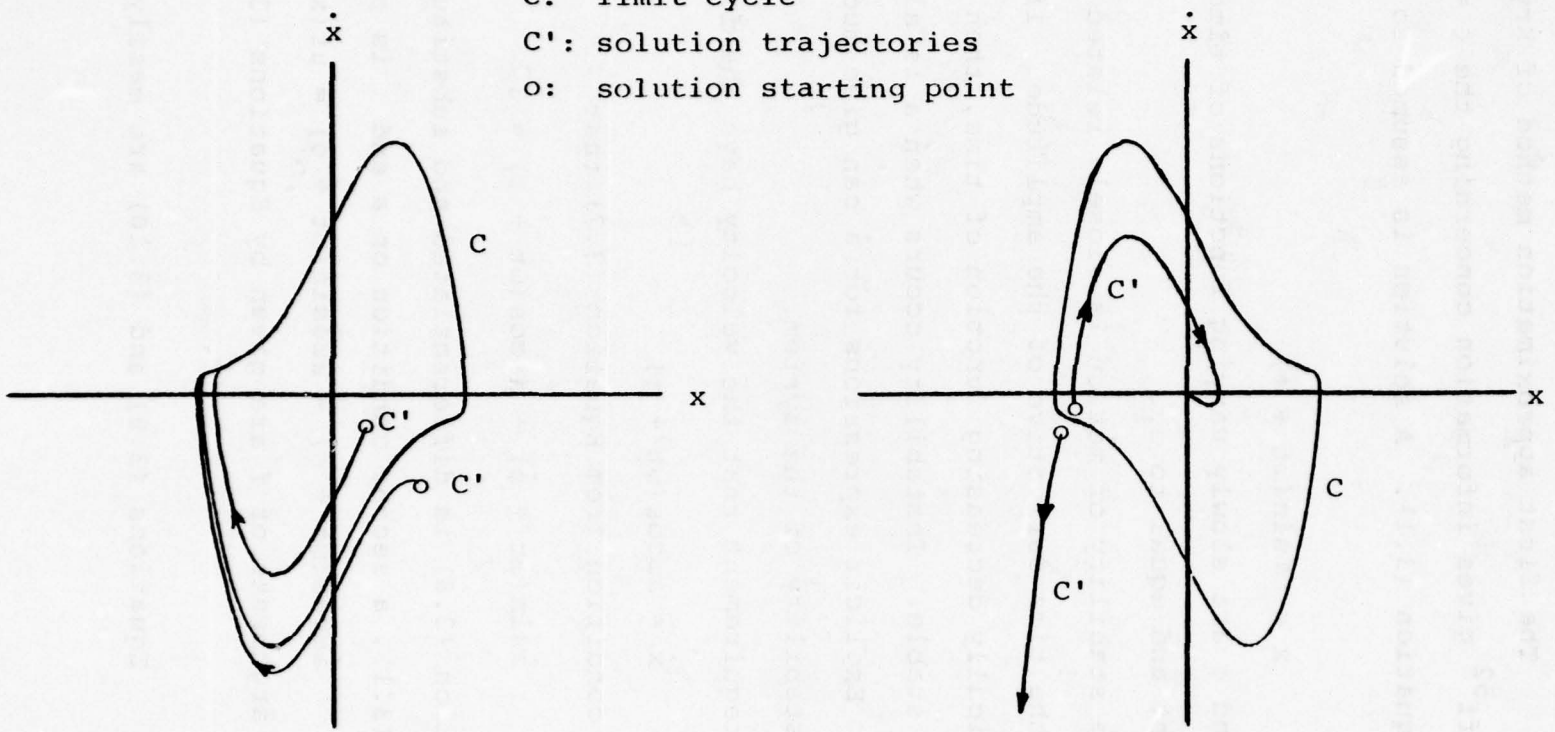

(a) Stable Limit Cycle

(b) Unstable Limit Cycle

Figure 1. Phase Plane Representation of Limit Cycle Behavior of a Nonlinear System.

3.1.2 Expressions for Amplitude Derivatives

The first approximation method of Kryloff-Bogoliuboff[52] gives information concerning the $\zeta = 0$ solution of Equation (3.1). A solution is assumed to be of the form

$$x = a\sin(\omega t + \phi) \tag{3.7}$$

where a and ϕ are slowly varying functions of time and ω is constant and equal to ω_1.

The stability of motion is closely related to the value of the time derivative of the amplitude. If a is a monotonically decreasing function of time, then the motion is stable. Instability occurs when $\dot{a}$ is always positive. Explicit expressions for $\dot{a}$ can give much insight into the stability of the system.

A requirement that the velocity have the form

$$\dot{x} = a\omega\cos(\omega t + \phi) \tag{3.8}$$

gives the condition from Equation (3.7) that

$$\dot{a}\sin(\omega t + \dot{\phi}) + a\dot{\phi}\cos(\omega t + \phi) = 0 \tag{3.9}$$

When Equation (3.8) is differentiated and substituted into Equation (3.1), a second condition on a and is obtained.

$$\dot{a}\omega\cos(\omega t + \phi) - a\omega\dot{\phi}\sin(\omega t + \phi) = \mu f(x,\dot{x}) \tag{3.10}$$

where the arguments of f are given by Equations (3.7) and (3.8).

Equations (3.9) and (3.10) are easily solved to get

(3.11a) $$\dot{a} = \mu f(x,\dot{x}) \cos(\omega t + \phi)/\omega$$

(3.11b) $$\dot{\phi} = -\mu f(x,\dot{x}) \sin(\omega t + \phi)/a\omega$$

Since the right hand sides of Equation (3.11) are almost periodic functions, they can be represented in the first approximation as a Fourier series of the form

(3.12a) $$\mu f(x,\dot{x}) \cos\gamma \approx P_0(a) + \sum_{n=1}^{\infty} [P_n(a) \cos n\gamma + P_n'(a) \sin n\gamma]$$

(3.12b) $$\mu f(x,\dot{x}) \sin\gamma \approx Q_0(a) + \sum_{n=1}^{\infty} [Q_n(a) \cos n\gamma + Q_n'(a) \sin n\gamma]$$

where $\gamma = \omega t + \phi$. Substitution of Equations (3.12) into (3.11) gives expressions which can be integrated over the time interval t to t + T where T is the period. Considering a and ϕ to be constant whtin this interval leads to

(3.13a) $$[a(t+T) - a(t)]/T = \mu P_0(a)/\omega$$

(3.13b) $$[\phi(t+T) - \phi(t)]/T = \mu Q_0(a)/a\omega$$

If the period is great enough, the difference quotients on the left sides of Equation (3.13) can be replaced by time derivatives. Thus using the usual Fourier expressions for P_0 and Q_0, the first approximation of the K-B theory is obtained as follows

(3.14a) $$\dot{a} = (\mu/2\pi\omega) \int_0^{2\pi} f(a \sin\gamma, a\omega \cos\gamma) \cos\gamma d\gamma$$

$$\dot{\phi} = -\mu/2\pi\omega a) \int_0^{2\pi} f(a \sin\gamma, a\omega \cos\gamma) \sin\gamma d\gamma$$

where a and ϕ are treated as constants in the integration.

The power of this method can be seen in an application to the van der Pol equation

(3.15) $$\ddot{x} + x = \mu(1-x^2)\dot{x}$$

In this case the time rate of change of amplitude as computed by Equation (3.14a) is

(3.16) $$\dot{a} = (\mu a/2)(1-a^2/4)$$

It is suggested by this equation that for positive μ, the motion tends toward a stable limit cycle of amplitude 2.0 (see Figure 1a). For negative μ, a is negative at amplitudes less than 2.0 and positive for those greater than 2.0. Hence in this case an unstable limit cycle is indicated (see Figure 1b). Such conclusions for the van der Pol equation are verified by numerical integration in Chapter 4. The K-B theory is shown to give accurate trend information concerning limit cycle behavior for even moderate values of μ (about 1.0).

The method just outlined gives equivalent results to the variation of parameter method described by Cunningham[85] and the van der Pol method (see Stoker,[86] pp. 149-153). In the latter method, a solution of the form

(3.17) $$x = a_1(t)\ \sin\omega t + a_2(t)\ \cos\omega t$$

is assumed. Such a form can be obtained from Equation (3.7) by elementary trigonometry.

3.1.3 The Harmonic Balance Form of the K-B Method

The harmonic balance form of the K-B method used by Shen[54] in his nonlinear flutter work takes on a slightly different but equivalent form. Again using the $\zeta = 0$ form of Equation (3.1), the first step is to assume a series solution

(3.18) $$x = \sum_{n=1}^{\infty} a_n \sin n\omega t$$

and substitute it into the given equation. This leads to

(3.19) $$\sum_{n=1}^{\infty} (-\omega^2 n^2 + b_n) \sin n\omega t = 0$$

where the b_n constants are the Fourier sine coefficients of $\omega_1^2 x = \mu f(x,\dot{x})$. In explicit form, the first coefficient is

(3.20) $$b_1 = \frac{\omega}{\pi} \int_0^{2\pi/\omega} [\omega_1^2 x - \mu f(x,\dot{x})] \sin\omega t\ dt$$

where the first term of the series Equation (3.18) is used to compute the integral. Balancing the first harmonic in Equation (3.19) gives

(3.21) $$\omega^2 = b_1/a_1$$

where $b_1 = b_1(a_1)$ is computed from Equation (3.20). The first order solution is thus

(3.22) $$x = a_1 \sin[b_1(a_1)t/a_1]$$

3.1.4 The K-B Estimate of Stability for the Reduced Pendulum Equation

As an example of harmonic balance procedure, consider the reduced nonlinear pendulum equation (see Reference 52, p. 14)

(3.23) $$\ddot{x} + (g/\ell)(x-x^3/6) = 0$$

where x is the angular displacement of the pendulum and g and ℓ are the acceleration due to gravity and the pendulum length, respectively. Equation (3.23) gives accurate results up to displacement angles of about 30 degrees. It will be shown below that larger angles can result in an instability. Although unstable motion is not observed in the physical system, it serves to point out a difficulty with the unjudicious application of the harmonic balance method.

A straightforward application of Equations (3.18) through (3.20) yields the following amplitude dependent frequency equation

(3.24) $$\omega^2 = (g/\ell)(1-a_1^2/8)$$

From this equation, it is concluded that real frequencies can be computed for all amplitudes of motion up to $a_1 = \sqrt{8}$. Beyond that point, Equation (3.24) has complex roots and the displacement solution of Equation (3.22) has a term which grows exponentially with time.

Figure 2 shows the solution of Equation (3.23) that is obtained by the Kutta-Merson integration technique.[87] A slightly more general equation has been included in the computer code, but the case shown in Figure 2 is for $\zeta = \omega_1 = 0$, $\mu = g/\ell = 1.0$ with an initial displacement of $x = 2.448$. The motion is stable and has a periodic frequency of 0.2527 radians per second which compares very well with the value of 0.2509 radians per second obtained from Equation (3.24) with $a_1 = 2.448$. At a slightly higher initial displacement of 2.449, the motion is divergent as shown in Figure 3. Thus Equation (3.24) overestimates the critical initial displacement which causes instability by about 15 percent. It is also important to note that the K-B estimate of rate of change of amplitude using Equation (3.14a) gives $\dot{a} \equiv 0$ for all amplitude levels.

The K-B method can be applied to an n-degree-of-freedom system; however, the expressions for the rate of change of amplitude require n multiple integrations of the nonlinear terms.[88] Such a calculation for prediction of aerodynamically nonlinear flutter could be quite formidable when explicit expressions for the aerodynamics are not available.

An additional difficulty with the K-B method is that strong linear damping terms cannot be included on the left hand side of the equations. As stated in the literature survey, Brunelle[56] modified the K-B method to include

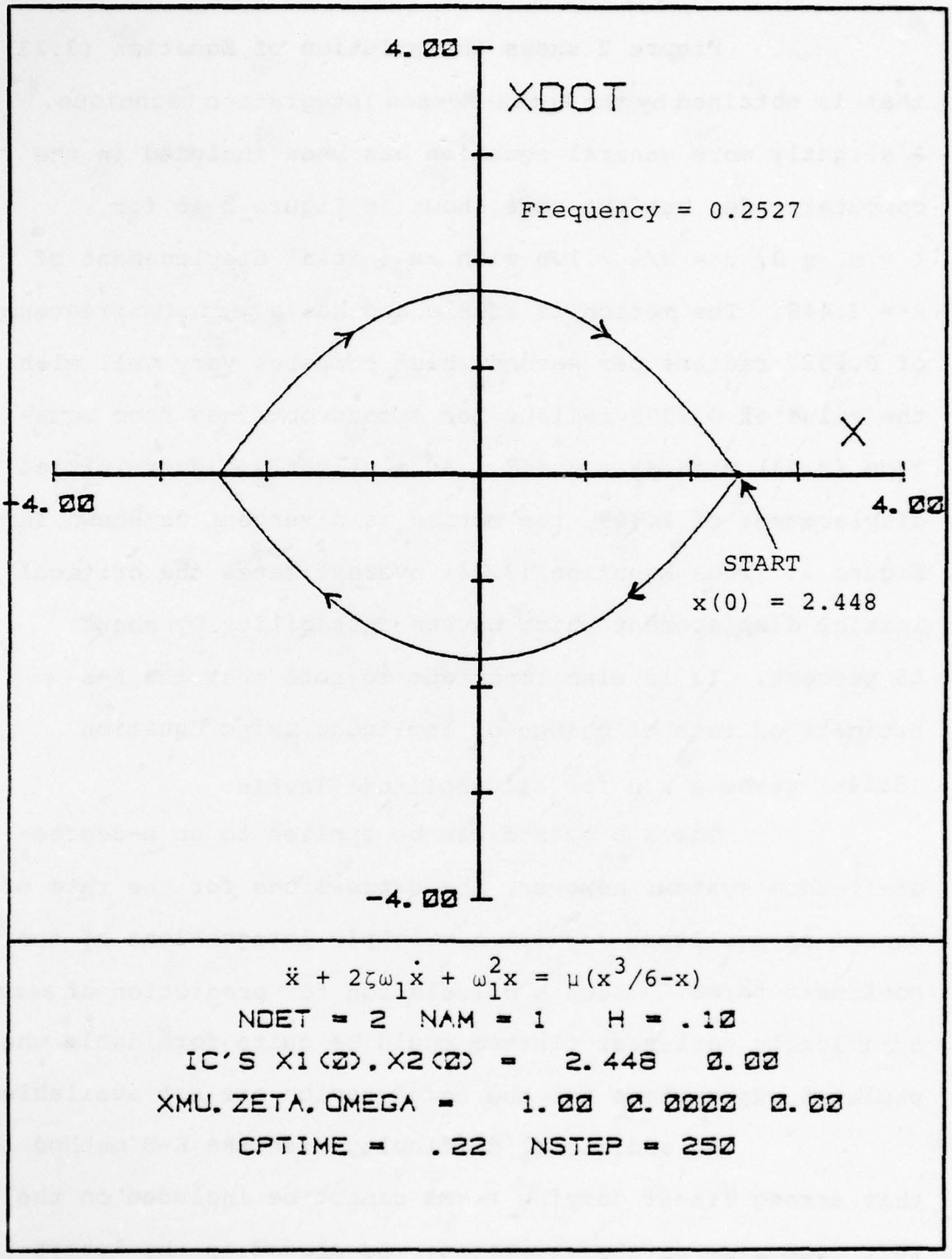

Figure 2. Stable Nonlinear Motion of Reduced Nonlinear Pendulum Equation (Kutta-Merson Integration).

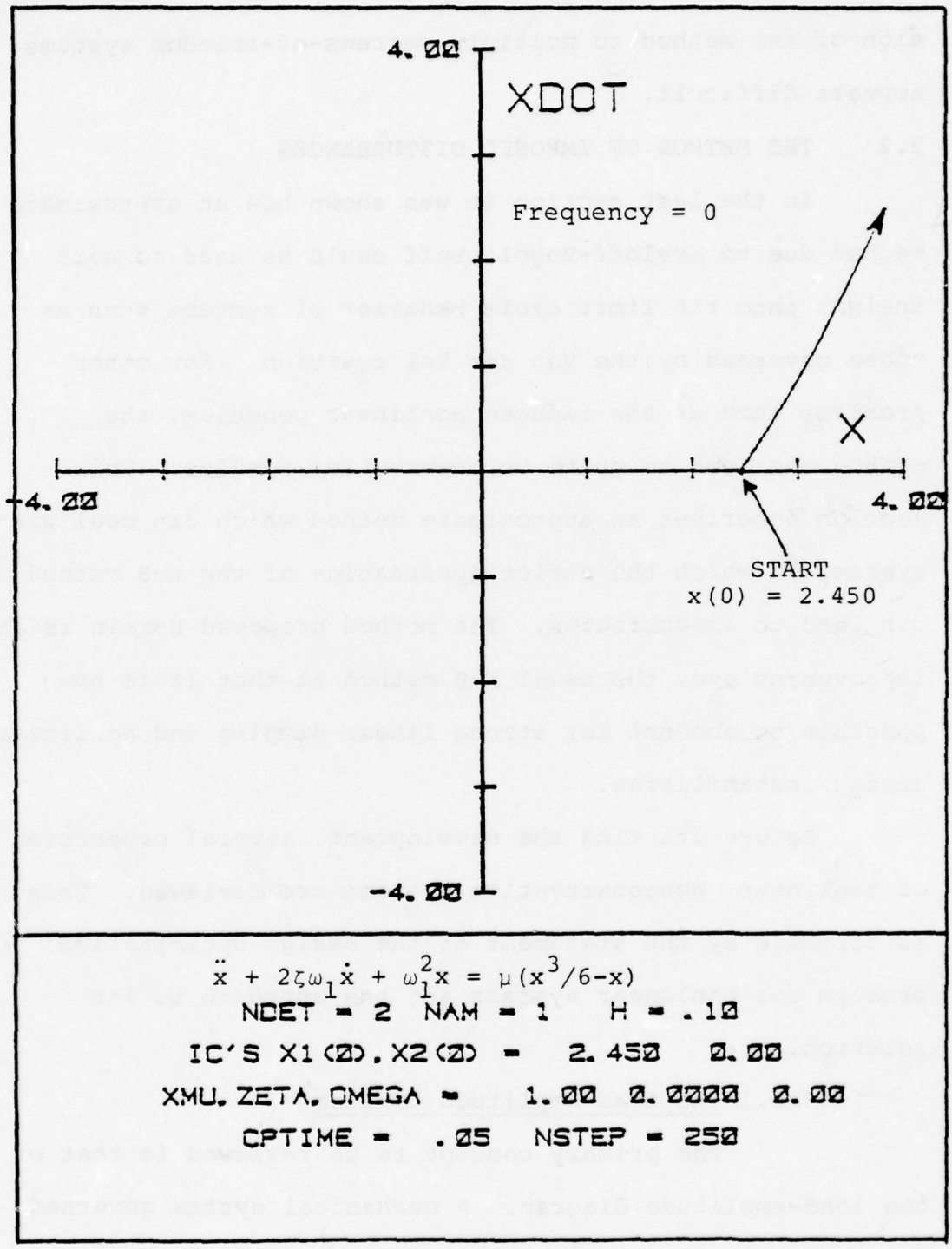

Figure 3. Unstable Nonlinear Motion of Reduced Nonlinear Pendulum Equation (Kutta-Merson Integration).

strong damping terms and nonlinearities; however, the extension of the method to multiple degrees-of-freedom systems appears difficult.

3.2 THE METHOD OF IMPOSED DISTURBANCES

In the last section it was shown how an approximate method due to Kryloff-Bogoliuboff could be used to gain insight into the limit cycle behavior of systems such as those governed by the van der Pol equation. For other problems such as the reduced nonlinear pendulum, the method can lead to quite unconservative results. This section describes an approximate method which can deal with systems in which the strict application of the K-B method can lead to inaccuracies. The method proposed herein is an improvement over the usual K-B method in that it is now possible to account for strong linear damping and nonlinear static instabilities.

Before starting the development, several properties of nonlinear, nonconservative systems are reviewed. This is followed by the statement of the design optimization problem for nonlinear systems and the approach to its solution.

3.2.1 The Load-Amplitude Diagram

The primary concept to be reviewed is that of the load-amplitude diagram. A mechanical system governed by the following set of matrix equations is to be studied:

$$\underset{\sim}{M}\,\ddot{\vec{x}} + \underset{\sim}{C}\,\dot{\vec{x}} - p\,\underset{\sim}{G}\,\vec{x} + \underset{\sim}{K}\,\vec{x} = \lambda\vec{f}(\vec{x},\dot{\vec{x}}) \tag{3.25}$$

where

$\underset{\sim}{M}$ = generalized mass matrix

$\underset{\sim}{C}$ = generalized damping matrix

$\underset{\sim}{G}$ = generalized geometric stiffness matrix

$\underset{\sim}{K}$ = generalized stiffness matrix

$\vec{x}$ = generalized coordinates

$\vec{f}$ = load vector which is nonlinear in the generalized coordinates and velocities

p = static load parameter

λ = dynamic load parameter

There may often exist a critical value of the dynamic load parameter, $\lambda = \Lambda$, beyond which the motion of the system increases without bound. A further important feature of the system is that Λ can depend upon the magnitude of the initial disturbance. It is sometimes possible to define a single disturbance parameter, A, and to numerically solve Equation (3.25) at a given A. For example, in nonlinear panel flutter problems the quantity A can be taken to be the maximum amplitude at the three-quarters chord point. Thus $(A,\Lambda(A))$ plots can be made as shown in Figure 4 by varying A until self-sustained motion is achieved.

Figure 4a depicts what can be termed a "hard instability" since increasing the amplitude of the disturbance also increases the critical value of the load. Thus there is an apparent increase in stiffness in the system.

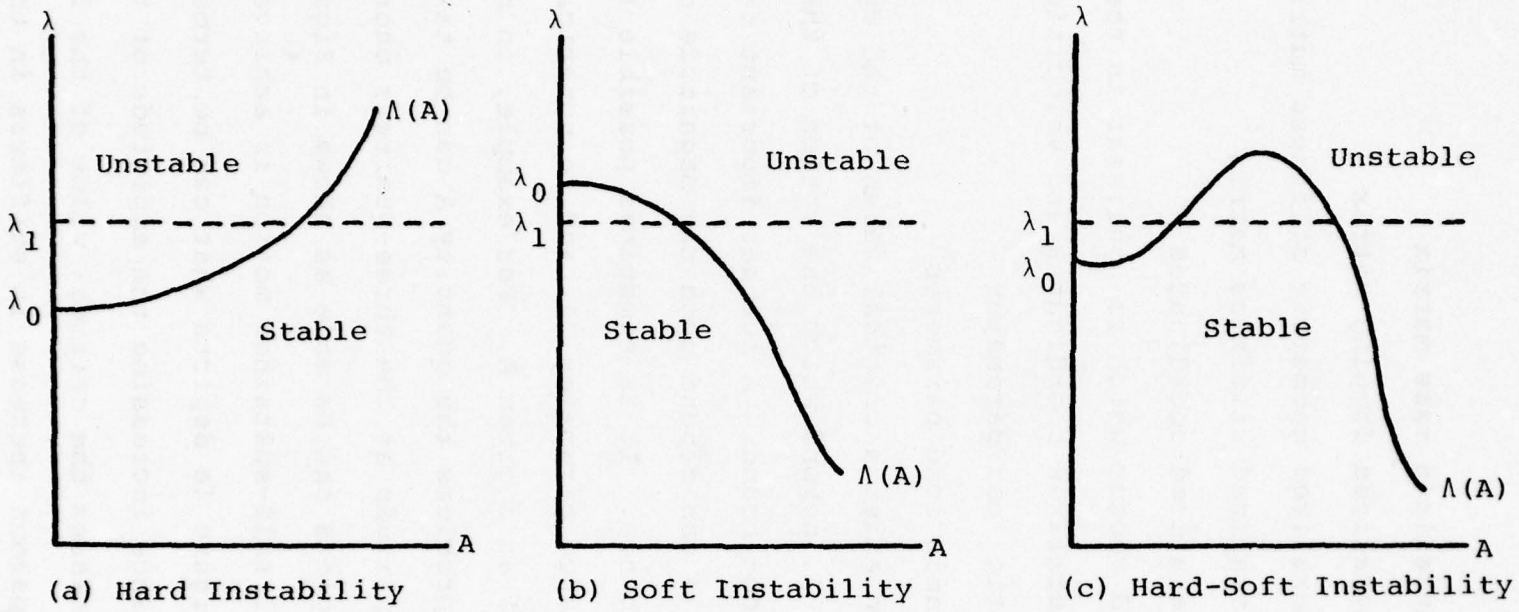

Figure 4. Possible Load-Amplitude Relationships for a Nonlinear, Nonconservative System.

system of Equations (3.25), deleting the nonlinear terms contained in the load vector. At some value of λ_1 greater than λ_0, i.e., λ_1 as shown in Figure 4a, the system is unstable at low amplitudes of disturbance. At higher disturbances the system is again stable. In the case of a single degree-of-freedom system, the phase plane representation would show the existence of stable limit cycle motion. From an energy standpoint, at low amplitude the system is gaining energy from the dynamic loads, but at higher amplitudes the system is losing energy, and the motion cannot be maintained.

A soft instability is shown in Figure 4b. In this case, a linearized analysis gives a critical value of λ which is an upper bound on the stable values of the loading parameter. At some value of λ less than λ_0, the system is unstable until a critical amplitude is reached and then unstable motion occurs. In the phase plane, unstable limit cycle motion would be observed. It is this case of soft instability which is of great technological importance. A linearized analysis proves to be highly misleading if large amplitude disturbances are expected to be applied to the system. Figure 4c shows a possible behavior which is a combination of both situations just described.

3.2.2 Optimization of Load-Amplitude Curves

At this point the (Λ,A) design optimization problem is discussed. As seen from Figure 4b, designing

the system so that λ_0 is greater than some fixed value is inadequate. It is apparent that the stability of the system must be assured within some rectangular domain bounded by both loading and amplitude requirements. Figure 5 shows possible "optimized" load-amplitude plots for these cases.

By changing system design variables in the generalized matrices, it is possible to reconfigure the load-amplitude curves. In Figure 5, the required load, λ_R, and the required amplitude, A_R, block off a region of the diagram in which it is desired to have only stable combinations of λ and A. The situation shown in Figure 5a dictates that system changes be made which primarily affect the λ requirement. In practice, it would not be immediately obvious what changes to make; however, the following comments concerning what is called here "design in the λ-mode" are in order.

A first order approximation to the solution of the design problem of Figure 5a is entirely covered within the framework of methodology already developed for the optimization of linear systems. For example, if Figure 5a is the load-amplitude plot for a panel in two-dimensional nonlinear flow, then λ is the dynamic pressure parameter, and A can be taken as the panel deflection amplitude at a selected point. In nonlinear panel flutter work, plots like this are frequently developed.[58] Thus, in order to achieve the λ_R requirement, the equations for the

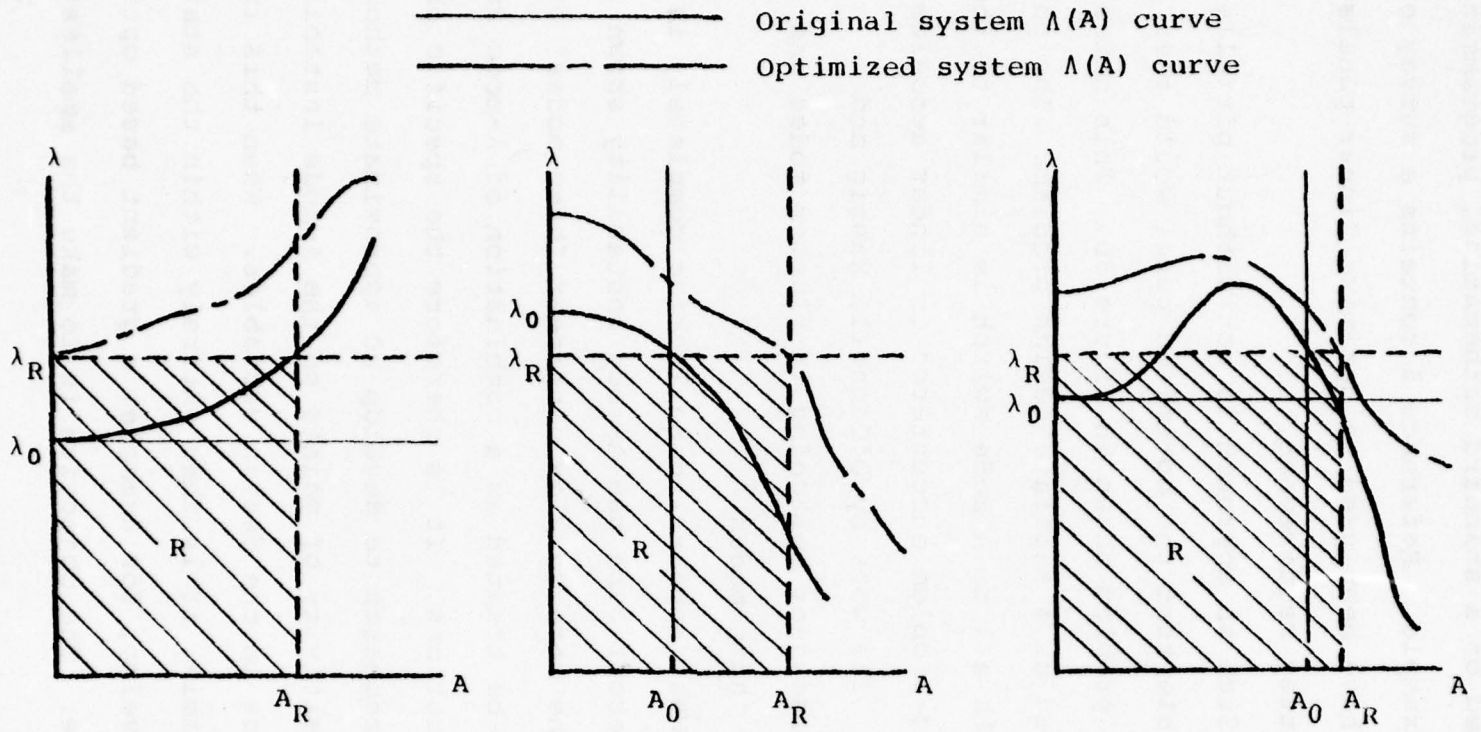

Figure 5. Optimized Load-Amplitude Relationships

panel are first linearized, and then structural resizing performed based on a standard mathematical programming method, for example. Reference 5 contains a survey of the methods that have been used to optimize linear panels to achieve a flutter requirement.

Such an approach is not without pitfalls. It is very possible that the optimized panel would then have the amplitude problem shown in Figure 5b. This situation must be treated as a separate design problem. The potential difficulty with a λ to A mode switch is similar to the mode switching problem encountered in linear aeroelastic optimization. The work by O'Connell, Hassig and Radovcich[89] discusses switching in flutter modes and the occurrence of "hump modes."

What appears to be lacking completely is an approach to reconfigure the A-mode instability shown in Figure 5b. The more complex nonlinear "hump modes" of Figure 5c can be treated as a combination of λ-mode and A-mode optimizations. It is therefore the specific objective of this research to develop an approximate method to determine sensitivity of points on the A-mode instability plot to changes in the design variables. When this information is available, it is then entirely within the state of the art to develop, for example, a gradient based optimization procedure. The objective is to make the smallest

possible changes in the system design variables which remove the $\Lambda(A)$ curve from the required instability region, R (shaded area in Figure 5).

The development of a method to compute A-mode sensitivities is the nonlinear analog to the key development in the dissertation by Gwin.[29] In the case of linear flutter, he derives sensitivity information for selected points on a V-g (velocity-damping) diagram. Moves are made in design space, based on these sensitivities, which reconfigure a specific flutter mode so that the system is stable below a required velocity. With the sensitivity calculation in hand, the most difficult part of the optimization problem is solved.

3.2.3 Mathematical Development of Sensitivities

Sensitivities for the A-mode optimization are now defined in more mathematical terms. It is assumed that there exists a set of independent design variables, $\vec{h}$, associated with the system described by Equations (3.25). When a specific set of these variables is known, the generalized mass, damping, and stiffness matrices can be determined: i.e.,

$$\underset{\sim}{M} = \underset{\sim}{M}(\vec{h}), \quad \underset{\sim}{C} = \underset{\sim}{C}(\vec{h}), \quad \underset{\sim}{K} = \underset{\sim}{K}(\vec{h})$$

The response of the system is a function of $\vec{h}, \lambda$, the initial conditions, and time.

$$\vec{x} = \vec{x}(\vec{h},\lambda,\vec{x}_0,\dot{\vec{x}}_0;t)$$

Let $(\vec{X}_0,\dot{\vec{X}}_0)$ denote a specific set of initial conditions which results in a self-sustained, periodic motion of the system. So at steady-motion,

$$\vec{x} = \vec{x}(\vec{h},\vec{X}_0,\dot{\vec{X}}_0;t) \tag{3.26}$$

$$\lambda = \Lambda(\vec{h},\vec{X}_0,\dot{\vec{X}}_0) \tag{3.27}$$

$$\omega = \Omega(\vec{h},\vec{X}_0,\dot{\vec{X}}_0) \tag{3.28}$$

$$T = T(\vec{h},\vec{X}_0,\dot{\vec{X}}_0) \equiv 2\pi/\Omega \tag{3.29}$$

where ω and T are frequency and period, respectively.

The characteristic amplitude, A, is defined as

$$A = \max_{i,t\varepsilon I} [\vec{X}_i(\vec{h},\vec{X}_0,\dot{\vec{X}}_0;t)] \tag{3.30}$$

where X_i are the components of $\vec{X}$ and I is the time interval for one period of motion. Thus $\vec{X}$ has the form

$$\vec{X} = A\vec{\Psi} \tag{3.31}$$

where $\vec{\Psi}$ is the "normalized" coordinate vector at the steady-state condition. In general,

$$\vec{\Psi} = (\vec{h},\vec{X}_0,\dot{\vec{X}}_0;t) \tag{3.32}$$

and

$$A = A(\vec{h},\vec{X}_0,\dot{\vec{X}}_0) \tag{3.33}$$

The required sensitivities of points on the A-mode instability boundary can be represented symbolically as

$$\Lambda_{,i} = G(h,\vec{X}_0,\dot{\vec{X}}_0) \quad i = 1,\ldots,N_p \tag{3.34}$$

where $(\ )_{,i}$ denotes partial differentiation with respect to the i^{th} component of h, and N_p is the total number of design variables. Equation (3.34) can be obtained by differentiation of Equation (3.27); however, that functional relationship is unknown.

It will now be shown how an exact expression for the right hand side of Equation (3.27) can be derived. Premultiply the governing Equations (3.25) by $\dot{\vec{X}}^T$ and integrate over one cycle of motion to get at the critical condition

$$\left[\frac{1}{2}\dot{\vec{X}}^T \underset{\sim}{M}\dot{\vec{X}} - \frac{1}{2}p\vec{X}^T \underset{\sim}{G}\vec{X} + \frac{1}{2}\vec{X}^T \underset{\sim}{K}\vec{X}\right]_{t=0}^{T} = \int_0^T (\Lambda \dot{\vec{X}}^T \vec{f}(\vec{X},\dot{\vec{X}}) - \dot{\vec{X}}^T \underset{\sim}{C}\dot{\vec{X}})\, dt \tag{3.35}$$

The fact that M, G, and K are symmetric has been used to compute the left side of Equation (3.35). Define the nonconservative work done during the steady-state motion as the right side of Equation(3.35),

$$W^{NC} = \int_0^T \left[\Lambda \dot{\vec{X}}^T \vec{f}(\vec{X},\dot{\vec{X}}) - \dot{\vec{X}}^T \underset{\sim}{C}\dot{\vec{X}}\right] dt \tag{3.36}$$

Note that the conservative terms on the left side of Equation (3.35) are identically equal to zero. This is a result of the fact that conservative terms evaluated at the upper time limit have the same value as at the lower limit.

3.2.4 Assumptions Used to Derive the Method of Imposed Disturbances

The method of imposed disturbances is based on the following assumptions:

1. The quantities A and $\vec{h}$ are the primary variables and the initial conditions can be expressed as

$$\vec{X}_0 = \vec{X}_0(A,\vec{h}), \quad \dot{\vec{X}}_0 = \dot{\vec{X}}_0(A,\vec{h})$$

2. The normalized response is only a function of time

$$\vec{\Psi} = \vec{\Psi}(t)$$

3. The period, T, is constant.

4. The stability is predicted by the following criterion:[83]

$$W^{NC}(\Lambda,A,\vec{h},\vec{\Psi},T) = \begin{cases} >0 & \text{unstable motion} \\ =0 & \text{marginally stable motion} \\ <0 & \text{stable motion of decreasing amplitude} \end{cases} \tag{3.37}$$

Assumption 1 simplifies the problem greatly. Instead of performing studies varying each component of displacement an and velocity, it is only necessary to deal with the amplitude of steady-state oscillation. This assumption does not limit the applicability of the method. It just provides an unambiguous way to define amplitude (see Equation (3.30)). From the study of limit cycle behavior, it is felt that it is reasonable to effectively remove the initial conditions

from the problem, since the long term amplitude (bounded or unbounded) can be achieved by any number of initial conditions. Hence $\vec{X}_0$ and $\dot{\vec{X}}_0$ are not single valued functions of A. It is the character of the normalized response, $\vec{\Psi}$, that is important. By treating A as a scale factor on $\vec{\Psi}$, the relation $\Lambda = \Lambda(A, \vec{\Psi}, \vec{h})$ can be obtained from the condition $W^{NC} = 0$. This is valid if Assumption 2 holds. Again, by studying typical nonlinear systems, it can be found that the character of the normalized response and period do not greatly change over a wide range of system parameters. Hence, Assumption 3 is justified. Assumption 4 is valid as long as the motion is steady-state. If the period becomes infinite, a static subcase must be considered. This is presented in Section 3.2.6.

It is very important to keep in mind that a rapid analysis tool is being developed here for application to optimization studies. A completely rigorous analysis step is not intended through the entire resizing process. It is felt that the assumptions used herein are reasonable considering the purpose for which the method is intended.

3.2.5 Statement of the Method

The method of imposed disturbances can now be stated. For a nonlinear, nonconservative system undergoing steady-state oscillations, the work done on the system by the nonlinear external forces must be balanced by the work done by the internal damping of the system.

This is represented by the condition $W^{NC} = 0$. Given a normalized response mode, $\vec{\Psi}$, which is a kinematically admissible motion, the amplitude parameters, A, can be varied independently to achieve $W^{NC} = 0$. This expression can then be solved for the critical load, Λ. The first result for steady-state motion is

$$(3.38) \qquad \Lambda(A,\vec{h}) = A \int_0^T \dot{\vec{\Psi}}^T C(\vec{h}) \dot{\vec{\Psi}} \, dt / \int_0^T \vec{\Psi}^T \vec{f}(A,\vec{\Psi},\dot{\vec{\Psi}}) \, dt$$

and the sensitivities are

$$(3.39) \qquad \Lambda_{,i}(A,\vec{h}) = A \int_0^T \dot{\vec{\Psi}}^T \underset{\sim}{C}_{,i} \vec{\Psi} \, dt / \int_0^T \vec{\Psi}^T \vec{f}(A,\vec{\Psi},\dot{\vec{\Psi}}) \, dt$$

The conclusion is that damping changes are the main quantities to be varied in order to remove steady-state A-mode instabilities.

No application of a procedure equivalent to the method of imposed disturbances has been found in the literature. Numerical studies are shown in Chapter 4 which indicate that the assumptions of Section 3.2.4 are not too severe. The method fills the important technological gap that exists between methods that are used for nonlinear analysis and those that are used for optimization.

3.2.6 The Static Solution Subcase

An important subcase can be found when the nonlinear external forces have the form

$$(3.40) \qquad \vec{f}(\vec{X},\dot{\vec{X}}) = \vec{f}_1(\vec{X}) + \vec{f}_2(\vec{X},\dot{\vec{X}})$$

Let $\vec{\Psi} = \vec{\Psi}_1$ be an unknown constant vector. When this is substituted into Equation (3.25) together with Equation (3.40), the following static force balance equations are obtained:

$$(3.41) \quad \vec{F} \equiv \Lambda \vec{f}_1(A, \vec{\Psi}_1) - [\underset{\sim}{K}(\vec{h}) - p\underset{\sim}{G}(\vec{h})]\ \vec{\Psi}_1 = \vec{0}$$

For some given $\Lambda = \Lambda_1$ and $A = A_1 \neq 0$, a solution of these nonlinear algebraic equations gives the static equilibrium solution $\vec{\Psi}_1$. Thus the entire $\Lambda(A,\vec{h})$ can be generated by solving Equation (3.41) in a parametric manner. Since stiffness terms appear in Equation (3.41), it can be concluded that changing these terms is important in removing static A-mode instabilities.

3.2.7 Use of the Method

In the next chapter a series of numerical examples are presented which show that the steady-state and static $\Lambda(A)$ curves computed by the method of imposed disturbances agree quite well with numerical integration. The method of imposed disturbances is particularly useful for aerodynamically nonlinear flutter and divergence calculations. In these cases, explicit forms for $\vec{f}$ and $\vec{f}_1$ are not always known, but may be evaluated instead by numerically solving some complex flow equation. By imposing a steady-state disturbance on the wing panel, the calculation of the W^{NC} involves only integrations and matrix multiplications. For flutter calculations, no interaction with the structural

part of the equations is necessary if $\vec{\Psi}$ is properly selected. The aerodynamic calculations are performed using $\vec{\Psi}$ to determine the imposed time dependent flow boundary conditions. The next chapter shows that good results can be obtained when $\vec{\Psi}$ is computed by just solving the linearized problem.

The procedure for flutter calculation is thus to solve either a low amplitude nonlinear problem, or, if possible, to solve a fully linearized problem. Then this solution is used as an imposed disturbance as input to a series of flow calculations. Each flow calculation involves a different scale factor, A, on the mode $\vec{\Psi}$. The approximate flutter solution is at that amplitude which causes the net nonconservative work to vanish. The method of imposed disturbances is proposed as an analysis tool which is complementary to time history flutter solutions. It can also give a first order estimate of the sensitivity of the system to various design changes.

SECTION IV

NUMERICAL RESULTS

In this chapter the method of imposed disturbances is applied to a series of nonlinear problems. The first section below describes the application of the method to several widely studied nonlinear equations. Comparisons are made with various numerical integration methods. Nonlinear flutter and divergence calculations are then studied which use the transonic aerodynamic code, LTRAN2, to compute the air loadings. The chapter is concluded with a follower load problem and a hypersonic panel flutter problem to demonstrate the applicability of the method to multiple degree-of-freedom systems.

4.1 NONLINEAR OSCILLATOR STUDIES

Two widely studied nonlinear differential equations are the van der Pol equation and the Lewis servomechanism equation. Accurate numerical solutions are given, for example, in the dissertation by Knese.[90] In what follows, the method of imposed disturbances is shown to give trend results which agree well with parametric studies performed using numerical integration.

4.1.1 The van der Pol Equation

The usual form of the van der Pol equation does not contain a strong linear damping term. It will, however, be included here to demonstrate the applicability of the method of imposed disturbances to such problems. Thus including the damping term the equation is

$$\ddot{x} + 2\zeta\omega_1\dot{x} + \omega_1^2 x = \mu(1-x^2)\dot{x} \tag{4.1}$$

The notation is the same as that used in Section 3.1.

An imposed disturbance is given to the system of the form

$$X = A\Psi \tag{4.2}$$

where

$$\Psi = \sin\Omega t \tag{4.3}$$

This is used in the total nonconservative work expression,

$$W^{NC} = \int_0^T \left[\mu(1-X^2)\dot{X} - 2\zeta\omega_1\dot{X}\right]\dot{X}\, dt \tag{4.4}$$

which can easily be computed as

$$W^{NC} = (\pi\mu\Omega A^2/4)\ [(8\omega_1/\mu)(\mu/2\omega_1-\zeta)-A^2] \tag{4.5}$$

It is observed that if $\mu>0$ and $\zeta<\mu/2\omega_1$, then $W^{NC}<0$ whenever $A^2>(8\omega_1/\mu)(\mu/2\omega_1-\zeta)$; i.e., the motion is stable. If the same condition holds on ζ, but A^2 is less than $(8\omega_1/\mu)(\mu/2\omega_1-\zeta)$ then the motion is unstable. The

optimum value of ζ which will preclude instability at any amplitude is

$$\zeta = \mu/2\omega_1 \qquad (\mu>0) \tag{4.6}$$

and in which case the motion is always of decreasing amplitude.

Figure 6 shows phase plane results for the damped van der Pol equation (NDET=1) using the Kutta-Merson numerical integration method (NAM=1). The step size (H) is 0.05 with 500 steps (NSTEP) taken. The initial displacement (X1(0)) is 0.01 and the initial velocity (X2(0)) is zero. Value of μ(XMU), ζ(ZETA), and Ω_1(OMEGA) are 1.0, 0.0, and 1.0, respectively. In this case, Equation (4.5) predicts $W^{NC}>0$ until an amplitude of 2.0 is reached. As shown in Figure 6, numerical integration indicates that the displacement increases initially and is limited to about 2.0 in absolute value for large time.

In Figure 7, an initial displacement amplitude of 3.3 is given and the motion decreases and again reaches a limiting amplitude of 2.0. Such behavior is consistent with the observation that $W^{NC}<0$ for this condition.

To further check the validity of Equation (4.5), assume that it is required that sufficient damping be added to the system which will make it stable for all (μ,A) in the range $-0.2<\mu<0$ and $0<A<\sqrt{6}$. Solving Equation (4.5) for

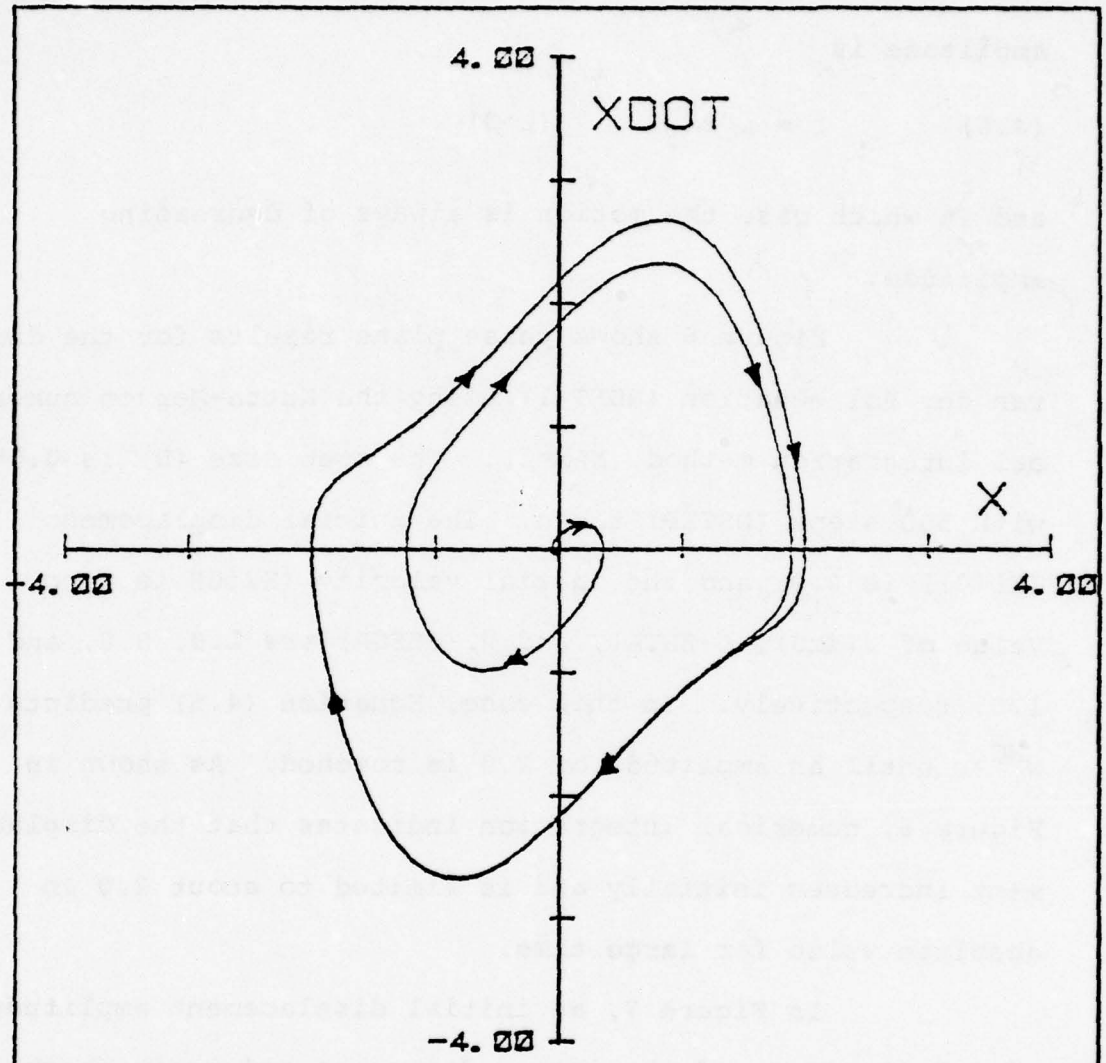

NDET = 1 NAM = 1 H = .05
IC'S X1(0).X2(0) = .01 0.00
XMU. ZETA. OMEGA = 1.00 0.0000 1.00
CPTIME = .46 NSTEP = 500

Figure 6. Stable Limit Cycle Behavior of van der Pol Equation (Small Disturbance).

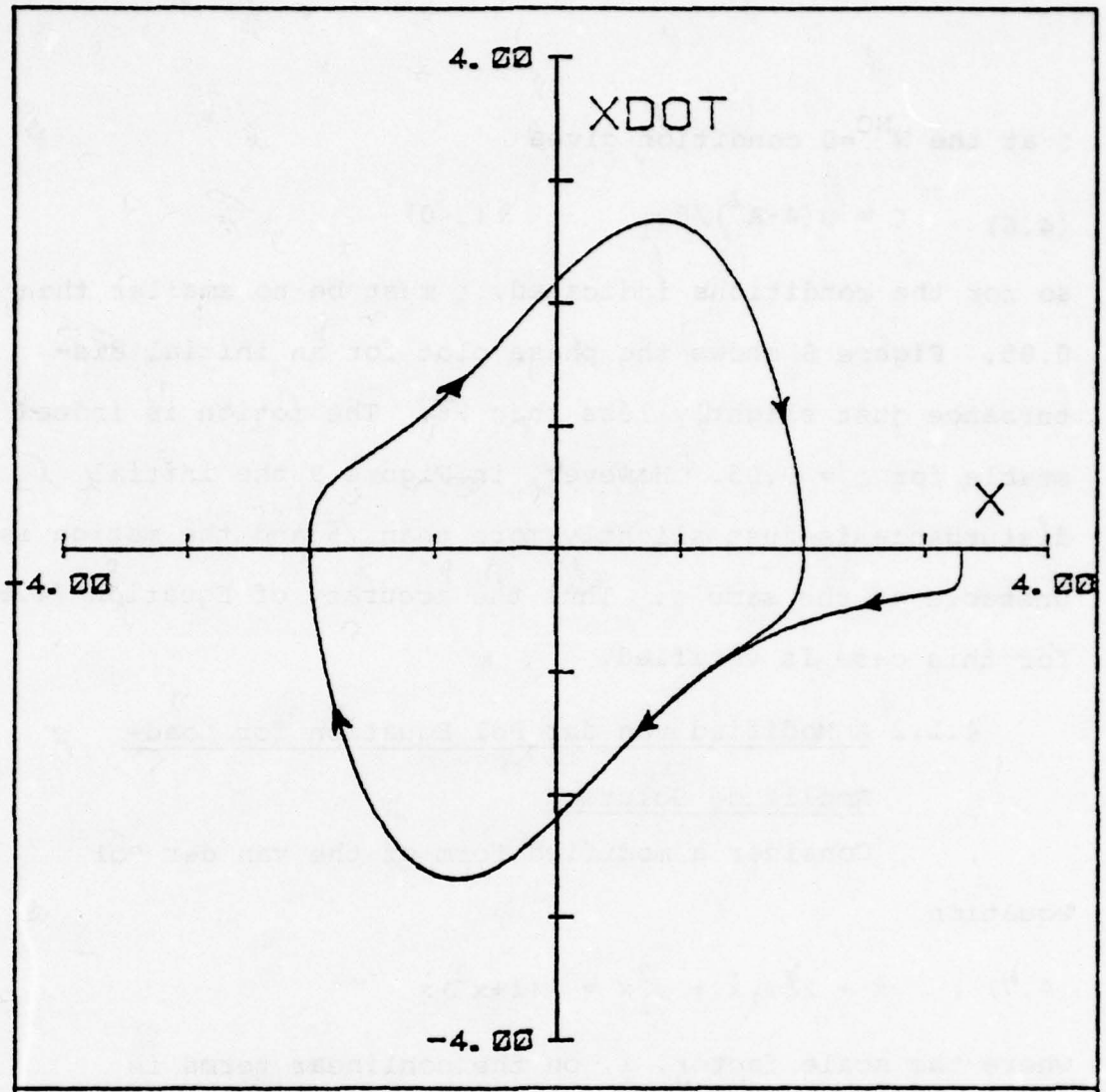

NDET = 1 NAM = 1 H = .05

IC'S X1(0).X2(0) = 3.30 0.00

XMU.ZETA.OMEGA = 1.00 0.0000 1.00

CPTIME = .47 NSTEP = 500

Figure 7. Stable Limit Cycle Behavior of van der Pol Equation (Large Disturbance).

ζ at the $W^{NC}=0$ condition gives

$$\zeta = \mu(4-A^2)/8\omega_1 \qquad (\mu<0) \tag{4.6}$$

so for the conditions indicated, ζ must be no smaller than 0.05. Figure 8 shows the phase plot for an initial disturbance just slightly less than $\sqrt{6}$. The motion is indeed stable for $\zeta = 0.05$. However, in Figure 9 the initial disturbance is just slightly more than $\sqrt{6}$ and the motion is unstable at the same ζ. Thus the accuracy of Equation (4.6) for this case is verified.

4.1.2 A Modified van der Pol Equation for Load-Amplitude Solution

Consider a modified form of the van der Pol equation

$$\ddot{x} + 2\zeta\omega_1\dot{x} + \omega_1^2 x = \lambda(1+x^2)\dot{x} \tag{4.7}$$

where the scale factor, λ, on the nonlinear terms is considered to be a dynamic loading parameter.

For vanishing nonlinearity, the critical load is

$$\lambda = \Lambda_o = 2\zeta\omega_1 \tag{4.8}$$

and a solution is

$$X_o = A_o\Psi_o \tag{4.9}$$

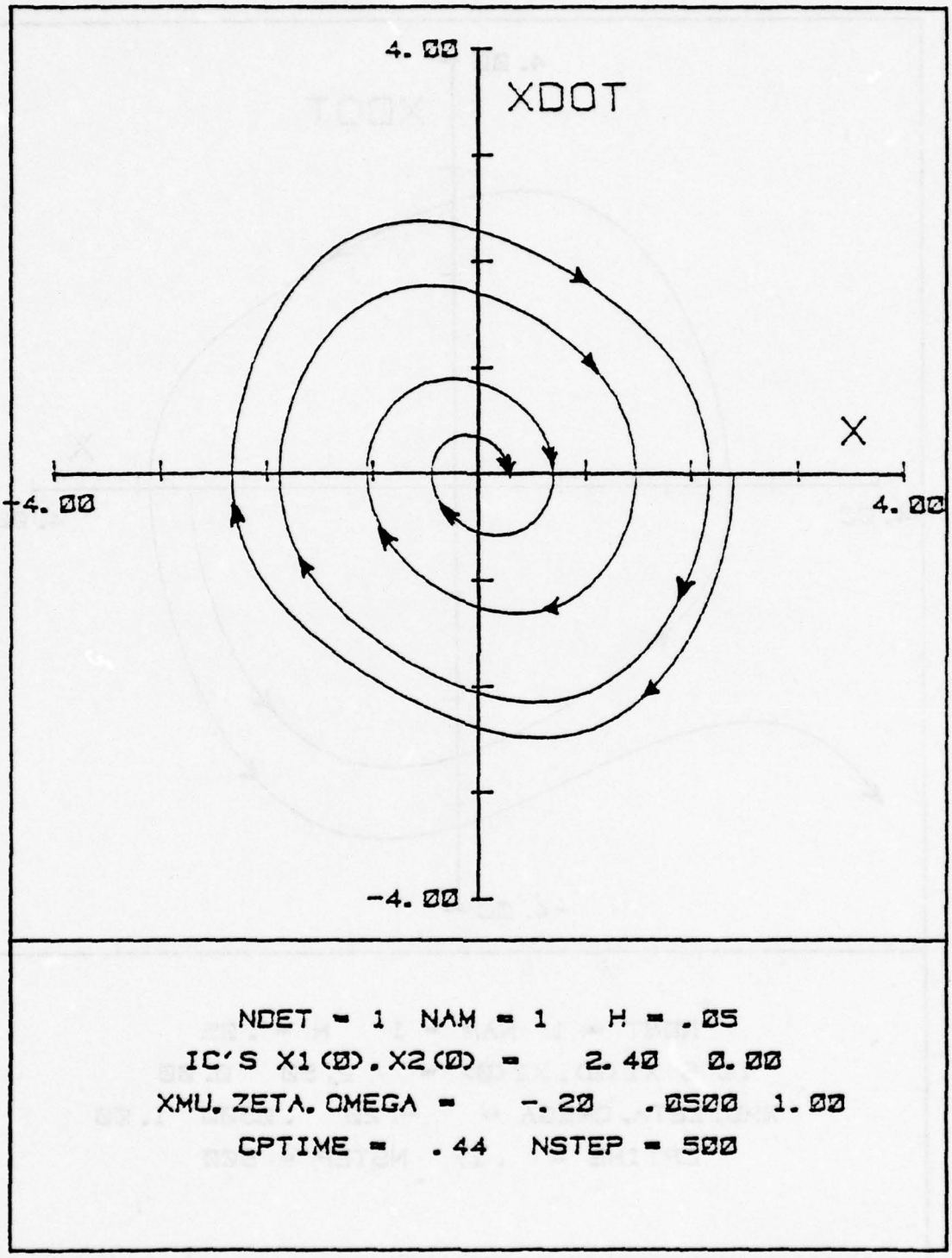

Figure 8. Unstable Limit Cycle Behavior of Damped van der Pol Equation (Small Disturbance).

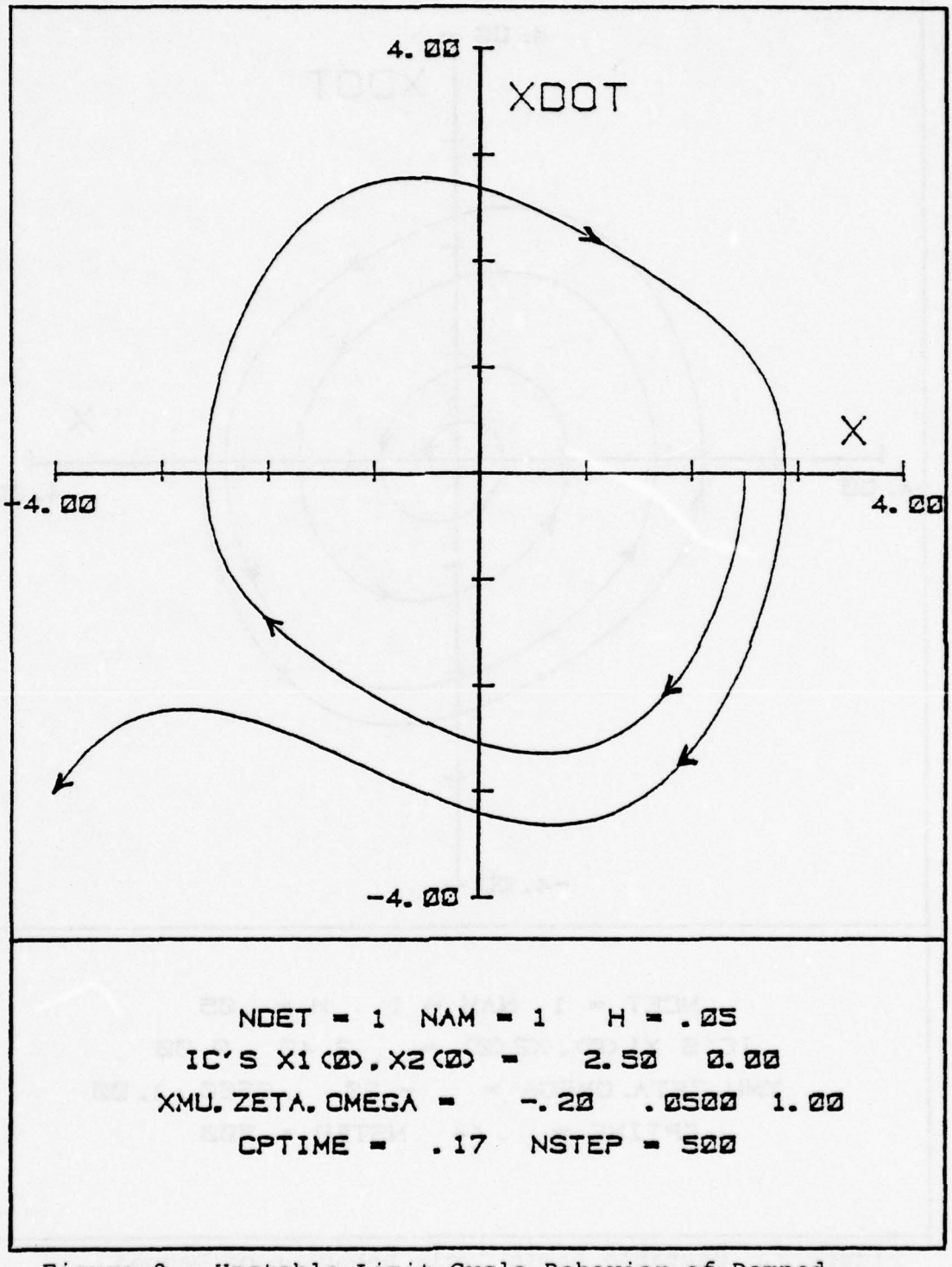

Figure 9. Unstable Limit Cycle Behavior of Damped van der Pol Equation (Large Disturbance).

where

$$(4.10) \qquad \Psi_o = \sin\omega_1 t$$

Equation (4.9) is the zero amplitude solution of Equation (4.7), and hence an imposed disturbance of the form of Equation (4.2) can be used to compute the total nonconservative work. This leads to

$$(4.11) \qquad W^{NC} = (A^2\pi/\Omega)\ [\lambda(1+A^2/4) - 2\zeta\omega_1]$$

At the condition of neutral stability, $W^{NC} = 0$, an appropriate relation between critical load and amplitude is

$$(4.12) \qquad \Lambda = 2\zeta\omega_1/(1+A^2/4)$$

Alternatively, A in terms of Λ is

$$(4.13) \qquad A = 2\sqrt{(2\zeta\omega_1-\Lambda)/\Lambda}$$

Curves of $W^{NC} = 0$ are shown on Figure 10 for various values of ζ. Time history integration results are shown to verify the accuracy of Equation (4.12). All "K-M" points are the result of Kutta-Merson numerical integration using $x(0) = A$ and $\dot{x}(0) = 0$ as the initial condition. Equation (4.13) predicts the shape of the load-amplitude curve quite accurately and gives the proper trend as ζ is increased.

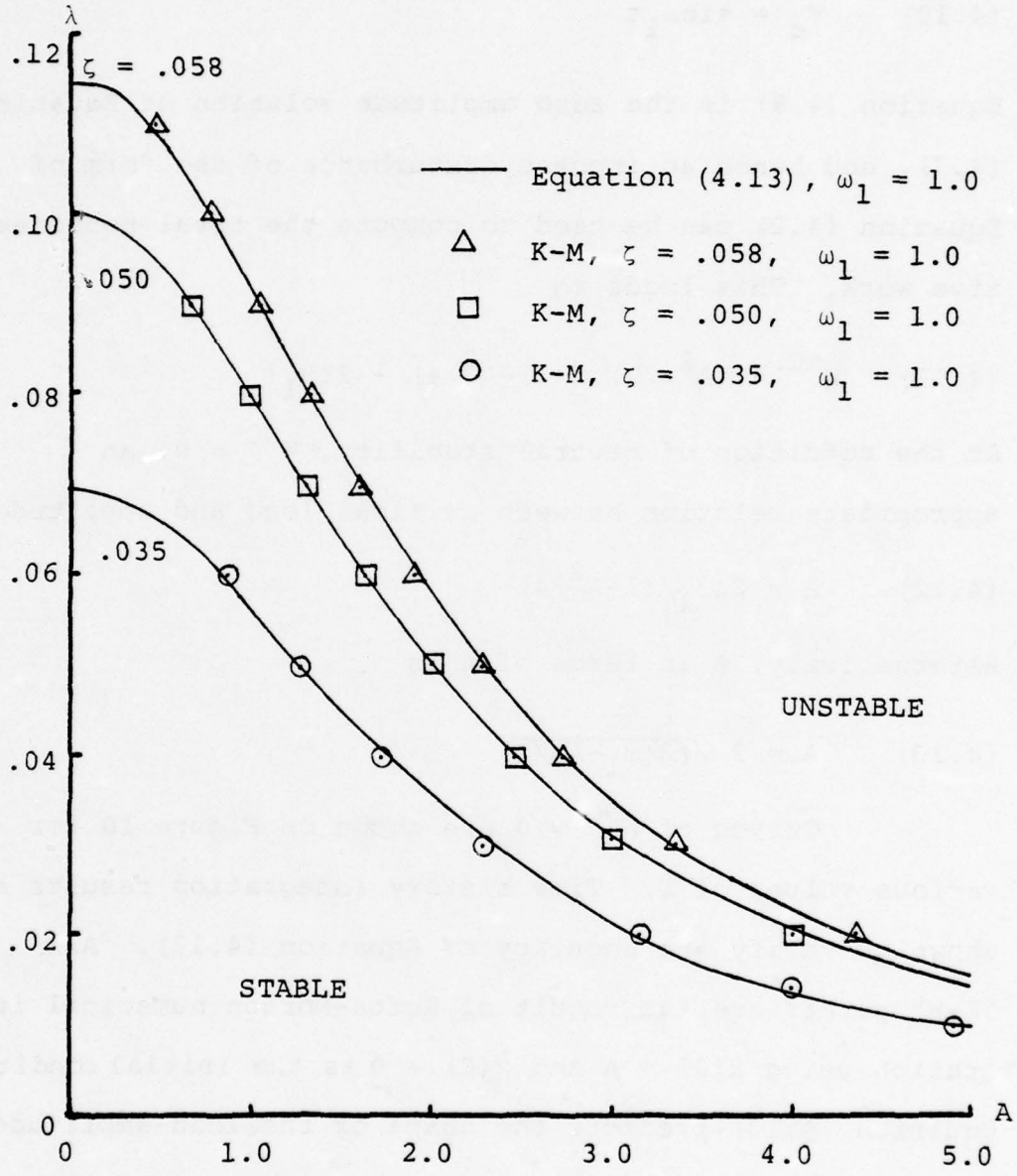

Figure 10. Load-Amplitude Relationships for Modified van der Pol Equation.

4.1.3 The Lewis Servomechanism Equation

In control theory, a nonlinear equation referred to as the Lewis Servomechanism equation is encountered.[90] For the purposes herein, it is useful to write it in the form

$$\ddot{x} + 2\zeta\omega_1\dot{x} + \omega_1^2 x = \lambda(|x| - 1)\dot{x} \tag{4.14}$$

Again using Equation (4.2) as the initial disturbance, the total nonconservative work is

$$W^{NC} = (A^2\Omega\Lambda/2)\ [4A/3-\pi(1+2\zeta\omega_1/\Lambda] \tag{4.15}$$

For small A, W^{NC} is negative and for large A it is positive. Hence the existence of an unstable limit cycle is indicated. This behavior is verified by Kutta-Merson numerical integration of the equation as shown in Figures 11 and 12. In Figure 11, the phase plane plot for the case $\lambda = 1.0$, $\zeta = 0$, $\omega_1 = 1.41$ is shown where a pure initial velocity condition of 3.30 is given the system. These conditions produce stable motion of decreasing amplitude; at a velocity condition of 3.40 the system is unstable as shown in Figure 12. Only the initial velocity condition is different between these two plots.

At the neutrally stable condition Equation (4.14) can be solved for A in terms of Λ, ω_1, and ζ to get

$$A = (3\pi/4)(1+2\zeta\omega_1/\Lambda) \tag{4.16}$$

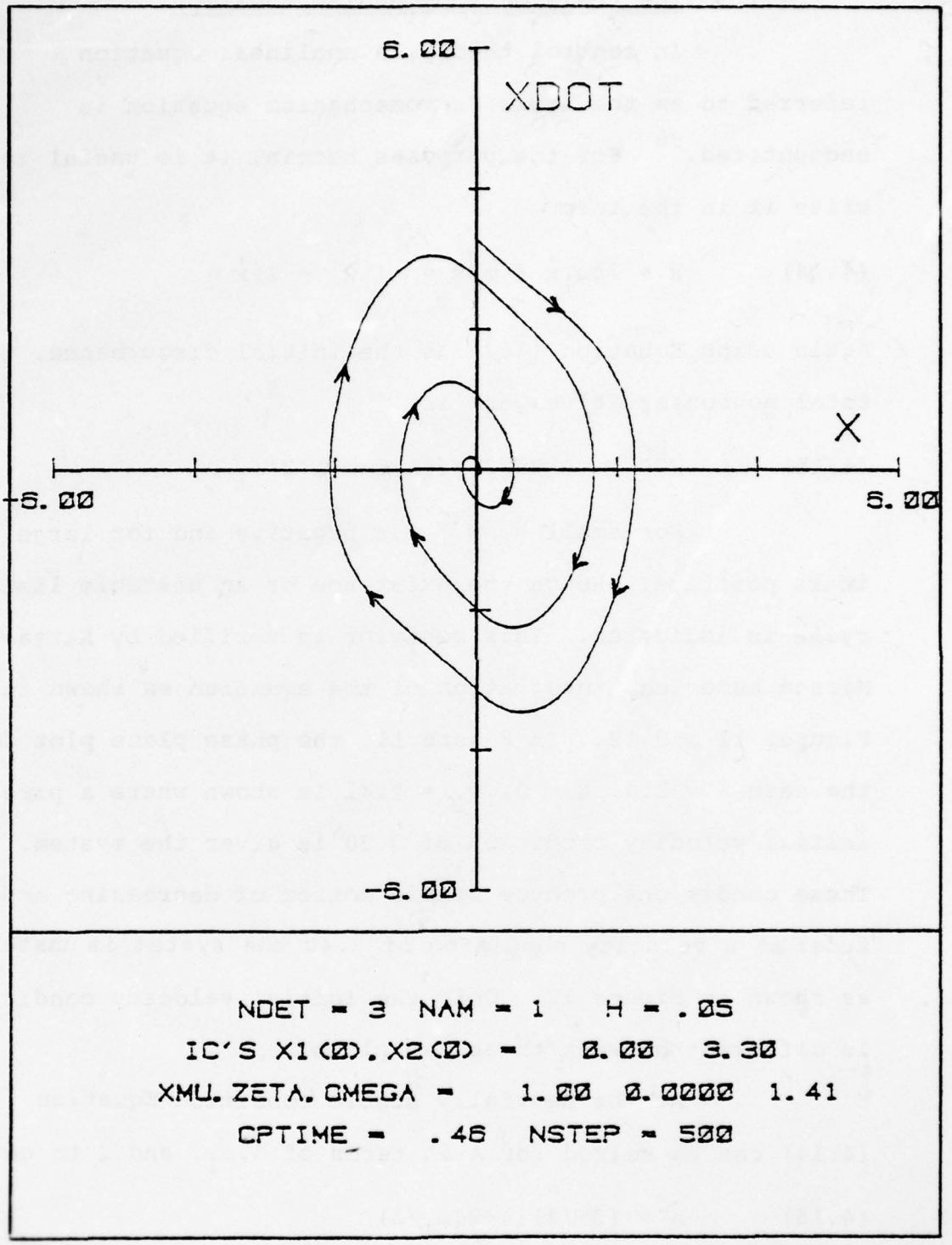

Figure 11. Unstable Limit Cycle Behavior of Lewis Servomechanism Equation (Small Disturbance).

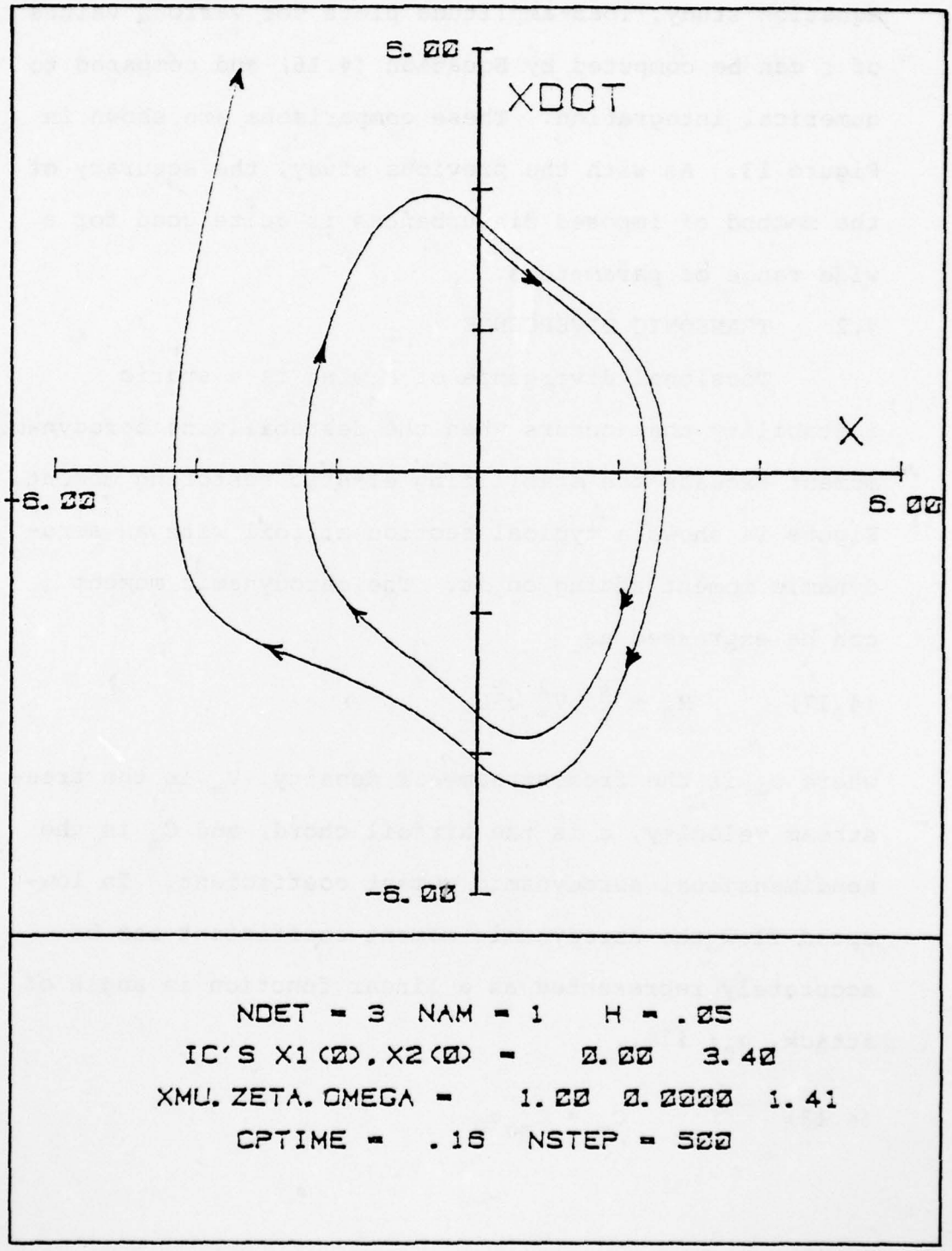

Figure 12. Unstable Limit Cycle Behavior of Lewis Servomechanism Equation (Large Disturbance).

In a manner identical with the modified van der Pol equation study, load-amplitude plots for various values of ζ can be computed by Equation (4.16) and compared to numerical integration. These comparisons are shown in Figure 13. As with the previous study, the accuracy of the method of imposed disturbances is quite good for a wide range of parameters.

4.2 TRANSONIC DIVERGENCE

Torsional divergence of a wing is a static instability that occurs when the destabilizing aerodynamic moment exceeds the stabilizing elastic restoring moment. Figure 14 shows a typical section airfoil with an aerodynamic moment acting on it. The aerodynamic moment can be expressed as

$$M_0 = \frac{1}{2}\rho_\infty V_\infty^2 \, c^2 C_m \tag{4.17}$$

where ρ_∞ is the free-stream air density, V_∞ is the free-stream velocity, c is the airfoil chord, and C_m is the nondimensional aerodynamic moment coefficient. In low-speed flow the aerodynamic moment coefficient can be accurately represented as a linear function in angle of attack, α_0; i.e.,

$$C_m = C_{m\alpha}\alpha_0 \tag{4.18}$$

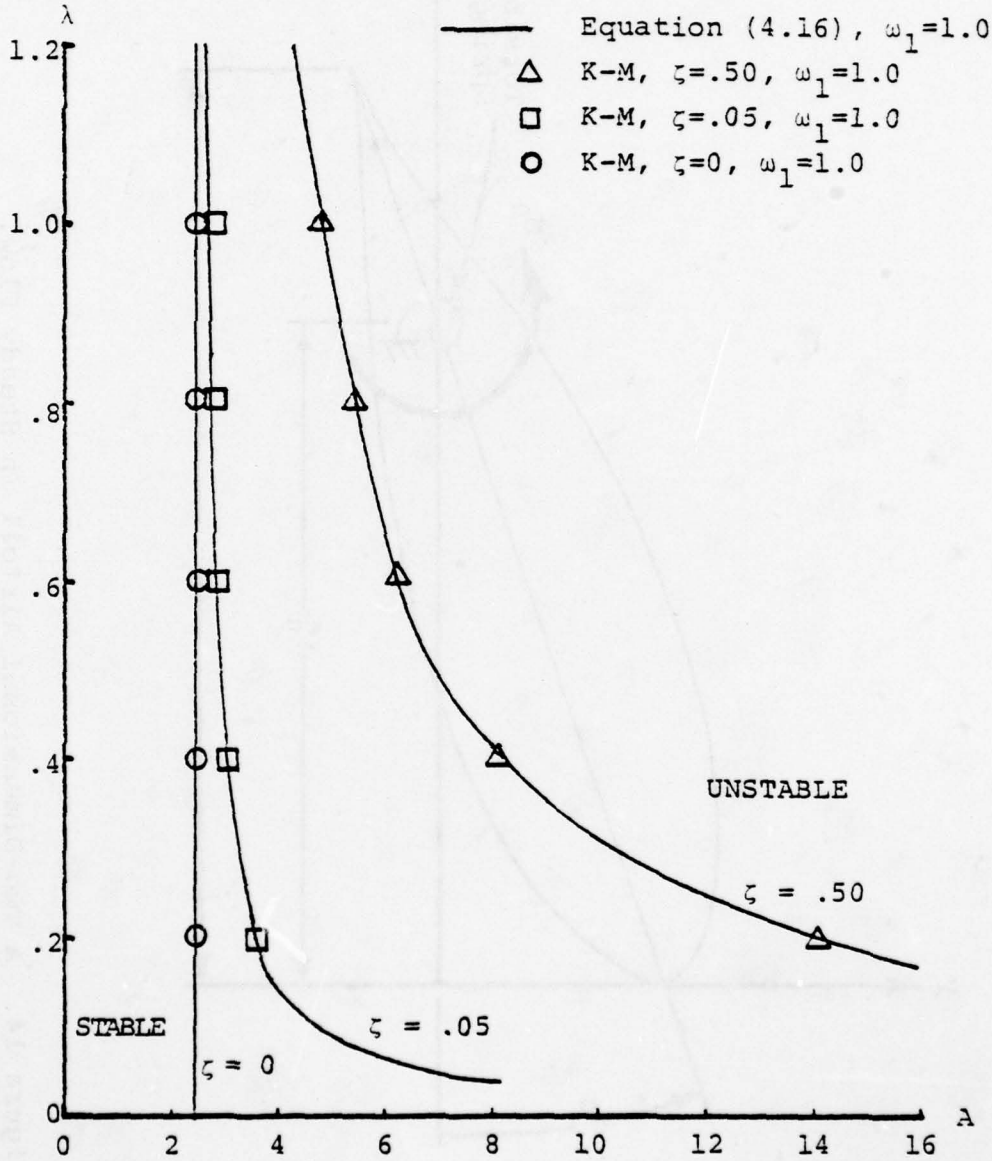

Figure 13. Load-Amplitude Relationship for Lewis Servomechanism Equation.

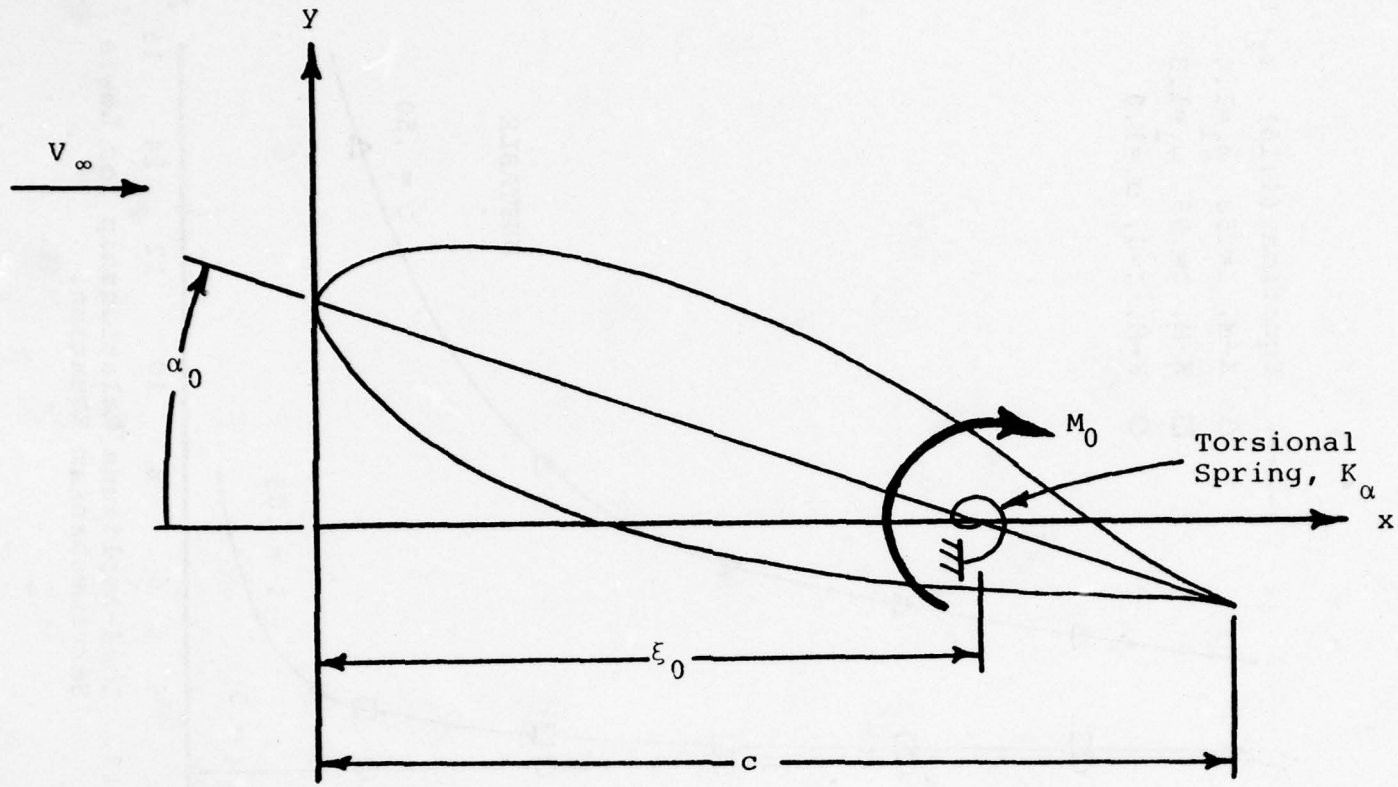

Figure 14. A Two-Dimensional Airfoil in Steady Flow.

If α_0 ia too large or if the flow is transonic, this linear relation may no longer hold over the range of α_0 of interest.

The onset of divergence occurs when

(4.19) $$M_J = M_e$$

where M_e is the elastic restoring moment which can be expressed as

(4.20) $$M_e = K_\alpha \alpha_0$$

It is assumed that the torsional spring is linear; hence the spring constant, K_α, is not a function of α_0. Equation (4.19) can be rewritten as

(4.21) $$C_K = C_m$$

where C_K is the nondimensional spring coefficient

(4.22) $$C_K = K_\alpha \alpha_0 / \tfrac{1}{2} \rho_\infty V_\infty^2 c^2$$

The LTRAN2 transonic aerodynamic code was used to investigate the case when $C_{m\alpha}$ is a function of α_0. Steady pressure coefficient distributions about a NACA 64A006 airfoil were calculated at a free stream Mach number of 0.88. A finite difference grid containing 113 chordwise points and 97 vertical points was used to solve the flow problem.

Table 1 shows the LTRAN2 lift coefficients and centers of pressure that were computed for various angles of attack. The lift coefficient is defined as

$$C_L = \int_0^c (P_L - P_u)\, dx / \tfrac{1}{2}\rho_\infty V_\infty^2 c \tag{4.23}$$

where $P_L = P_L(x)$ and $P_u = P_u(x)$ are the pressures on the lower and upper surface, respectively, of the airfoil. The moment coefficient can be computed from

$$C_m = (\xi_0 - \xi_c)\, C_L \tag{4.24}$$

where ξ_0 and ξ_c are the locations of the spring pitch axis and center of pressure, respectively, expressed as a fraction of the chord.

Figures 15 through 21 show the steady pressure coefficient distribution, C_p, on the upper and lower surfaces for angles of attack between zero and one-half degrees. The critical pressure coefficient C_p^* is also shown.

If the spring pitch axis is assumed to be located at .586, it is observed that at about $\alpha_0 = .25°$ the center of pressure is located at the pitch axis. For smaller angles it is forward of this axis and for larger angles it is to

TABLE 1

LIFT COEFFICIENTS AND CENTERS OF PRESSURE
FOR NACA 64006 AIRFOIL IN STEADY FLOW

MACH NUMBER = .88

α	C_L	ξ_c
.05	.080743	.567475
.10	.160636	.567611
.15	.232955	.576185
.20	.286957	.582854
.25	.325688	.586350
.30	.358254	.589188
.35	.386346	.591300
.40	.408527	.592814
.45	.430277	.593120
.50	.447601	.593464
.75	.501767	.586323
1.00	.533986	.567874
1.50	.578334	.540518

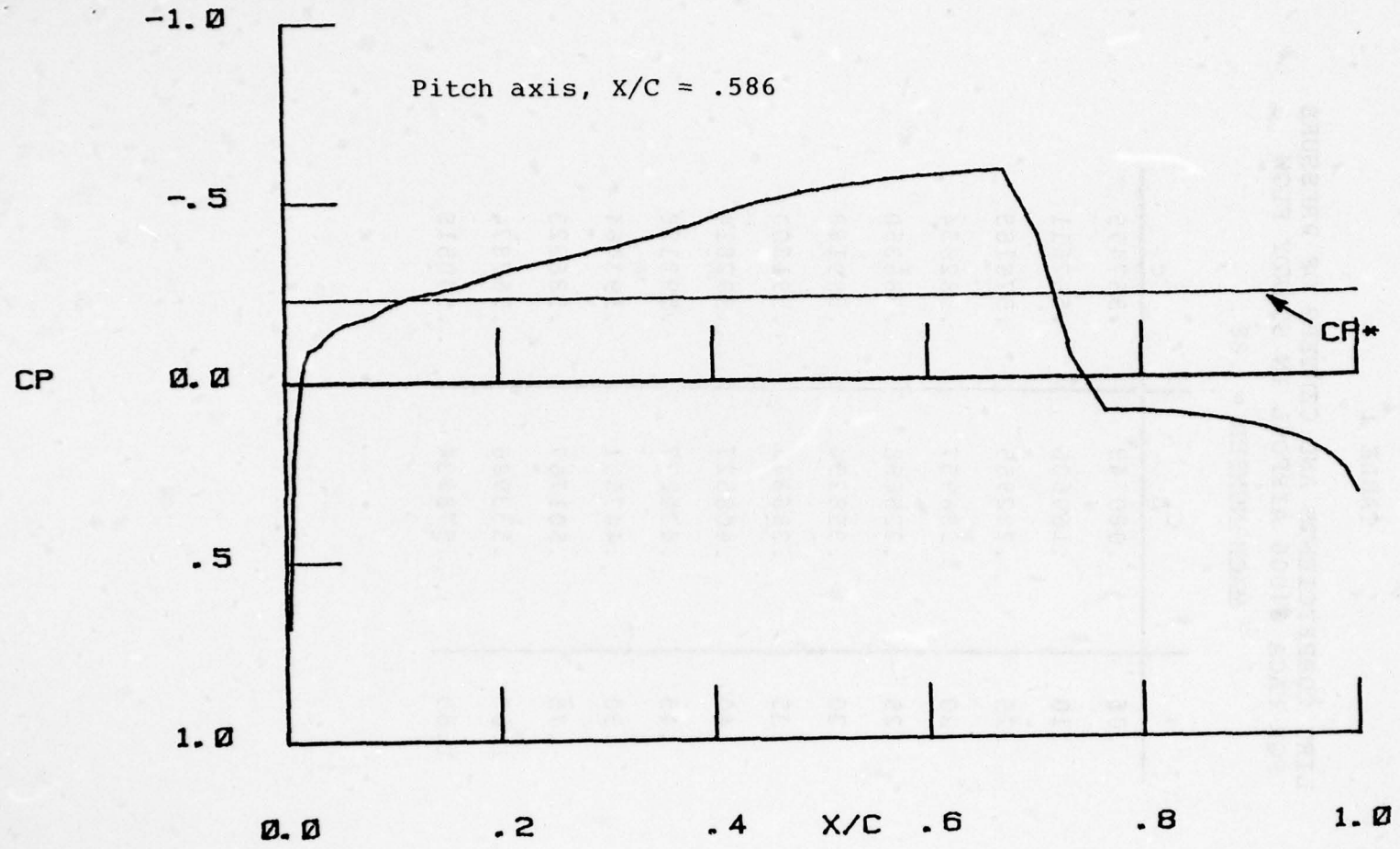

Figure 15. Steady Pressure Coefficient Distribution, 64A006 Airfoil, M_∞ = .88, α_0 = 0.

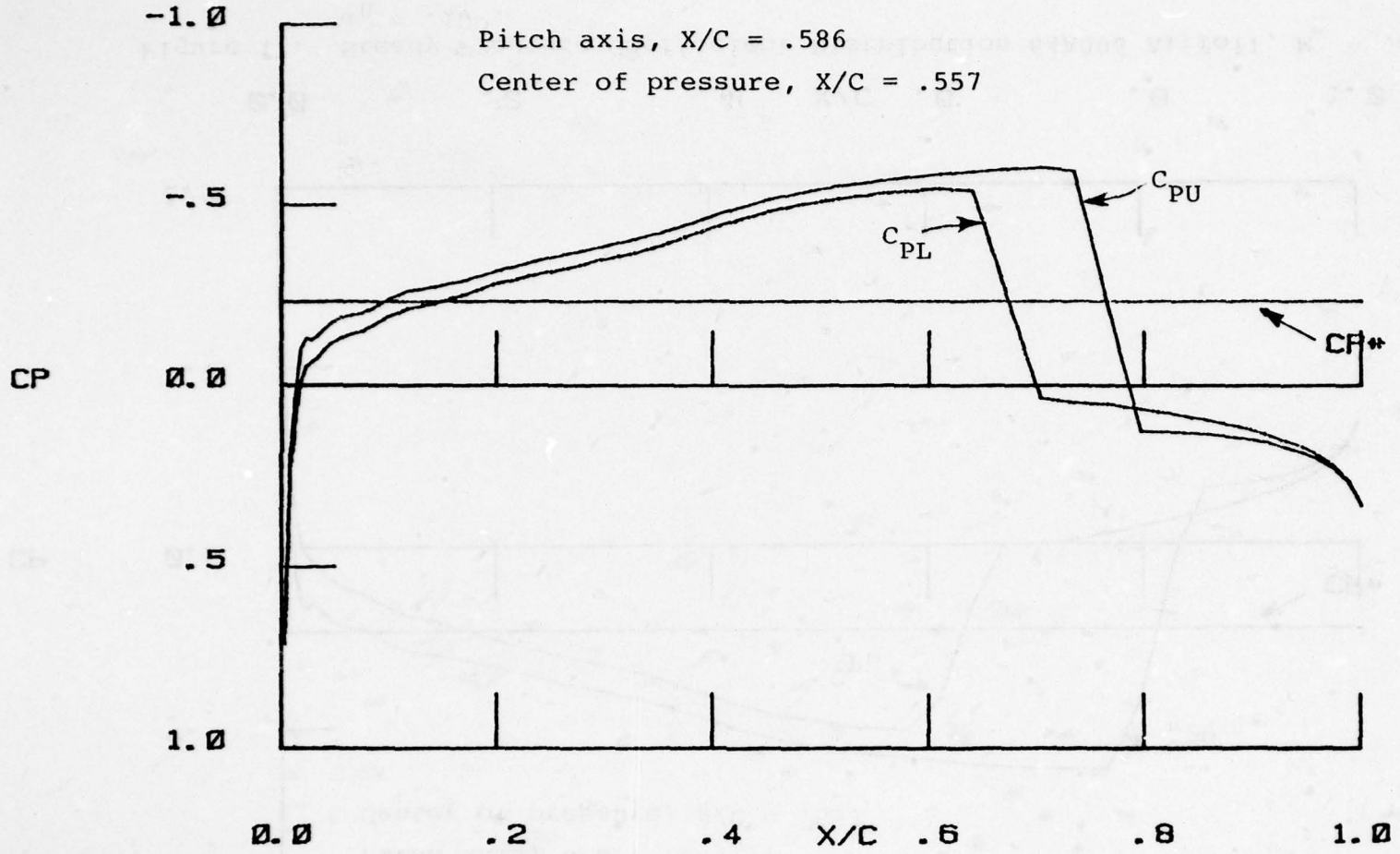

Figure 16. Steady Pressure Coefficient Distribution 64A006 Airfoil, M_∞ = .88, α_0 = .05°.

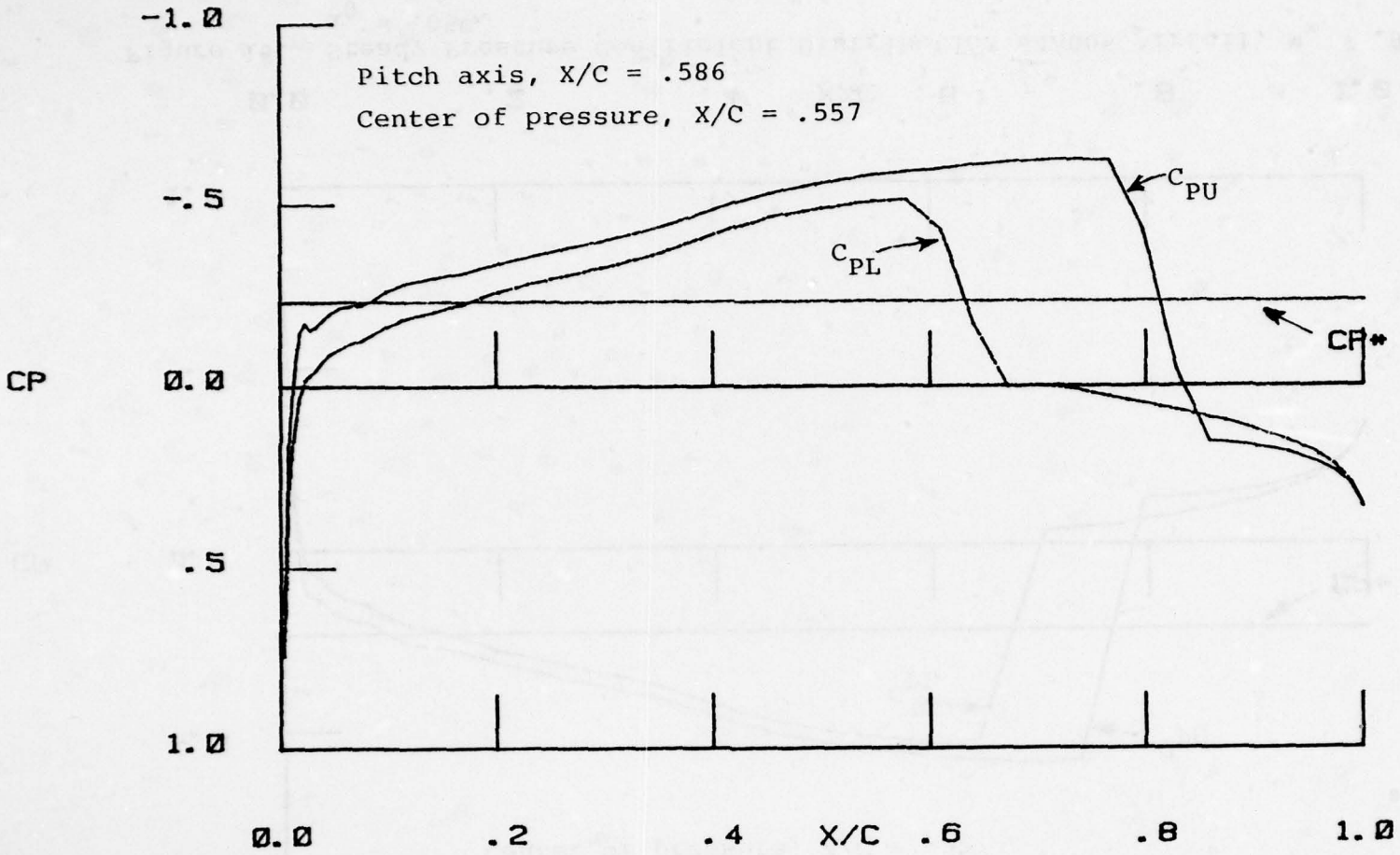

Figure 17. Steady Pressure Coefficient Distribution 64A006 Airfoil, M_∞ = .88, α_0 = .10°.

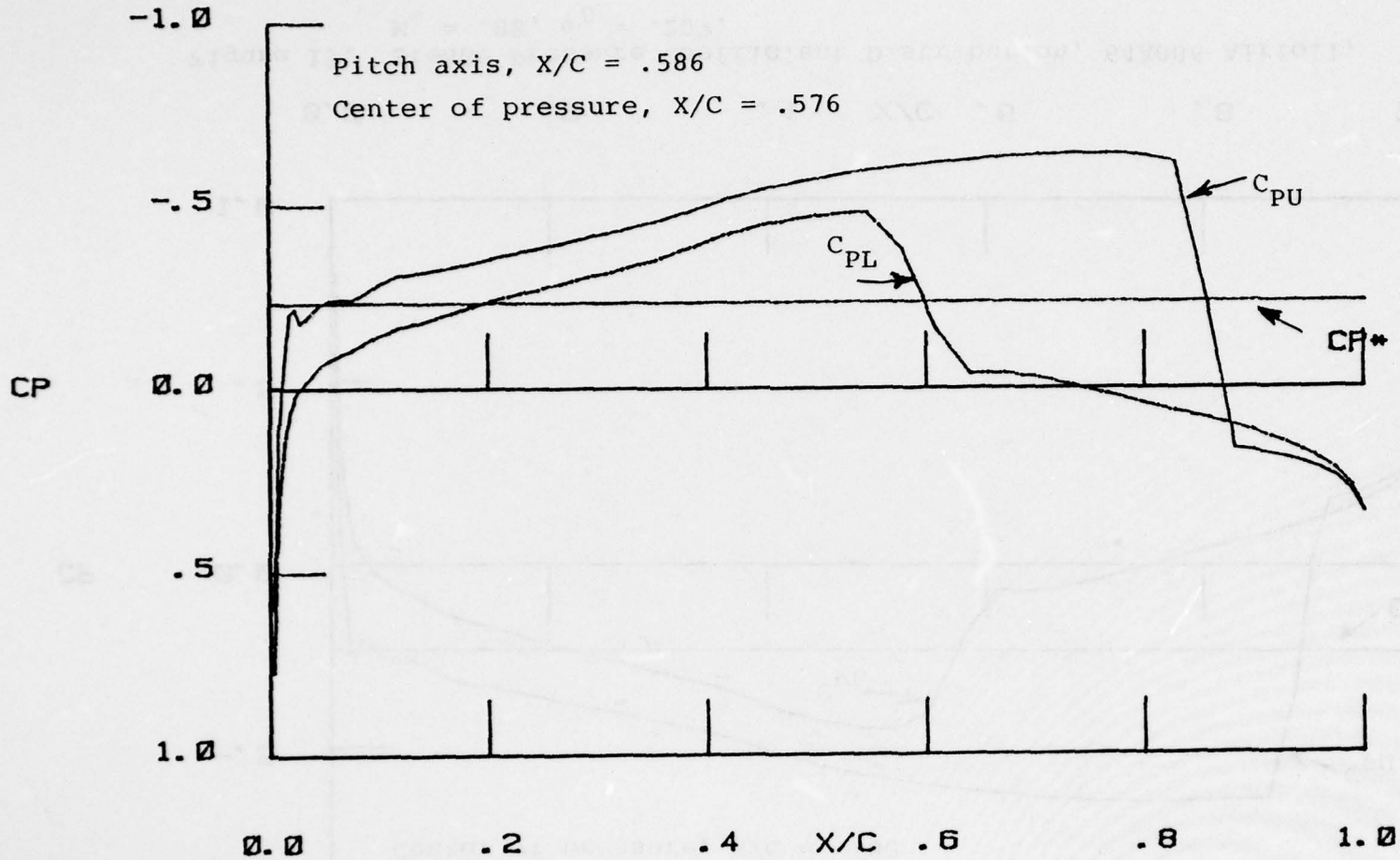

Figure 18. Steady Pressure Coefficient Distribution, 64A006 Airfoil, M_∞ = .88, α_0 = .15°.

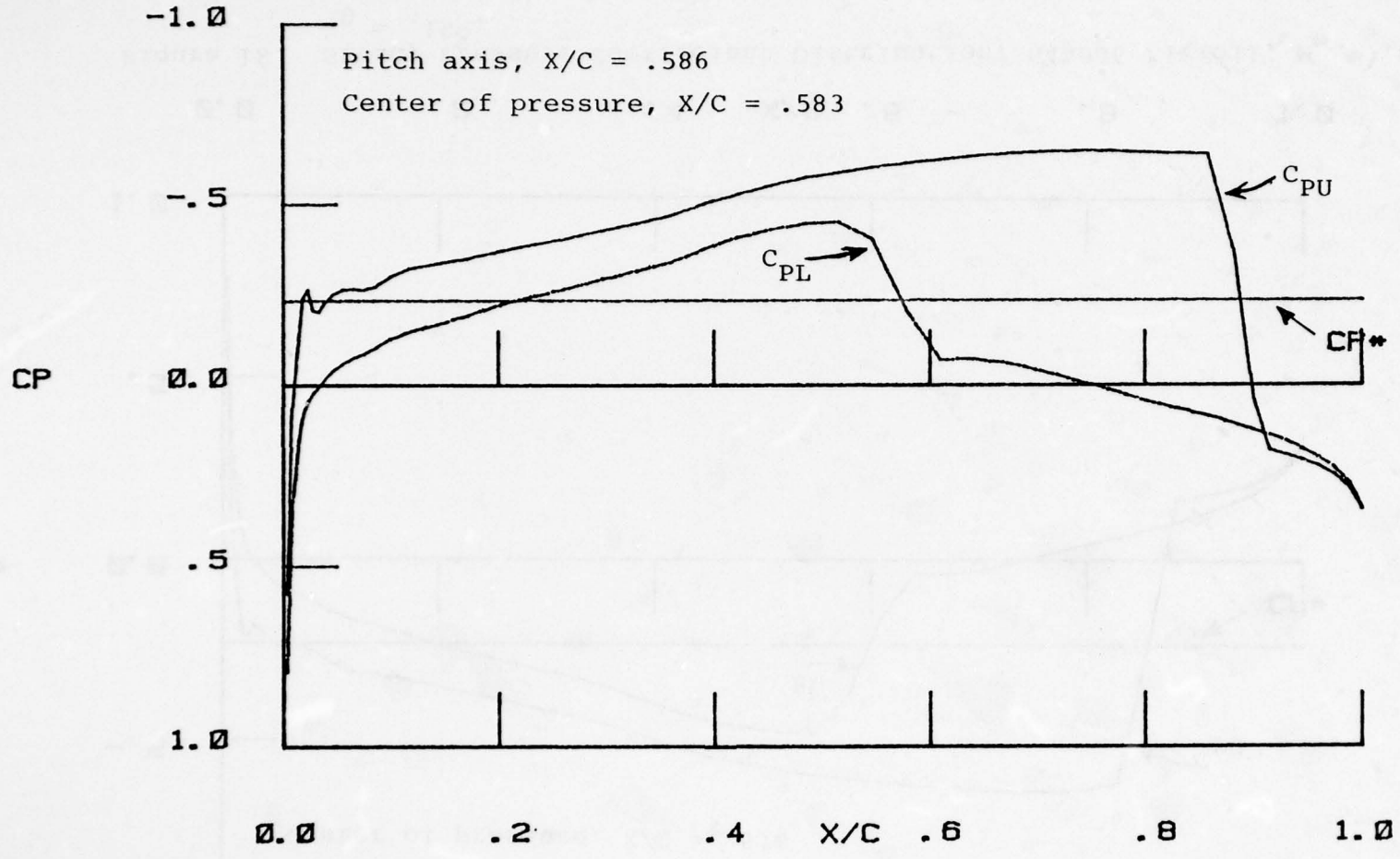

Figure 19. Steady Pressure Coefficient Distribution, 64A006 Airfoil, $M_\infty = .88$, $\alpha_0 = .20^o$.

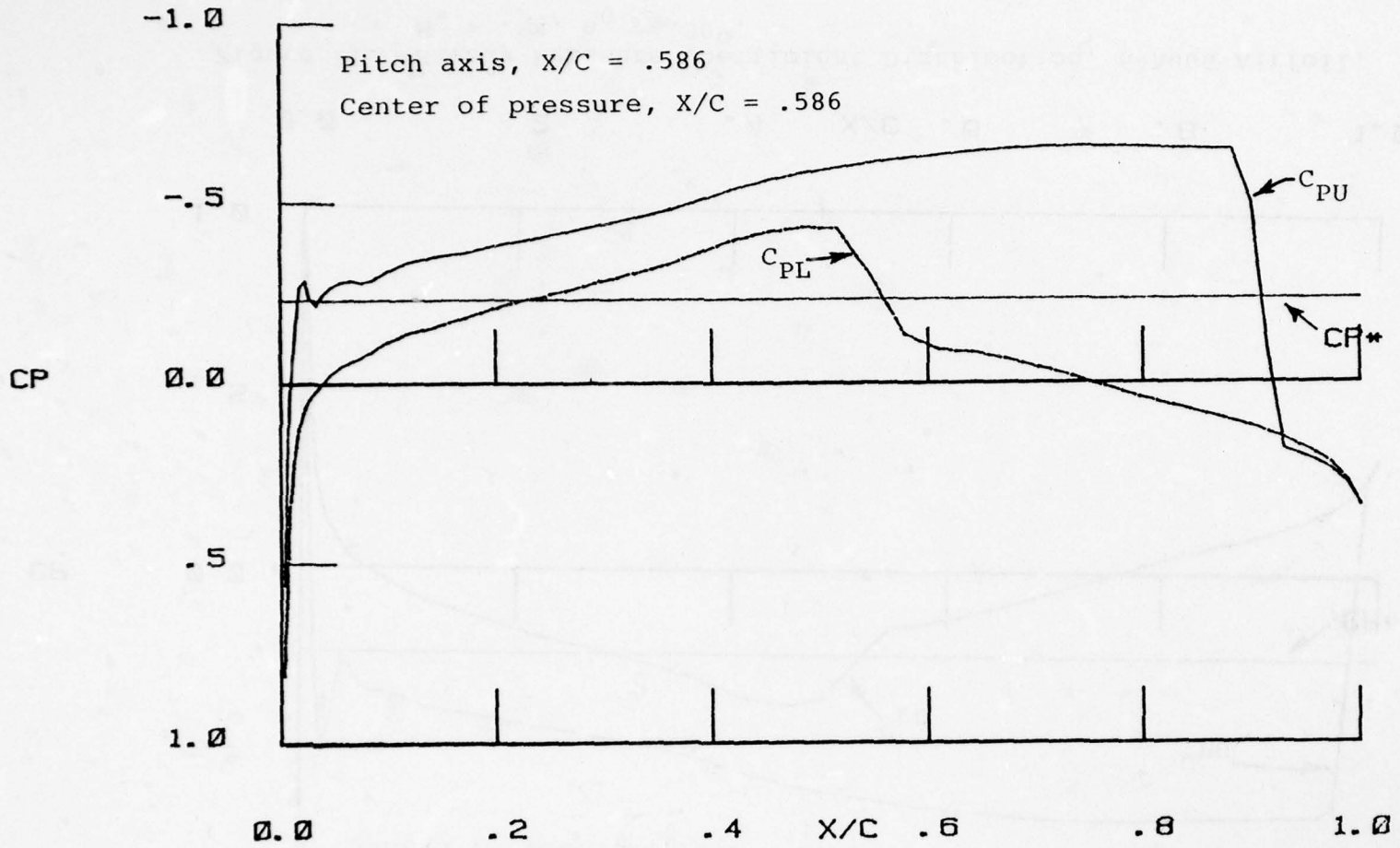

Figure 20. Steady Pressure Coefficient Distribution 64A006 Airfoil, $M_\infty = .88$, $\alpha_0 = .25^o$.

AD-A077 851 DAYTON UNIV OH RESEARCH INST F/G 20/4
DEVELOPMENT OF STABILITY METHODS FOR APPLICATION TO NONLINEAR A--ETC(U)
JUL 79 R F TAYLOR AFOSR-78-3487
UNCLASSIFIED UDR-TR-79-64 AFFDL-TR-79-3114 NL

2 OF 2
AD A
077851

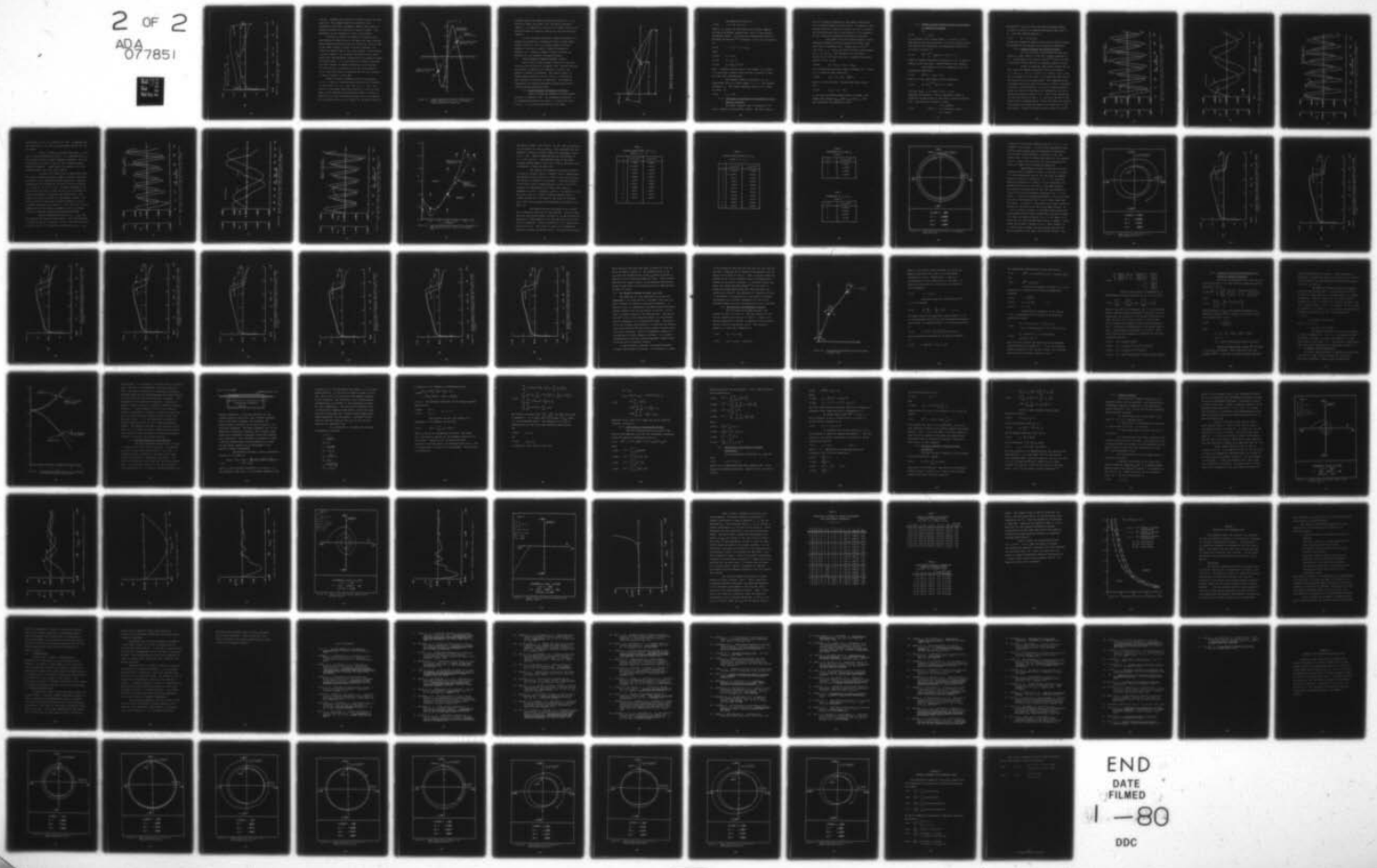

END
DATE FILMED
1-80
DDC

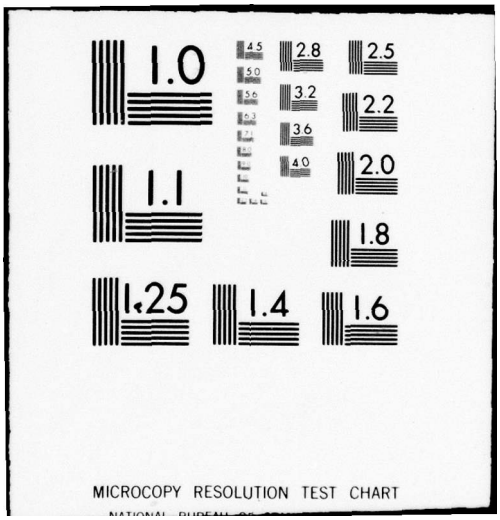
1.0
1.1
1.25
1.4
1.6
1.8
2.0
2.2
2.5
2.8
3.2
3.6
4.0
4.5
5.0
5.6
MICROCOPY RESOLUTION TEST CHART

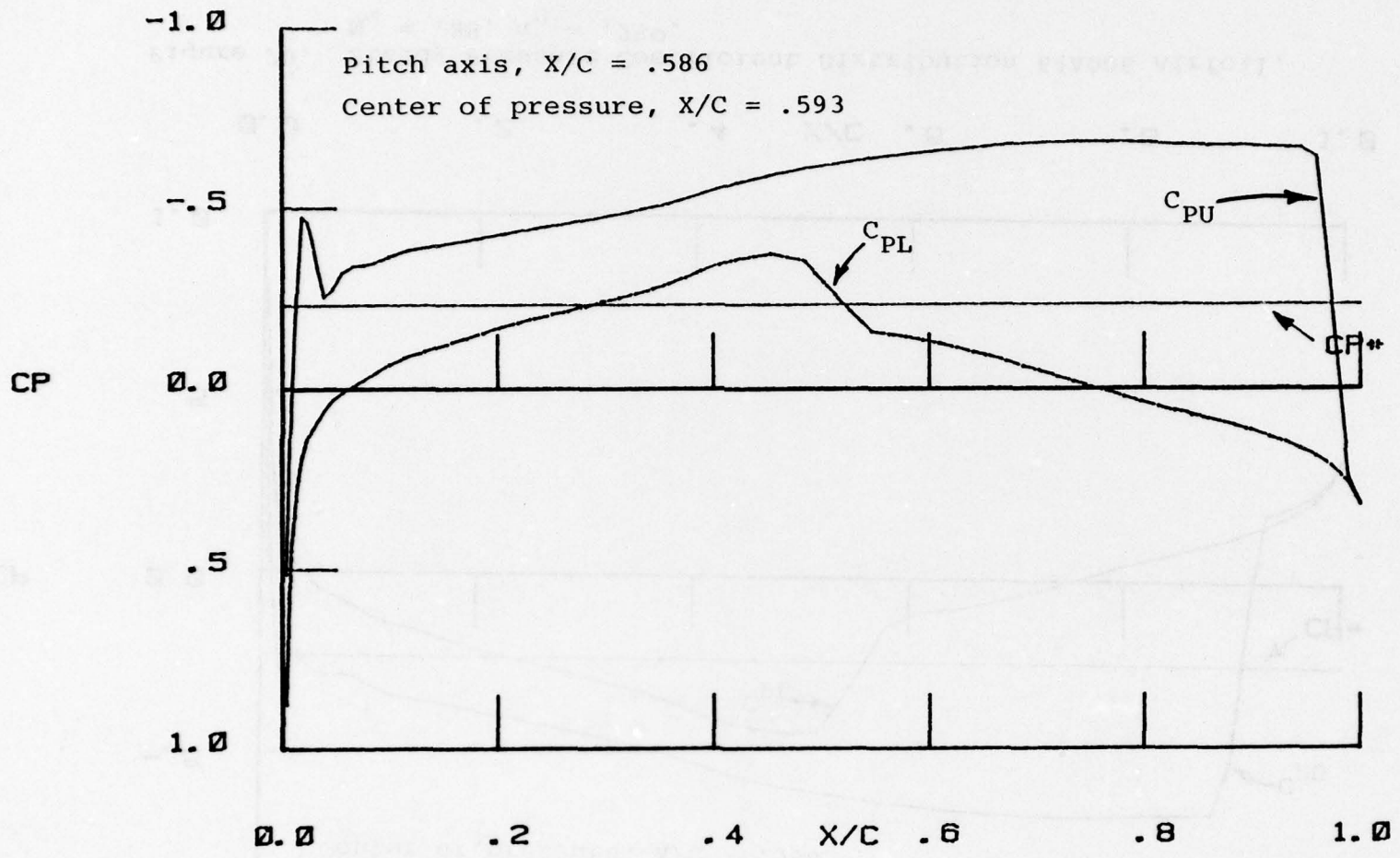

Figure 21. Steady Pressure Coefficient Distribution, 64A006 Airfoil, $M_\infty = .88$, $\alpha_0 = .50^O$.

the aft. Although this pitch axis location may not be very realistic, this example serves to highlight a key mechanism of nonlinear divergence; namely, that center of pressure location is a function of angle of attack. This phenomenon is not observed in linear flow problems.

The shift in center of pressure is directly due to the pressure of shock waves on the upper and lower surfaces. These pressure discontinuities move toward the trailing edge on the upper surface as angle of attack increases, and toward the leading edge on the lower surface. This produces a lateral change in the pressure distribution which grows faster than the transverse changes which are occurring toward the leading edge. It is this feature of pressure distribution which causes the moment coefficient to be nonlinear. The fact that C_m is nonlinear can be seen from Equation (4.24) since both center of pressure and lift are functions of angle of attack in this case.

Figure 22 shows a graphical solution to Equation (4.21). A total of three quilibrium positions are observed: (1) the origin, (2) $\alpha_0 = +.20°$, and (3) $\alpha_0 = -.20°$. The origin is an unstable equilibrium position, since for very small α_0 the destabilizing aerodynamic moment is larger in absolute value than the restoring moment due to the spring. For α_0 positive such as A_1 on Figure 22, the motion tends to

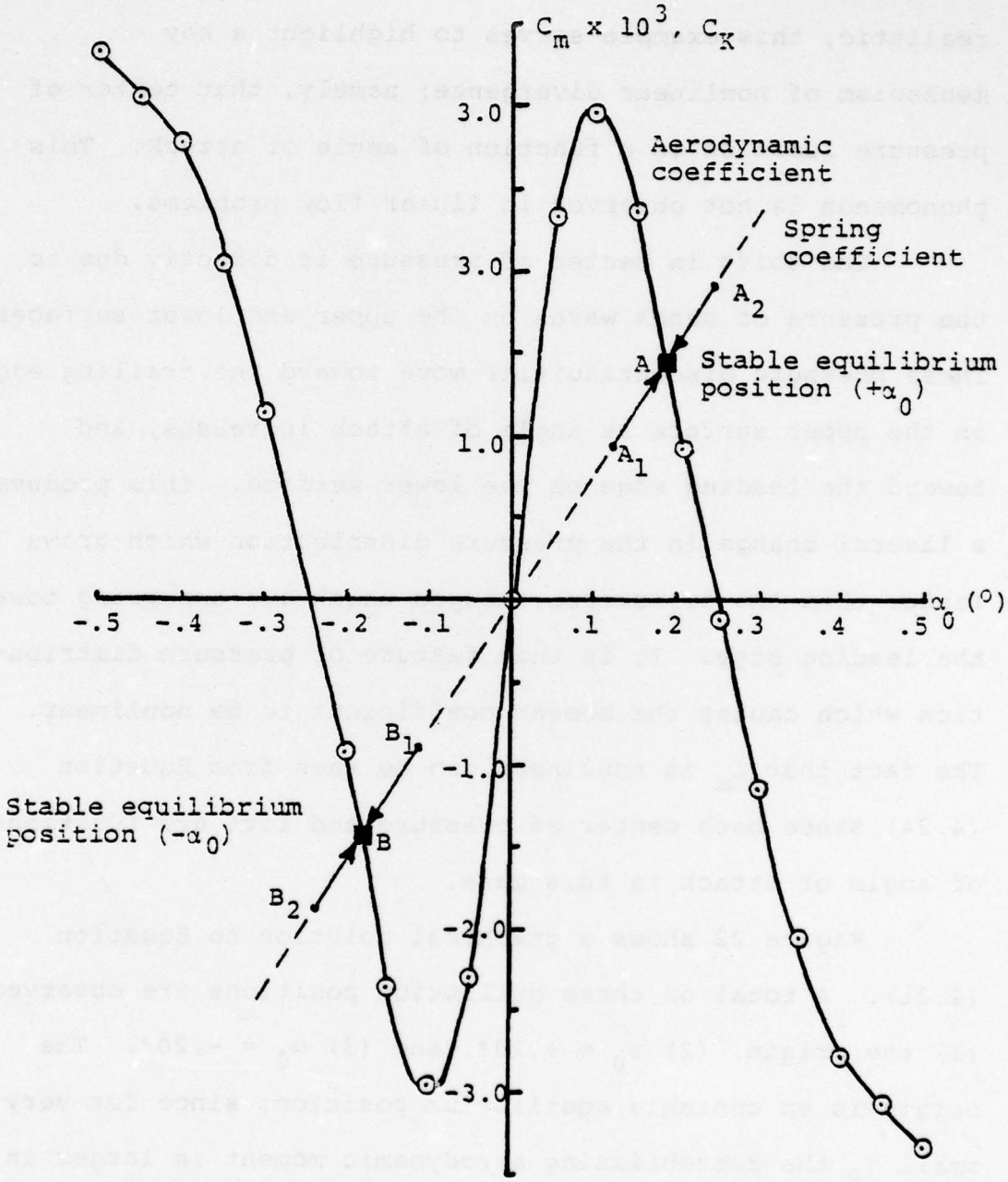

Figure 22. Steady Aerodynamic Moment Coefficient for 64A006 Airfoil at M_∞ = .88, and Spring Force Coefficient versus α_0.

increase toward the stable equilibrium position A. At α_0 positions larger than about .20°, the motion decreases toward A. At negative α_0, poiint B is a stable position and motions started at points B_1 and B_2 will quickly stabilize toward B.

In this divergence study the imposed disturbance is a constant and stability is determined from a simple moment balance relation. This is a single degree-of-freedom example of the static solution subcase discussed in Section 3.2.6. However, moments instead of forces are balanced for the transonic divergence problem.

4.3 SINGLE DEGREE-OF-FREEDOM TRANSONIC FLUTTER

Time history flutter analysis results are obtained for an airfoil pitching in transonic flow. Results obtained by numerical integration are compared to those of the method of imposed disturbances. The optimal amount of system damping needed to prevent flutter is computed by both methods as a function of amplitude. The numerical integration and imposed disturbance methods both predict similar damping-amplitude trends.

4.3.1 System Geometry and Equation of Motion

Figure 23 shows the geometry of a NACA 64A006 pitching in transonic flow. The streamwise coordinate, ξ, is nondimensionalized by the chord c. A pitch axis location of $\xi = 0.5$ has been selected for this study.

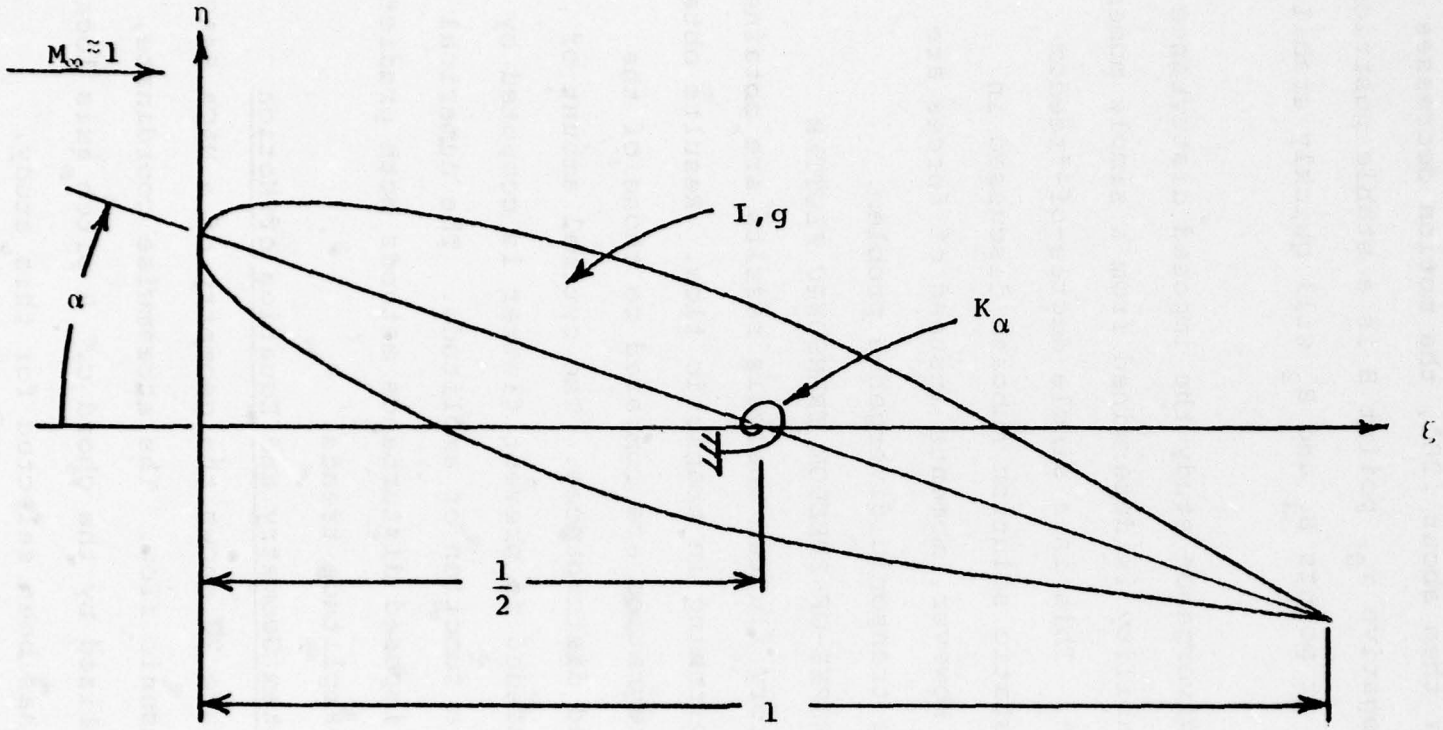

Figure 23. Geometry of NACA 64A006 Airfoil Pitching in Transonic Flow (Airfoil Thickness Scaled 3.5x).

The equation of motion is

$$I\ddot{\alpha} + g\dot{\alpha} + K_\alpha \alpha = M \tag{4.25}$$

where I, g, and K_α are the system pitch inertia, damping, and spring stiffness, respectively, and M is the unsteady aerodynamic moment. Following the nondimensionalization of Ballhaus and Goorjian,[47] the Equation (4.25) can be rewritten as

$$\alpha'' + A_1\alpha' + A_2\alpha = A_3 C_m \tag{4.26}$$

where

$$A_1 = g/\omega I \tag{4.27a}$$

$$A_2 = K_\alpha/\omega^2 I \tag{4.27b}$$

$$A_3 = \tfrac{1}{2}\rho_\infty V_\infty^2 c^2/\omega^2 I \tag{4.27c}$$

and ( )' denotes differentiation with respect to ωt where ω is an arbitrary frequency that has been introduced to make the time scale nondimensional.

The transonic moment coefficient, C_m, is a complicated function of Mach number, ωt, α, α', and reduced frequency, k_c. The reduced frequency definition is based on chord; i.e.,

$$k_c = \omega c/V_\infty \tag{4.28}$$

4.3.2 Aerodynamic Calculations and Integration of the Equation of Motion

The LTRAN2 computer code of Reference 47 is used to compute the aerodynamic moment. The basic code is

set up to compute unsteady lift and moment coefficients for an imposed harmonic airfoil motion. To compute a time history solution in which the airfoil is free to interact with the structural term in the equation, it is necessary to add a numerical integration algorithm to the code.

Goorjian[91] uses the following explicit finite difference scheme to solve the same pitch flutter problem[47] that is presented here. Assume that at the n^{th} time step, α, α', and C_m are known and have values denoted by α_n, α'_n, and C_{mn}. The expression for the second derivative of α at this time step is computed by solving Equation (4.26) to get

$$\alpha''_n = -A_1\alpha'_n - A_2\alpha_n + A_3C_{mn} \tag{4.29a}$$

The following two-term Taylor series expansion for α gives α_{n+1} in terms of known quantities

$$\alpha_{n+1} = \alpha_n + h\alpha'_n + \frac{1}{2}h^2\alpha''_n \tag{4.29b}$$

where h is the time step. The one-term Taylor series for α'

$$\alpha'_{n+1} = \alpha'_n + h\alpha''_n \tag{4.29c}$$

is the final difference equation that is needed. The LTRAN2 code computes C_{mn+1} after α_{n+1} and α'_{n+1} have been determined from Equations (4.29).

4.3.3 Transonic Pitch Flutter Analysis by the Method of Imposed Disturbances

Let

$$\alpha = \alpha_1 \sin\gamma \tag{4.30}$$

be an imposed airfoil motion where $\gamma = \omega t$ and α_1 is the amplitude of pitching oscillation. The total nonconservative work done by the aerodynamic and dissipative terms during one period of motion is

$$W^{NC} = \int_0^{2\pi} [A_3 C_m(\alpha,\alpha',\gamma) - A_1\alpha'] \; \alpha' \; d\gamma \tag{4.31}$$

where the imposed disturbance of Equation (4.30) is used to compute C_m and the other α related terms in the integral.

Using Equation (4.30) in Equation (4.31) and rearranging terms gives

$$W^{NC}/\alpha_1\pi = a_1 A_3 - \alpha_1 A_1 \tag{4.32}$$

where a_1 is the usual Fourier cosine coefficient

$$a_1 = \frac{1}{\pi} \int_{\gamma_1}^{\gamma_1+2\pi} C_m(\alpha,\alpha',\gamma) \cos\gamma d\gamma \tag{4.33}$$

The time value, γ_1, is taken to be 6π in the numerical calculations. This is required in order to establish the periodicity of the airfoil pressure distribution. The stability criterion is thus

$$W^{NC}/\alpha_1\pi = \begin{cases} >0 & \text{unstable} \\ =0 & \text{neutrally stable} \\ <0 & \text{stable} \end{cases} \tag{4.34}$$

Solving $W^{NC} = 0$ for A_1 gives the required damping needed to prevent flutter at an imposed disturbance amplitude of α_1. Thus the required damping is

$$A_1 = a_1(\alpha_1)A_3/\alpha_1 \tag{4.35}$$

In the next subsection specific data will be used to compare the results of this equation with numerical integration.

4.3.4 Numerical Results for Pitching Airfoil

All the following calculations have been performed at a Mach number of 0.88 and a reduced frequency of 0.1. These appear to be typical values[47,80] which can lead to nonlinear flutter behavior at moderate angles of attack.

Figure 24 shows the time history results for C_m and α using the LTRAN2 aerodynamic code for the case of $\alpha_1 = .25°$, $A_1 = .99$, $A_2 = 1.2278$, $A_3 = 0.9596$. Only α_1 and A_1 are variables in this study. All cases have been run for the values of A_2 and A_3 shown above. Four complete cycles of imposed motion are given the airfoil in order to establish a periodic airflow condition. This is followed by approximately two cycles of free motion as computed by the finite difference method of Section 4.3.2. The initial conditions for the free motion are the α, α', and C_m at the end of the fourth cycle of imposed motion. Figure 24a shows the complete time history and Figure 24b shows a full scale plot of the free motion. Figure 25 shows the time history of the lift

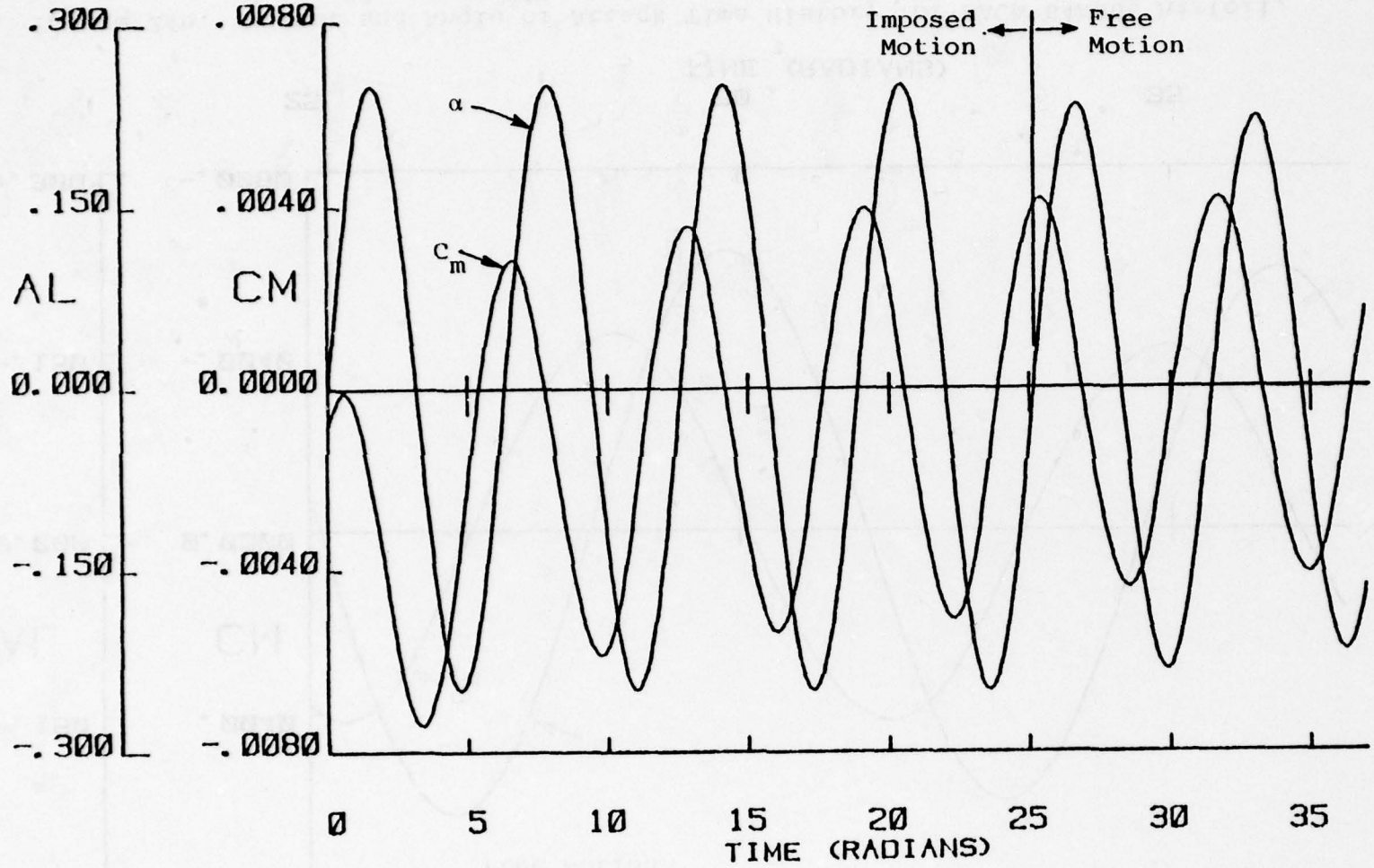

Figure 24a. Moment and Angle of Attack Time History for NACA 64A006 Airfoil, M_∞ = .88, α_1 = .25°, A_1=1.05, A_2 = 1.2275, A_3 = 0.9596.

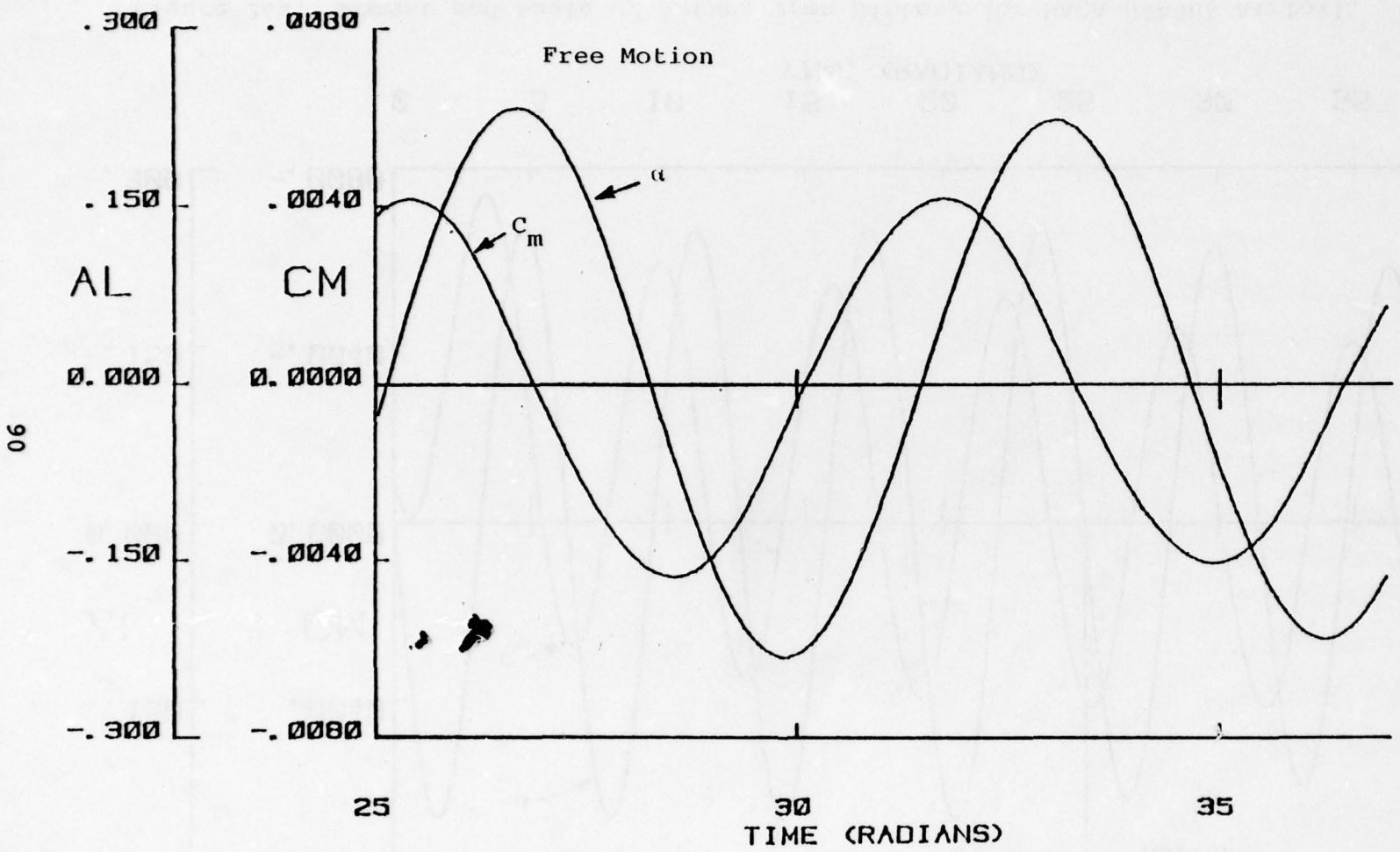

Figure 24b. Moment and Angle of Attack Time History for NACA 64A006 Airfoil, $M_\infty = .88$, $\alpha_1 = .25°$, $A_1 = 1.05$, $A_2 = 1.2275$, $A_3 = 0.9596$.

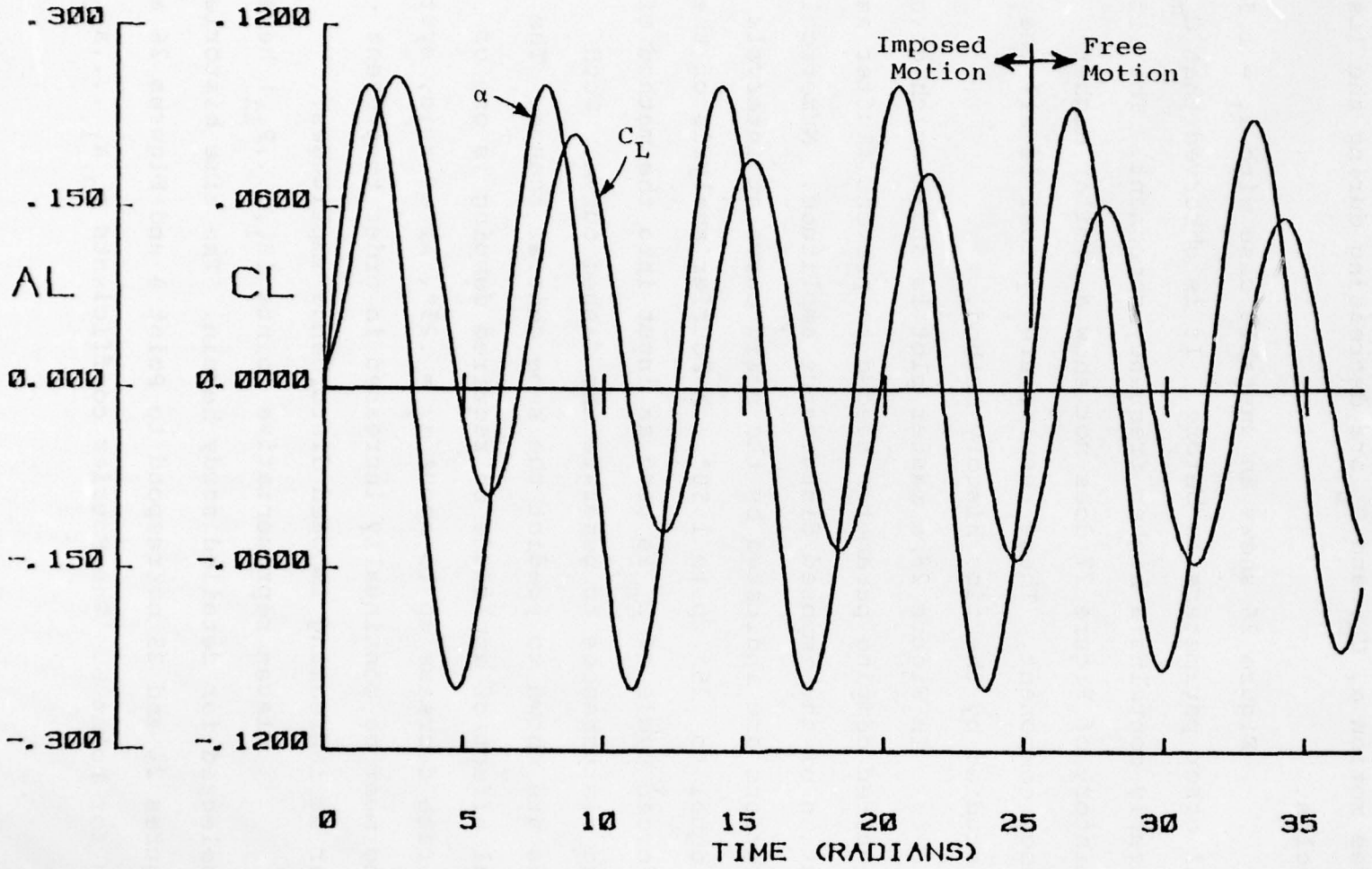

Figure 25. Lift and Angle of Attack Time History for NACA 64A006 Airfoil, $M_\infty = .88$, $\alpha_1 = .25°$, $A_1 = 1.05$, $A_2 = 1.2275$, $A_3 = 0.9596$.

coefficient C_L and α as a function of time. It appears that the free motion α, C_m, and C_L are decreasing during the last two cycles.

Figure 26 shows an unstable case with $\alpha_1 = 1.50°$ and all other parameters as before. It is observed that C_m now clearly contains a higher frequency component. The lift time history of Figure 27 does not show a similar higher frequency component. These results are typical of all the cases studied by the time history method.

In Figure 28, a master plot is shown which gives the required damping parameter needed to prevent flutter as a function of the imposed disturbance amplitude. Numerical integrations are indicated by the solid curve at intervals of α, equal to .25° up to 1.50°. A Fourier analysis of the last forced cycle of C_m is used as input into the method of imposed disturbances to generate the dashed curve. Both methods are shown to predict the same general trends. The initial effect of amplitude on required damping is one of a moderate decrease up to about $\alpha_1 = .25°$. After this, system damping must be continually increased in order to prevent flutter at increasing imposed disturbance amplitudes.

Eleven representative points ($P_1,\ldots,P_{11}$) have been selected for detailed study herein. The time histories of Figures 24 and 25 correspond to Point 4 and Figures 26 and 27 are for Point 6. The Fourier coefficients $a_0, a_1, \ldots, a_{10}$

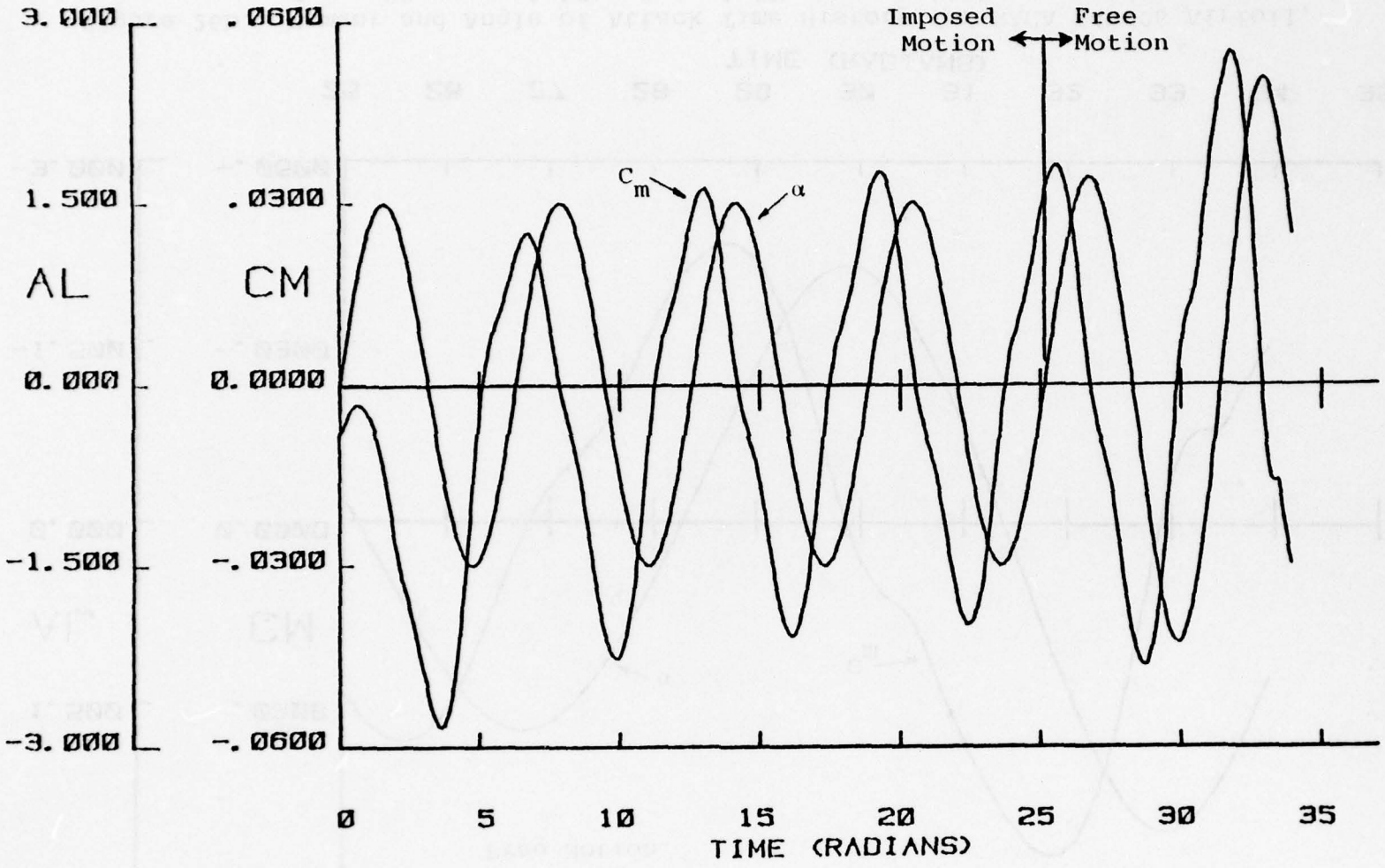

Figure 26a. Moment and Angle of Attack Time History for NACA 64A006 Airfoil, $M_\infty = .88$, $\alpha_1 = 1.50°$, $A_1 = 1.05$, $A_2 = 1.2275$, $A_3 = 0.9596$.

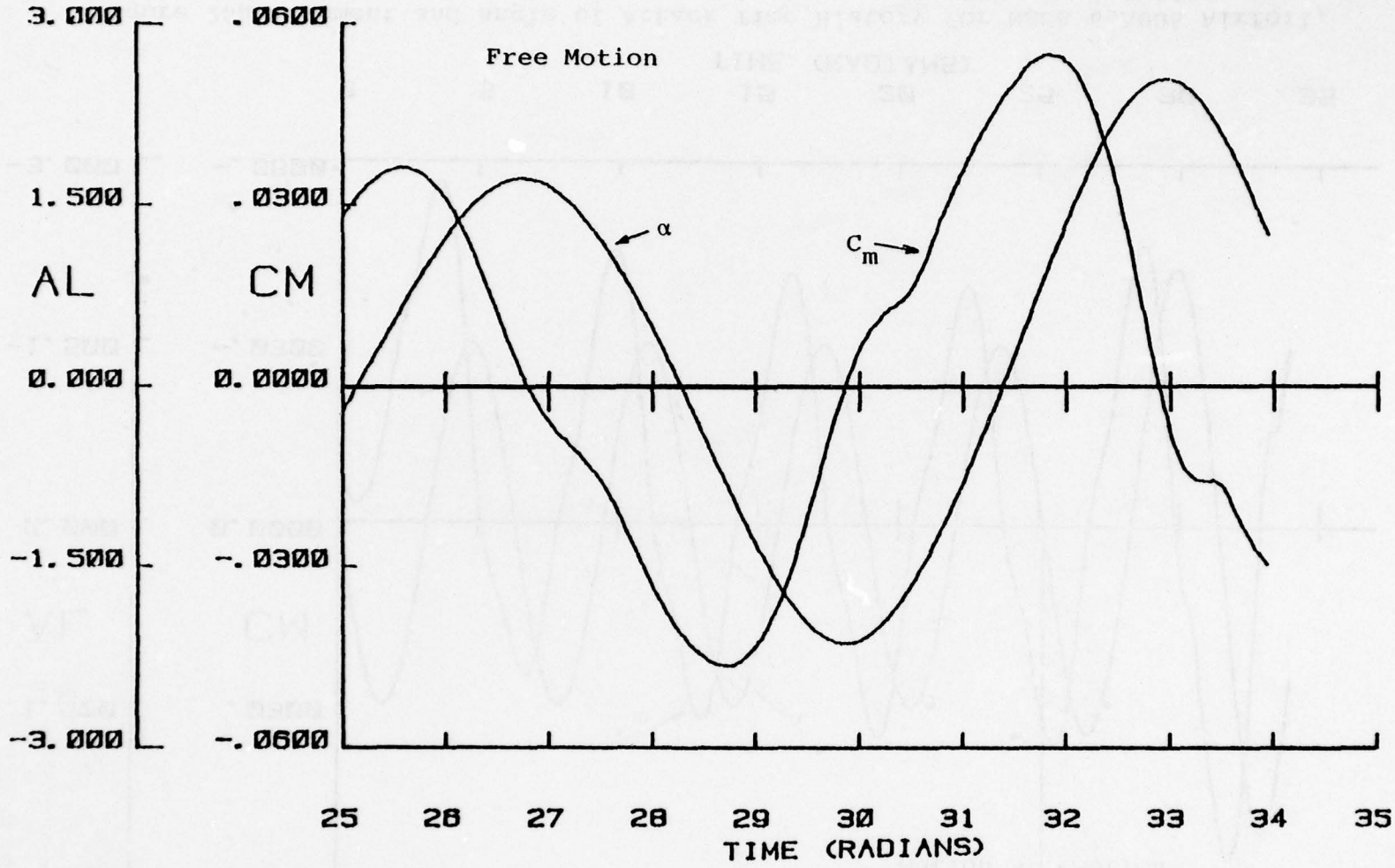

Figure 26b. Moment and Angle of Attack Time History for NACA 64A006 Airfoil, $M_\infty = .88$, $\alpha_1 = 1.50°$, $A_1 = 1.05$, $A_2 = 1.2275$, $A_3 = 0.9596$.

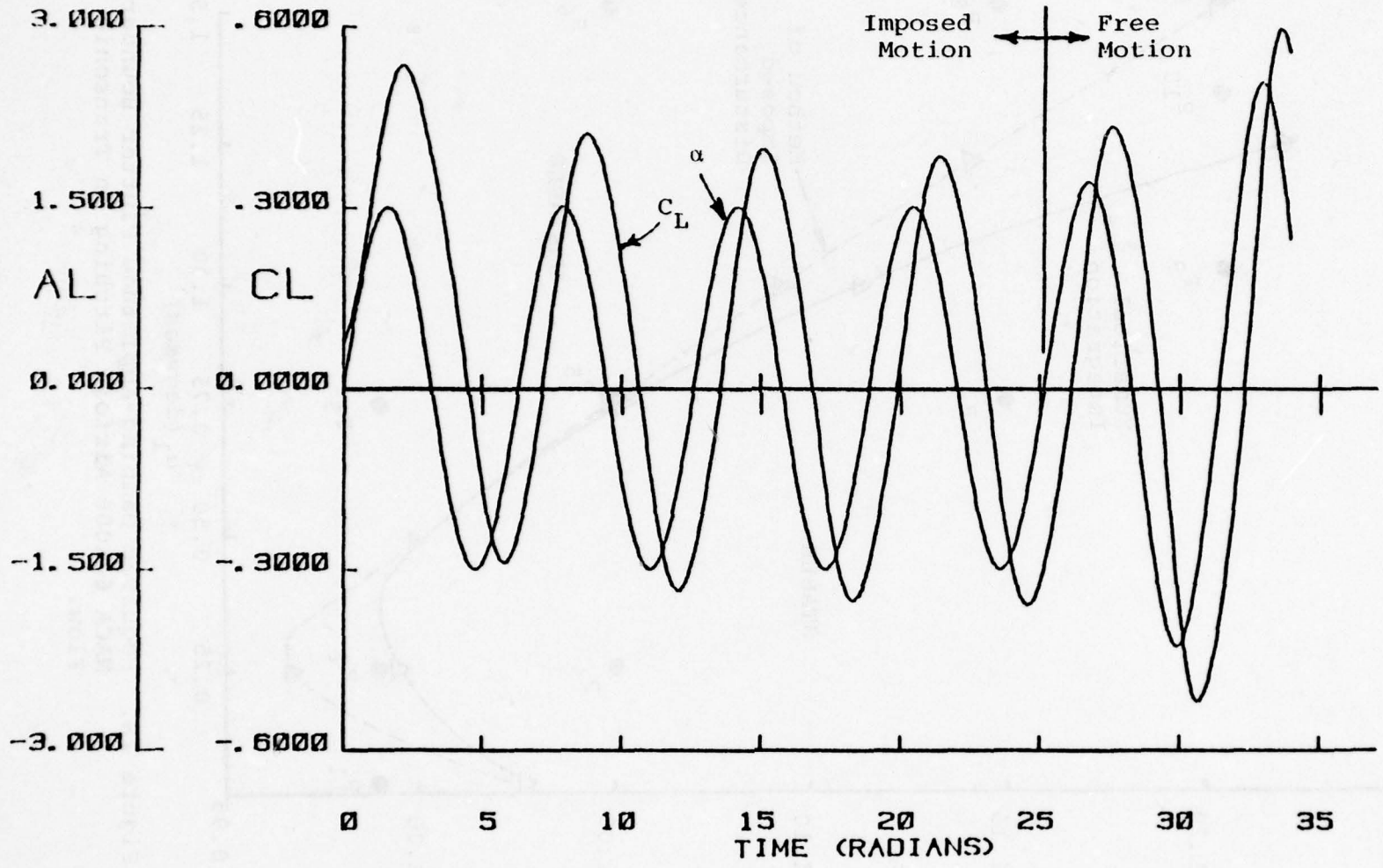

Figure 27. Lift and Angle of Attack Time History for NACA 64A006 Airfoil, M_∞ = .88, α_1 = .25°, A_1 = .99, A_2 = 1.2275, A_3 = 0.9596.

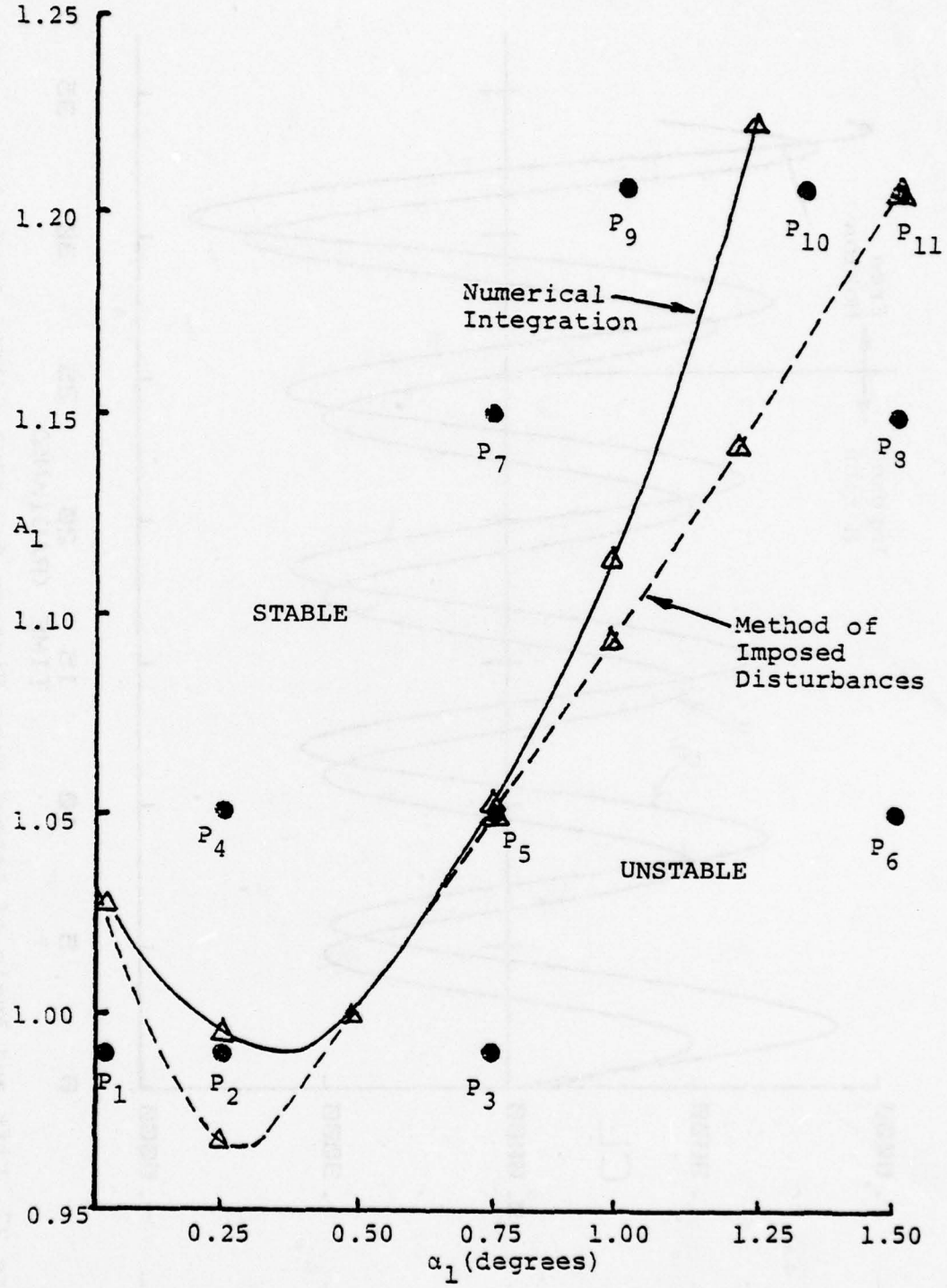

Figure 28. Required Damping-Amplitude Flutter Boundary for NACA 64A006 Airfoil Pitching in Transonic Flow.

are shown in Table 2 for Point 4. By far, the a_1 coefficient is the largest for both C_m and C_L. This indicates that the equation of motion is nearly linear at a disturbance level of $\alpha_1 = .25°$. Table 3 shows the Fourier coefficients at $\alpha_1 = 1.50°$ (Point 6). The greatest order of magnitude increase between Tables 2 and 3 is in the a_5 term which has increased by a factor of about 250.

The results of a sequence of Fourier analyses is given for Points 6 and 9 in Tables 4 and 5, respectively. The parameter being varied is α_1 which is the iime after which the airflow is assumed to be periodic. A Fourier analysis of the first cycle of imposed motion ($\gamma_1/2\pi=0$) for Point 6 is shown to underestimate a_1 by about seven percent, compared to a cycle 4 analysis ($\gamma_1/2\pi=3$). By Equation (4.35) this also leads to a value of required damping which is fifteen percent low. For Point 9, the trend is reversed and a first cycle analysis overestimates a_1 and hence A_1 by about 13%.

The phase plane plot has shown to be a useful way to determine stability for this problem. As can be seen from the time history plots in Figure 24, it can be difficult sometimes to judge whether or not the amplitude of the free motion is decaying. Figure 29 shows the (α,α') phase plane plot for Point 4. The circle of radius .25 is generated during the imposed sinusoidal motion. The free motion starts

TABLE 2

FOURIER COEFFICIENTS FOR C_L, C_m

POINT 4, $\gamma_1 = 6\pi$

i	$a_i(C_L) \times 10^2$	$a_i(C_m) \times 10^2$
0	.70929	-.04751
1	-5.61950	.44031
2	- .00006	.00052
3	.00317	-.00438
4	- .00022	-.00017
5	.00070	.00042
6	- .00011	.00009
7	.00064	.00009
8	.00032	-.00003
9	- .00011	.00017
10	.00032	.00019

TABLE 3

FOURIER COEFFICIENTS FOR C_L, C_m

POINT 6, $\gamma_1 = 6\pi$

i	$a_i(C_L) \times 10^2$	$a_i(C_m) \times 10^2$
0	2.79110	-.34660
1	-31.5790	3.30140
2	-.24121	-.03080
3	.84785	-.09042
4	.00984	-.01697
5	-.01732	.06526
6	-.00438	.00623
7	.00788	-.00382
8	-.00206	.00195
9	.00001	-.00168
10	-.00107	.00001

TABLE 4

CONVERGENCE OF a_1 FOR C_m

POINT 6

$\gamma_1/2\pi$	$a_1(C_m) \times 10^2$
0	3.06340
1	3.24630
2	3.29070
3	3.30140

TABLE 5

CONVERGENCE OF a_1 for C_m

POINT 9

$\gamma_1/2\pi$	$a_1(C_m) \times 10^2$
0	2.24520
1	2.04880
2	2.00330
3	1.99330

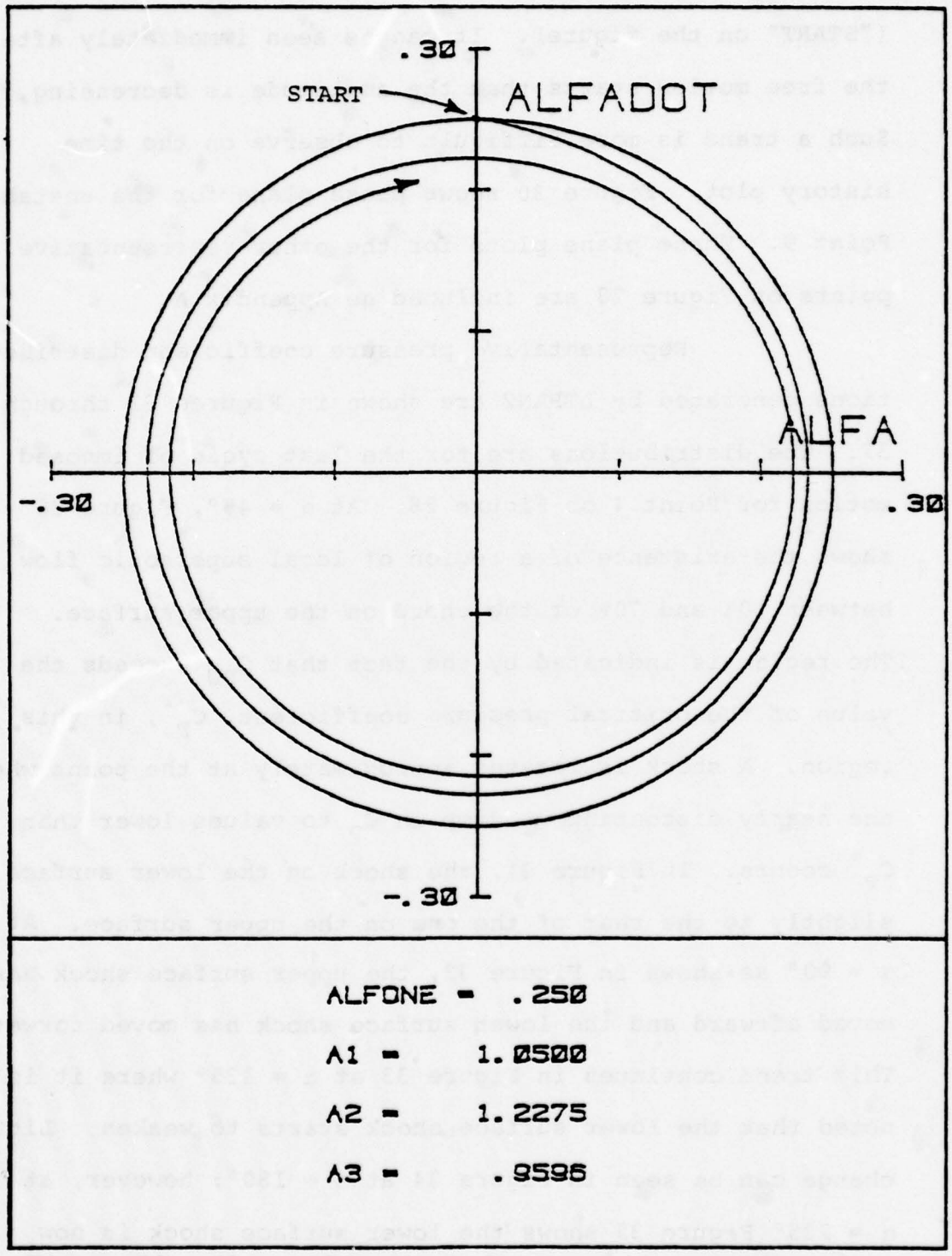

Figure 29. Phase Plane Plot for Point 4 on Damping-Amplitude Plot.

at the end of the fourth imposed cycle at $\alpha = 0$, $\alpha' = .25$ ("START" on the figure). It can be seen immediately after the free motion starts that the amplitude is decreasing. Such a trend is more difficult to observe on the time history plot. Figure 30 shows phase plane for the unstable Point 9. Phase plane plots for the other representative points on Figure 28 are included as Appendix A.

Representative pressure coefficient distributions generated by LTRAN2 are shown in Figures 31 through 37. The distributions are for the last cycle of imposed motion for Point 4 on Figure 28. At $\alpha = 45°$, Figure 30 shows the existence of a region of local supersonic flow between 10% and 70% of the chord on the upper surface. The region is indicated by the fact that C_{PU} exceeds the value of the critical pressure coefficient, C_p^*, in this region. A shock is located approximately at the point where the nearly discontinuous drop in C_p to values lower than C_p^* occurs. In Figure 31, the shock on the lower surface is slightly to the rear of the one on the upper surface. At $\alpha = 90°$ as shown in Figure 32, the upper surface shock has moved aftward and the lower surface shock has moved forward. This trend continues in Figure 33 at $\alpha = 135°$ where it is noted that the lower surface shock starts to weaken. Little change can be seen in Figure 34 at $\alpha = 180°$; however, at $\alpha = 225°$ Figure 35 shows the lower surface shock is now moving aftward and the upper one is moving forward. The

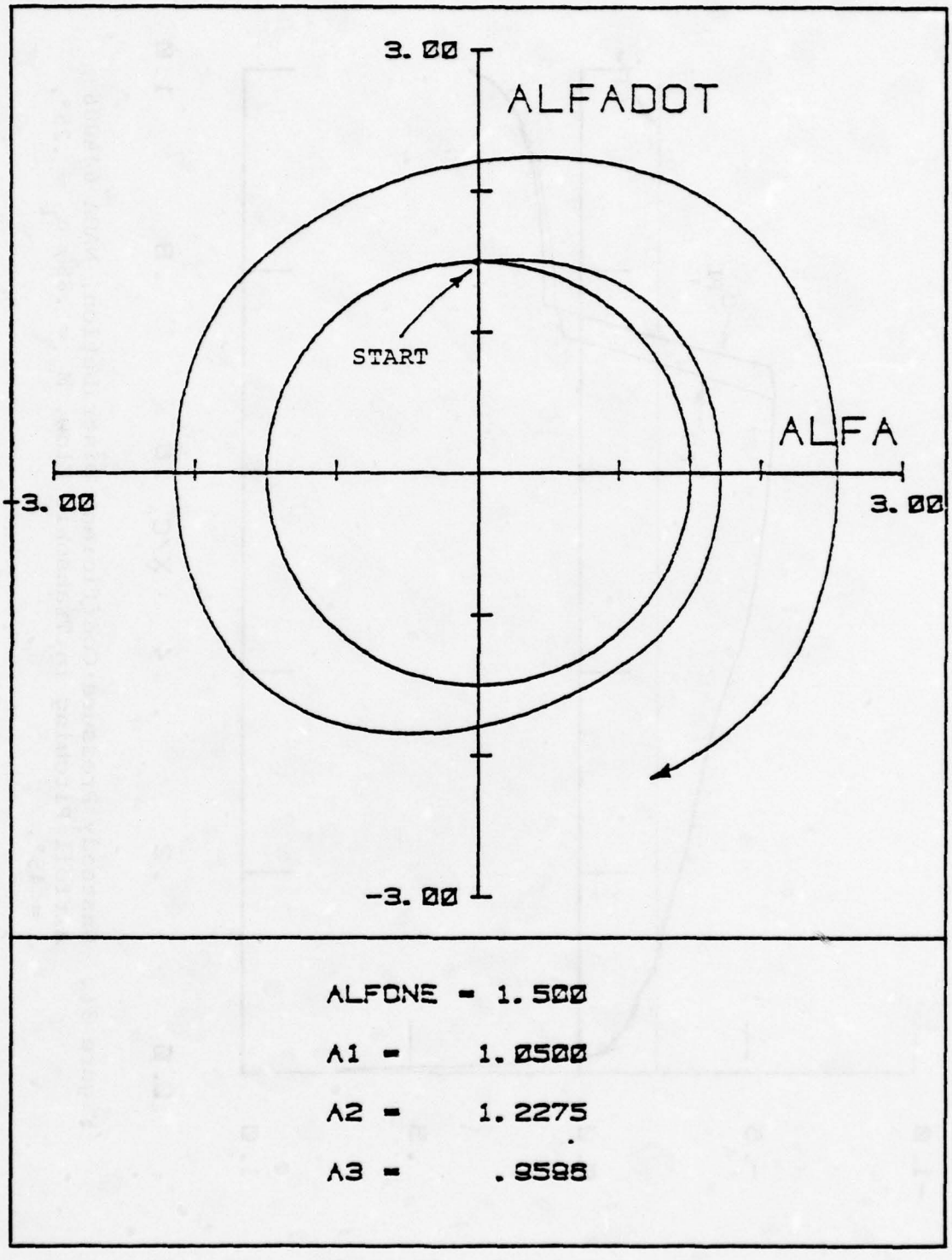

Figure 30. Phase Plane Plot for Point 6 on Damping-Amplitude Plot.

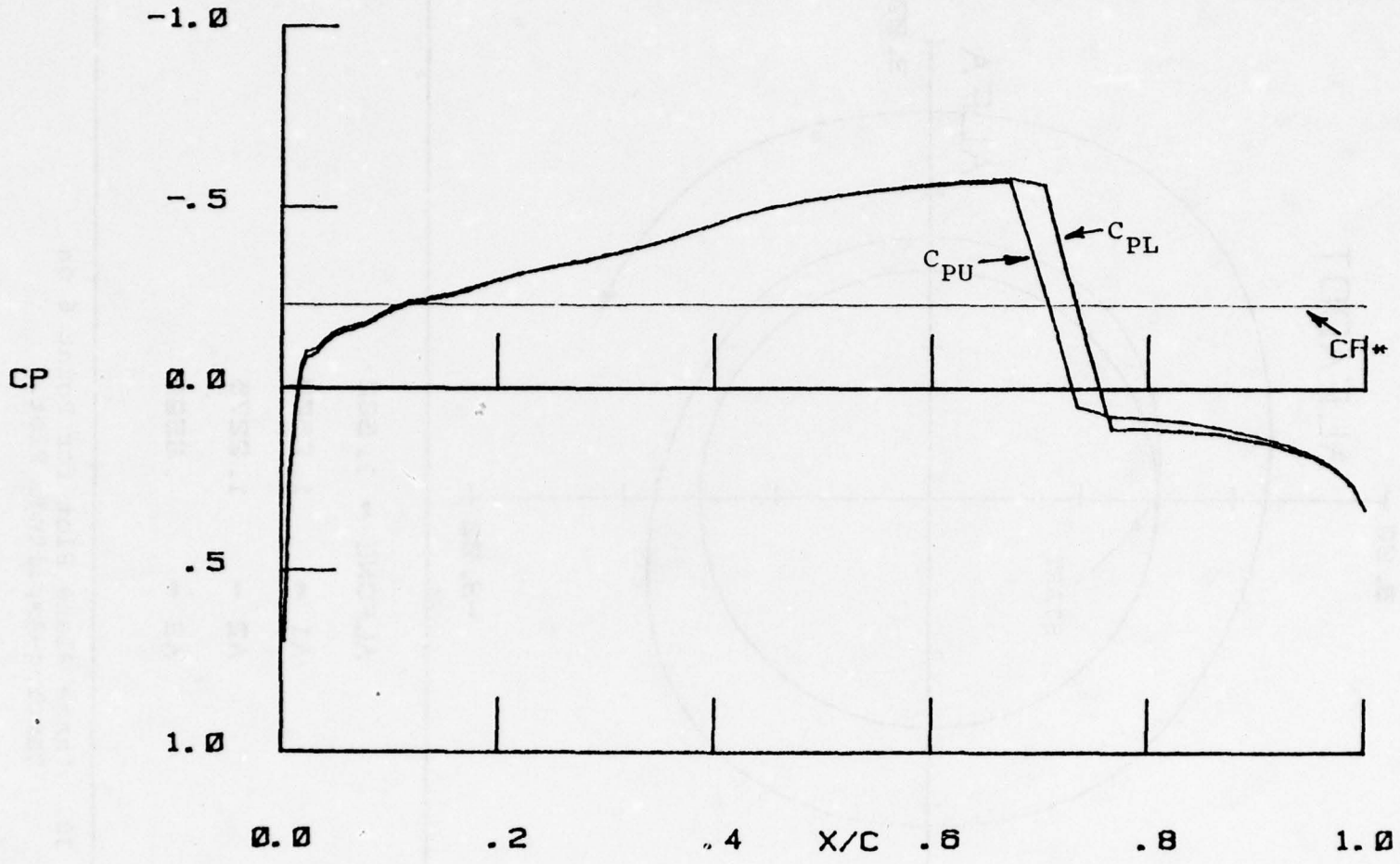

Figure 31. Unsteady Pressure Coefficient Distribution, NACA 64A006 Airfoil Pitching in Transonic Flow, $M_\infty = .88$, $\alpha_1 = .25°$, $\alpha = 45°$.

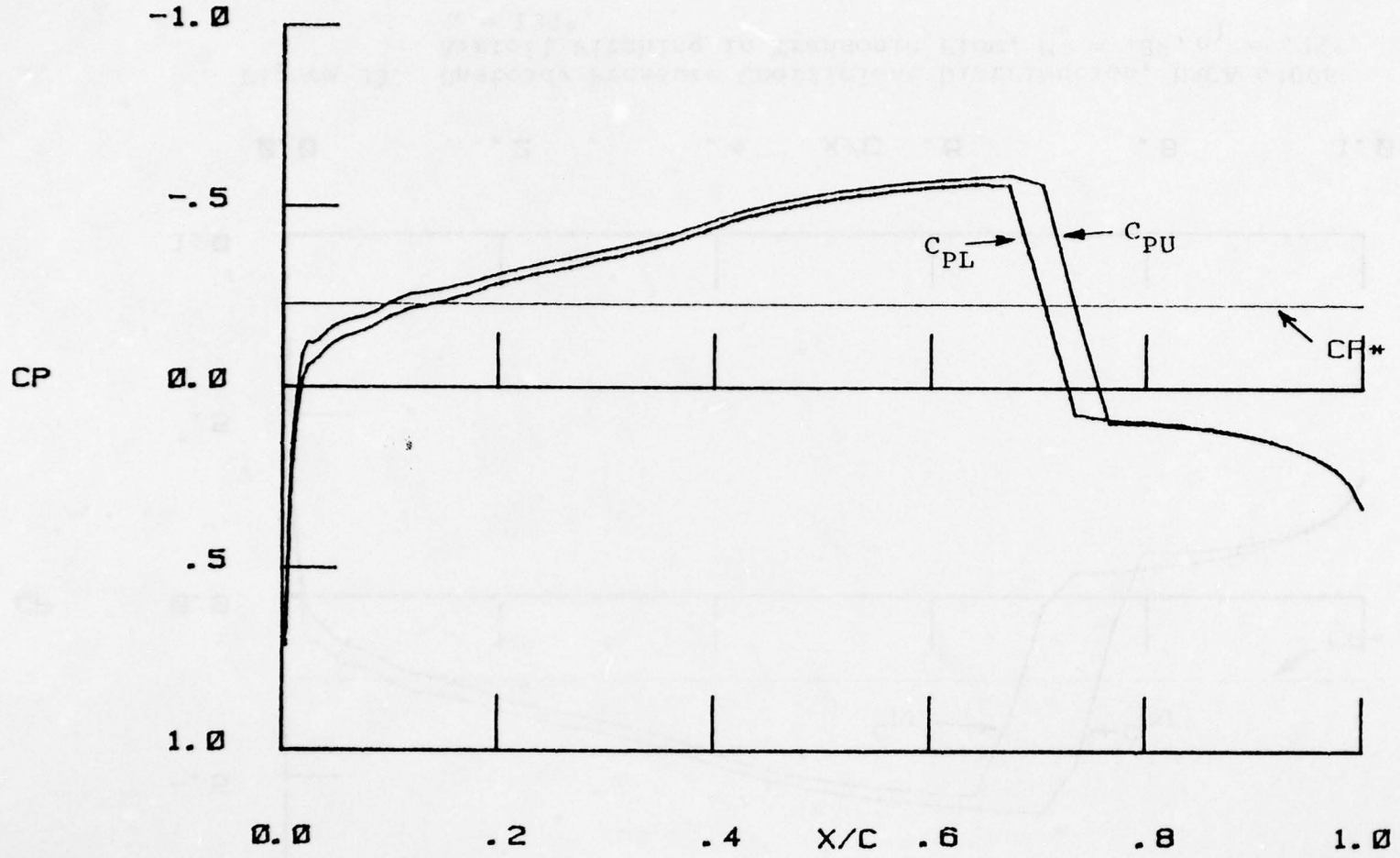

Figure 32. Unsteady Pressure Coefficient Distribution, NACA 64A006 Airfoil Pitching in Transonic Flow, $M_\infty = .88$, $\alpha_1 = .25°$, $\alpha = 90°$.

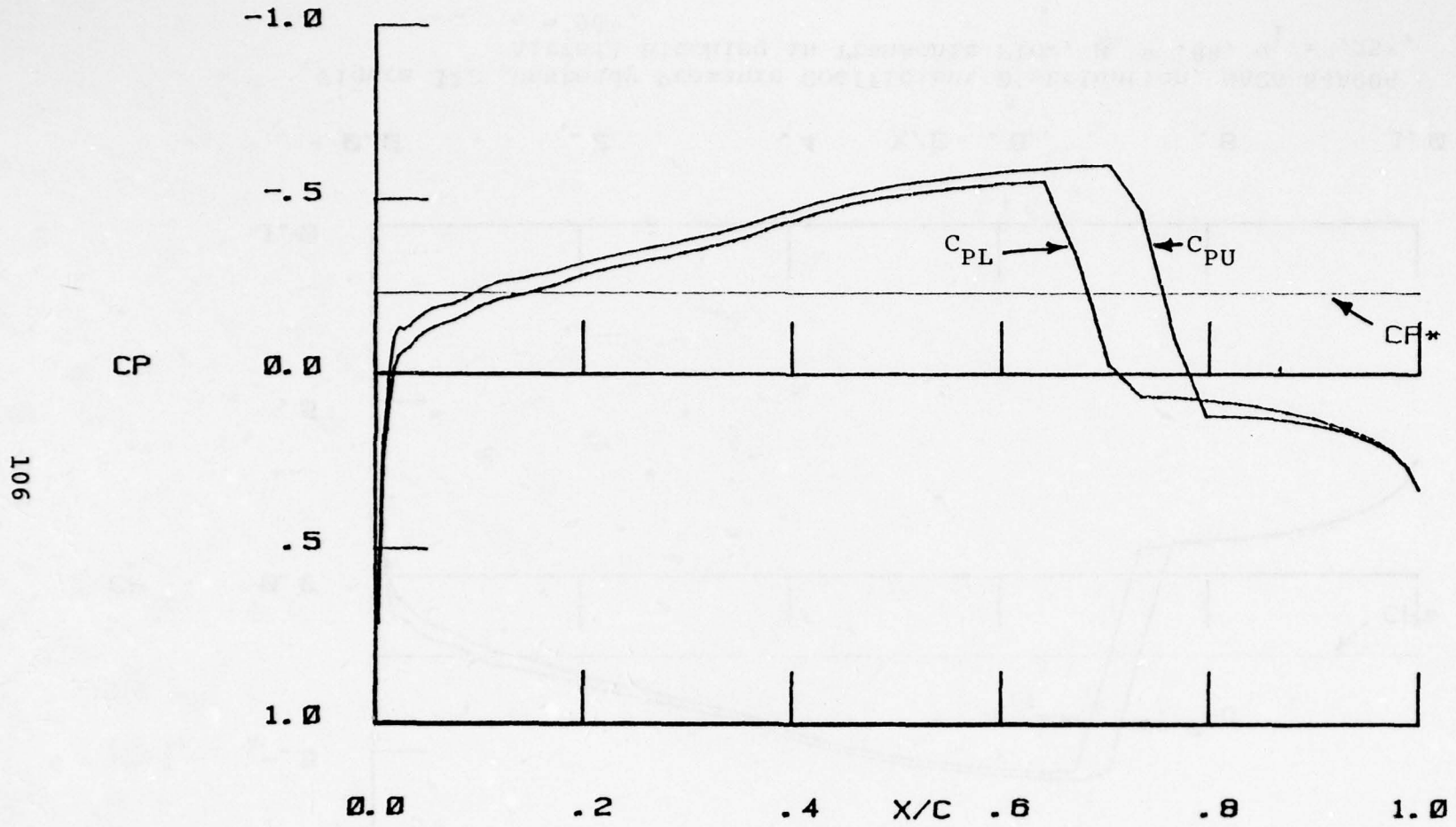

Figure 33. Unsteady Pressure Coefficient Distribution, NACA 64006 Airfoil Pitching in Transonic Flow, $M_\infty = .88$, $\alpha_1 = .25°$, $\alpha = 135°$.

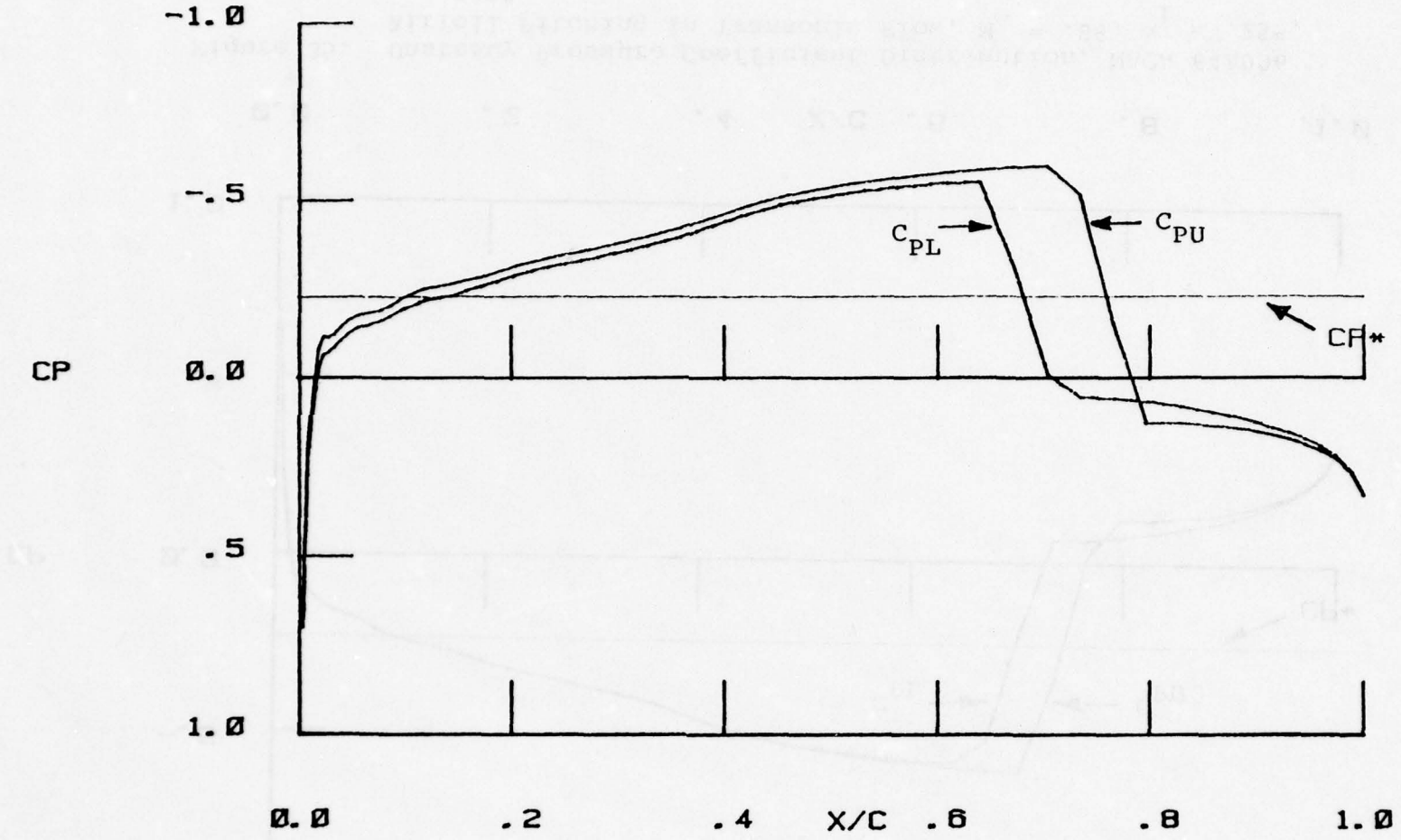

Figure 34. Unsteady Pressure Coefficient Distribution, NACA 64A006 Airfoil Pitching in Transonic Flow, $M_\infty = .88$, $\alpha_1 = .25°$, $\alpha = 180°$.

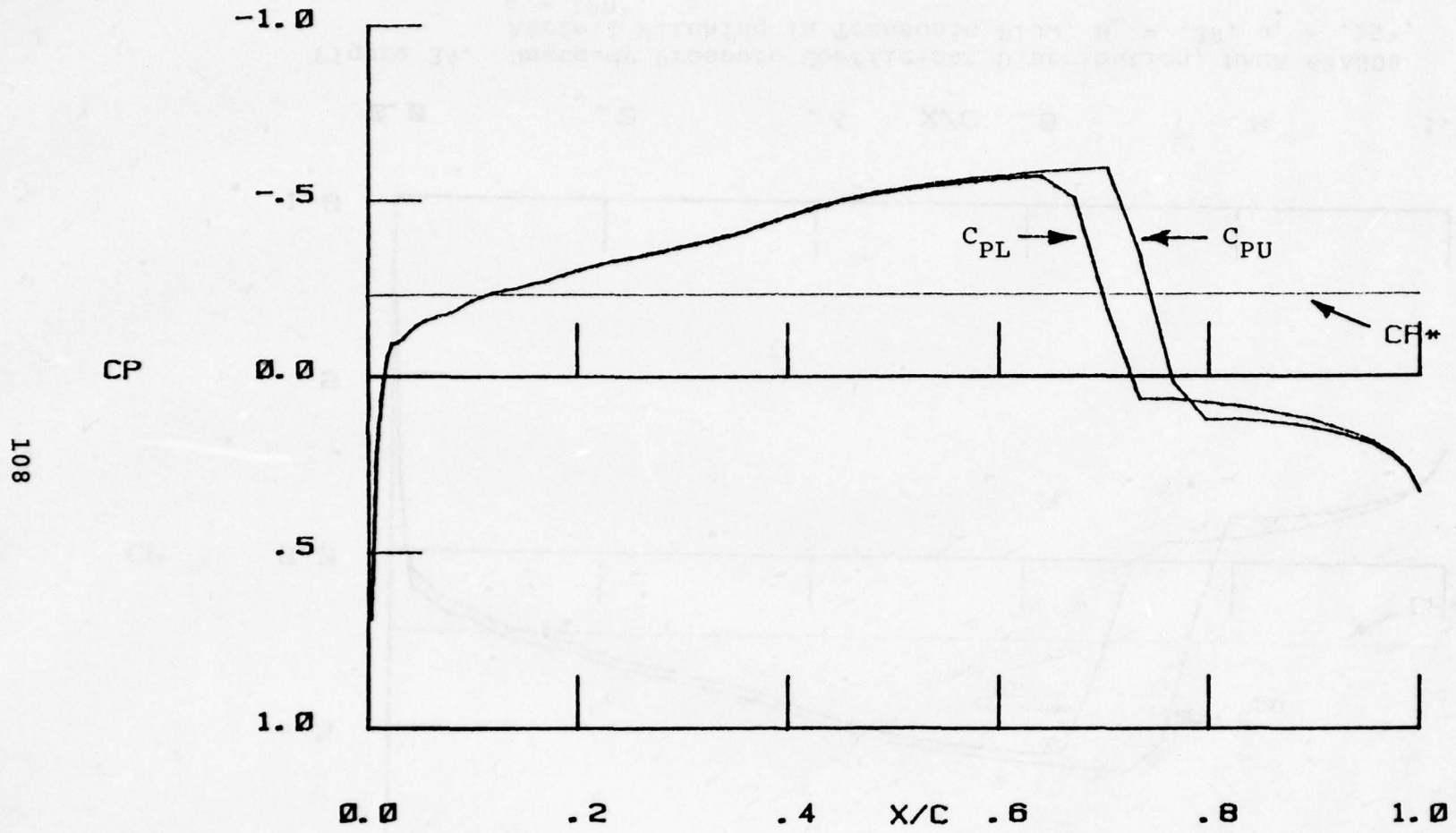

Figure 35. Unsteady Pressure Coefficient Distribution, NACA 64A006 Airfoil Pitching in Transonic Flow, $M_\infty = .88$, $\alpha_1 = .25°$, $\alpha = 225°$.

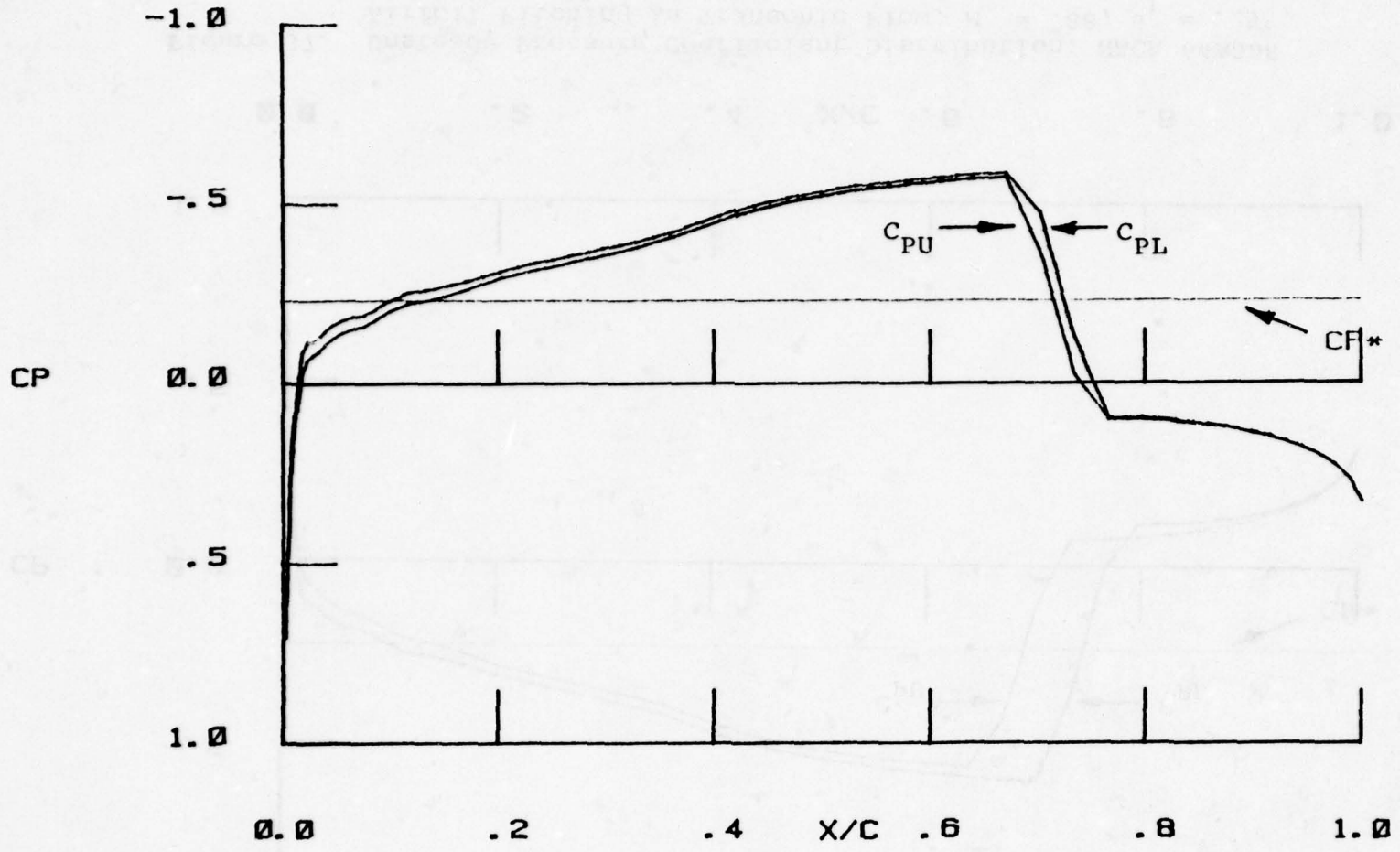

Figure 36. Unsteady Pressure Coefficient Distribution, NACA 64A006 Airfoil Pitching in Transonic Flow, $M_\infty = .88$, $\alpha_1 = .25°$, $\alpha = 270°$.

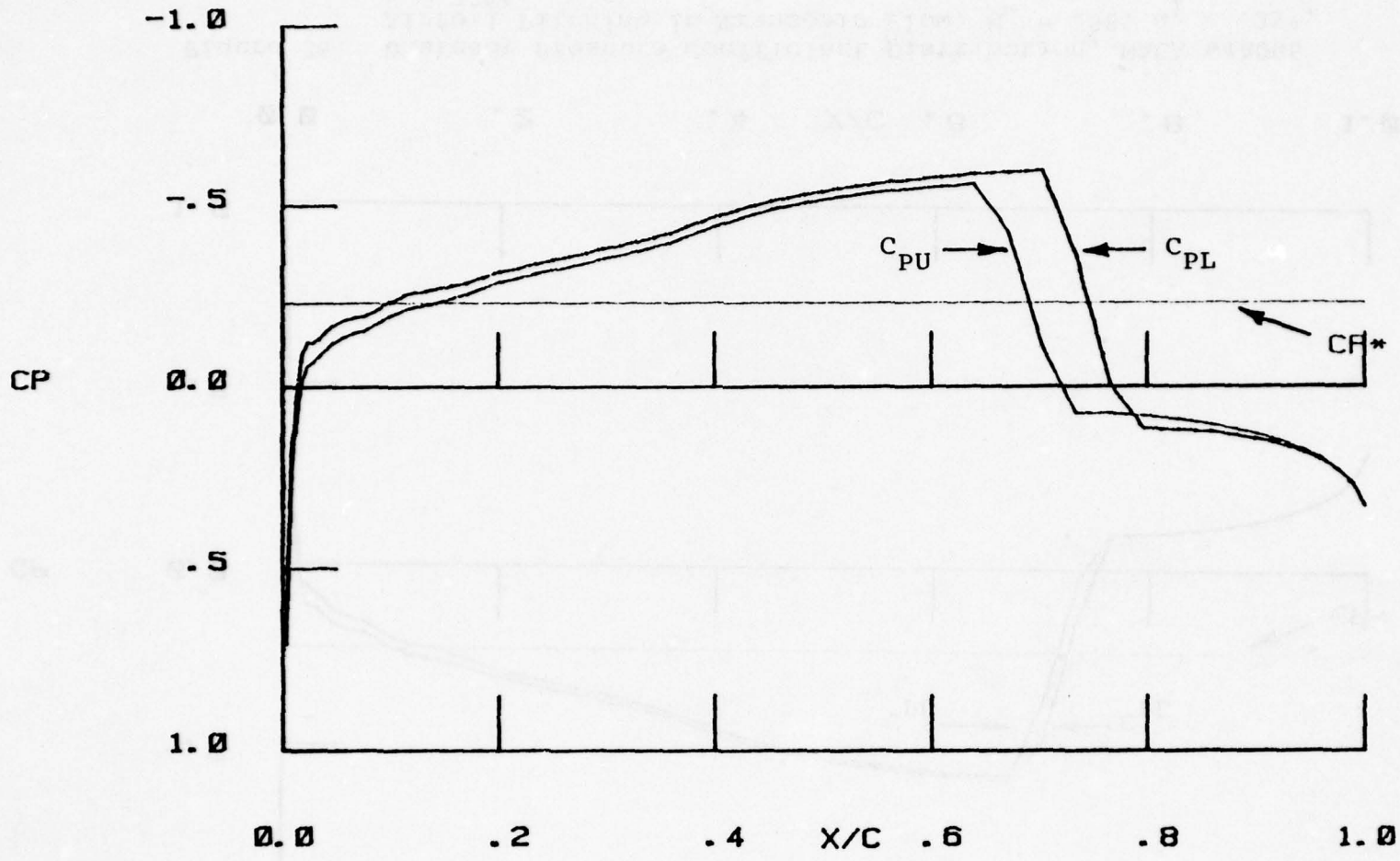

Figure 37. Unsteady Pressure Coefficient Distribution, NACA 64A006 Airfoil Pitching in Transonic Flow, M_∞ = .88, α_1 = .25°, α = 315°.

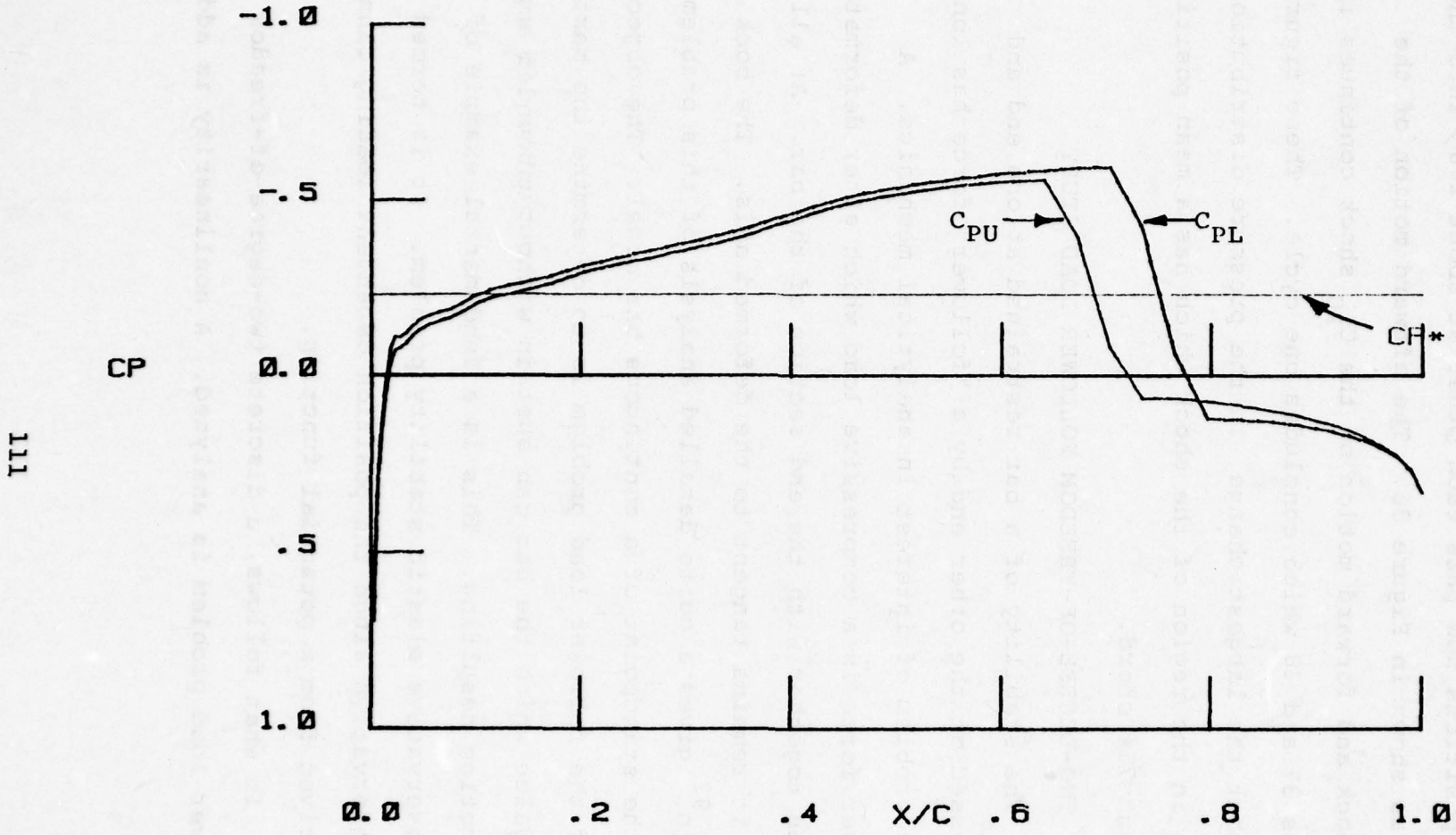

Figure 38. Unsteady Pressure Coefficient Distribution, NACA 64A006 Airfoil Pitching in Transonic Flow, $M_\infty = .88$, $\alpha_1 = .25°$, $\alpha = 360°$.

shock positions now pass each other at about 270° into the cycle as shown in Figure 36. The aftward motion of the C_{PL} shock and forward motion of the C_{PU} shock continues in Figures 37 and 38 which concludes one cycle. These figures show that the largest change in the pressure distribution occurs in the region of the shock which has a mean position of about 75% chord.

4.4 TWO-DEGREE-OF-FREEDOM FOLLOWER LOAD STUDY

The stability of a bar restrained at one end and compressed at the other end by a "follower" force has long been a problem of interest in analytical mechanics. A follower force is a compressive load which after deformation rotates together with the end section of the bar. At all times it remains tangent to the deformed axis. The book by Bolotin[92] gives a quite detailed analysis of this problem from the standpoint of a continuous bar model. The objective of the follower load problem is to determine the maximum load value which the bar can sustain without unbounded amplitude motion resulting. This is a fundamental example of a nonconservative elastic stability problem. It is termed nonconservative since the position dependent loading cannot be derived from a potential function.

In what follows, a discrete two-degree-of-freedom follower load problem is analyzed. A nonlinearity is added

to the problem by requiring that the load not only "follow" but that a component of its magnitude be dependent upon the square of the slope at the tip. Such a nonlinear stability problem is not in such standard works on nonconservative systems as the Bolotin reference. A literature search has shown that Roorda and Nemat-Nasser[83] are the first to present an energy based method for this nonlinear, nonconservative problem. The Reference 83 linearized solution is used below in an application of the method of imposed disturbances, and excellent agreement with the Roorda and Nemat-Nasser nonlinear load-amplitude curve is obtained.

4.4.1 Derivation of the Equations of Motion

The two-degree-of-freedom follower load problem is shown in Figure 39. The bar segments A-B and B-C are assumed rigid and are of length ℓ. Elastic and damping properties of the bar are modeled as two torsional springs located at positions A and B. The restoring moments at A and B are, respectively,

$$M_A = c\phi_1 = B_1\dot{\phi}_1 \tag{4.36a}$$

$$M_B = c(\phi_2-\phi_1) + B_2(\dot{\phi}_2-\dot{\phi}_1) \tag{4.36b}$$

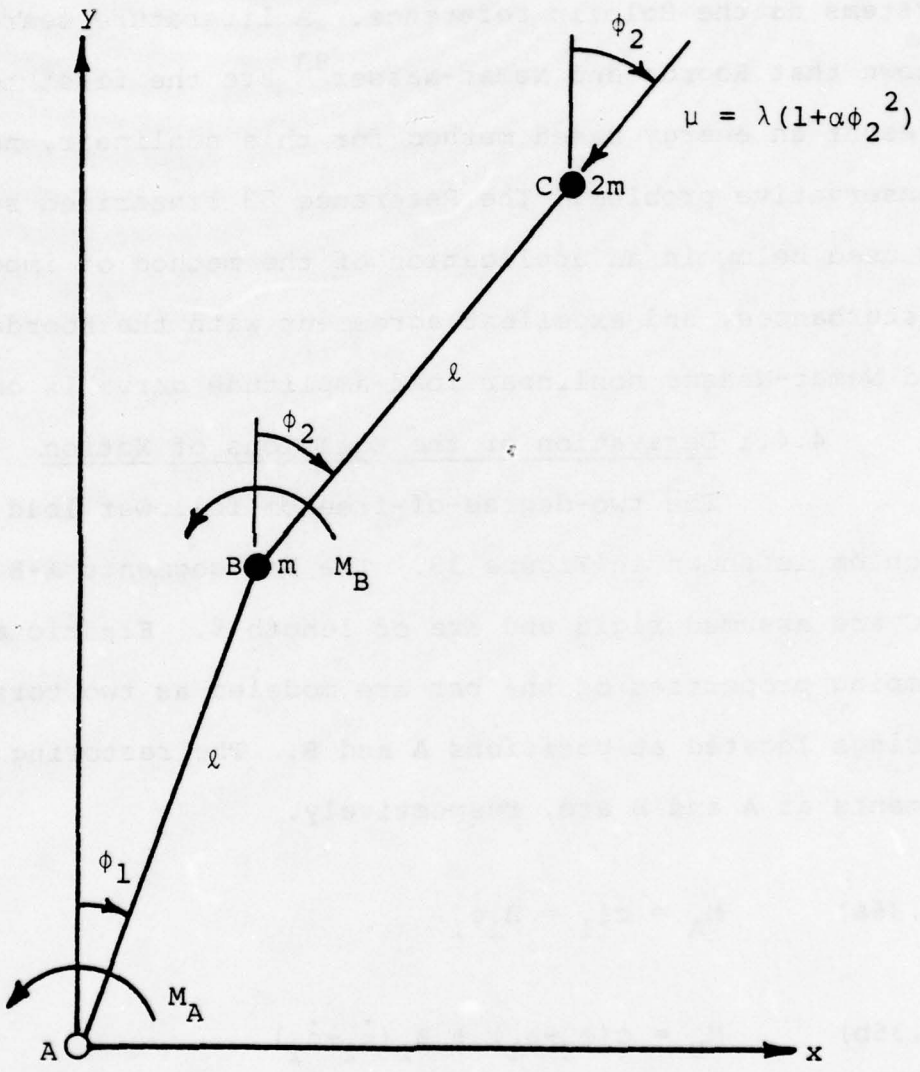

Figure 39. Two-Degree-of-Freedom Bar with Nonlinear Follower Load.

where c is an elastic spring constant, b_1 and b_2 are damping constants, and ϕ_1 and ϕ_2 are the angular rotations at A and B, respectively. A mass m is concentrated at B and a mass 2m at C. The load μ is always directed along the line B-C and is related to the tip slope by

$$\mu = \lambda(1+\alpha\phi_2^2) \tag{4.37}$$

Lagrange's equations (see Meirovitch,[93] p. 50, for example)

$$\frac{d}{dt}\frac{\partial L}{\partial \dot{\phi}_i} - \frac{\partial L}{\partial \phi_i} = Q_i^{NC} . \quad i = 1,2 \tag{4.38}$$

are used to derive the equations of motion where L = T-V is the Lagrangian and Q_i^{NC} are the nonconservative generalized forces. The kinetic energy, T, can easily be written as

$$T = \frac{1}{2} m\ell^2 [3\dot{\phi}_1^2+\dot{\phi}_2^2+2\dot{\phi}_1\dot{\phi}_2 \cos(\phi_1-\phi_2)] \tag{4.39}$$

and the potential energy due to the spring constants, V, is

$$V = \frac{1}{2}c(2\phi_1^2 - 2\phi_1\phi_2 + \phi_2^2) \tag{4.40}$$

The generalized nonconservative forces are given by

$$Q_i^{NC} = \lambda\ell(1+\alpha\phi_2^2)\sin(\phi_1-\phi_2) - (b_1+b_2)\dot{\phi}_1+b_2\dot{\phi}_2 \tag{4.41}$$

and

$$Q_2^{NC} = b_2(\dot{\phi}_1-\dot{\phi}_2) \tag{4.42}$$

In writing the equation of motion it is found convenient to introduce the following nondimensional variables

$$\gamma = \sqrt{c/m\ell^2}\ t \tag{4.43a}$$

$$B_i = b_i/\ell\sqrt{cm} \qquad i = 1,2 \tag{4.43b}$$

$$F = \lambda\ell/c \tag{4.43c}$$

Substitution of Equations (4.39) through (4.43) into Equations (4.38) results in the nonlinear equations of motion

$$\begin{aligned} &3\ddot{\phi}_i + \ddot{\phi}_2\cos(\phi_1-\phi_2) + \phi_1^2\sin(\phi_1-\phi_2) \\ &+ 2\phi_1-\phi_2 + (B_1+B_2)\dot{\phi}_1-B_2\dot{\phi}_2 = F(1+\alpha\phi_2^2)\sin(\phi_1-\phi_2) \end{aligned} \tag{4.44a}$$

$$\begin{aligned} &\ddot{\phi}_2 + \ddot{\phi}_1\cos(\phi_1-\phi_2) - \phi_1+\phi_2-B_2\dot{\phi}_1+B_2\dot{\phi}_2 \\ &-\dot{\phi}_1^2\sin(\phi_1-\phi_2) = 0 \end{aligned} \tag{4.44b}$$

where the "dot notation" for derivatives now represents differentiation with respect to γ. If all the nonlinear terms in Equations (4.44) are set to zero, the linearized equations can be written in matrix form as

$$(4.45)\qquad \begin{bmatrix} 3 & 1 \\ 1 & 1 \end{bmatrix}\begin{bmatrix} \ddot{\phi}_1 \\ \ddot{\phi}_2 \end{bmatrix} + \begin{bmatrix} B_1+B_2 & -B_2 \\ -B_2 & B_2 \end{bmatrix}\begin{bmatrix} \dot{\phi}_1 \\ \dot{\phi}_2 \end{bmatrix} + \begin{bmatrix} 2 & -1 \\ -1 & 1 \end{bmatrix}\begin{bmatrix} \phi_1 \\ \phi_2 \end{bmatrix} = F \begin{bmatrix} 1 & -1 \\ 0 & 0 \end{bmatrix}\begin{bmatrix} \phi_1 \\ \phi_2 \end{bmatrix}$$

Following the notation of Reference 83, a steady-state solution of Equation (4.45) can be written

$$(4.46)\qquad \begin{bmatrix} \phi_1 \\ \phi_2 \end{bmatrix} = A\left(\begin{bmatrix} 1 \\ Z_a \end{bmatrix} \cos\Omega\gamma - \begin{bmatrix} 0 \\ Z_b \end{bmatrix} \sin\Omega\gamma\right)$$

where A, Z_a, and Z_b are constants, and Ω is the nondimensional linearized solution frequency. Equations (4.46) are substituted into Equations (4.45) and the coefficients of $\cos\Omega\gamma$ and $\sin\Omega\gamma$ set to zero to obtain a fourth order set of homogeneous equations in the unknown parameters Ω and F. By setting the determinant of the system equal to zero, a characteristic polynomial in Ω results. Reference 83 solves this polynomial and obtains the following linearized solution

$$(4.47a)\qquad \Omega_o^2 = (B_1+B_2)/(B_1+6B_2)$$

$$(4.47b)\qquad Z_a = 1-2\Omega_o^2(\Omega_o^2-1)/[(\Omega_o^2-1)^2+\Omega_o^2B_2^2]$$

$$(4.47c)\qquad Z_b = -2\Omega_o^3B_2/[(\Omega_o^2-1)^2+\Omega_o^2B_2^2]$$

$$(4.47d)\qquad F_o = (4B_1^2+33B_1B_2+4B_2^2)/2(B_1+B_2)(B_1+6B_2)+B_1B_2/2$$

4.4.2 Solution of the Nonlinear Problem by the Method of Imposed Disturbance

The total nonconservative work done over one period of motion, T, for the nonlinear system described by Equations (4.44) is

$$(4.48)\quad W^{NC} = \int_0^T \begin{bmatrix} \dot{\phi}_1 \\ \dot{\phi}_2 \end{bmatrix}^T \left(F \begin{bmatrix} f_1 \\ f_2 \end{bmatrix} - \begin{bmatrix} B_1+B_2 & -B_2 \\ -B_2 & B_2 \end{bmatrix} \begin{bmatrix} \dot{\phi}_1 \\ \dot{\phi}_2 \end{bmatrix} \right) d\gamma$$

where

$$(4.49)\quad \begin{bmatrix} f_1 \\ f_2 \end{bmatrix} = \begin{bmatrix} (1+\alpha\phi_2^{\,2})(\sin(\phi_1-\phi_2) \\ 0 \end{bmatrix}$$

Using Equations (4.46) as the imposed disturbance, the stability condition $W^{NC} = 0$ results in an equation which can be solved for F to get

$$(4.50)\quad F = \frac{C_1 \Omega}{C_2 - C_3 A^2}$$

where

$$C_1 = B_1 + B_2 - 2B_2 Z_a + B_2 Z_a^{\,2} + B_2 Z_b^{\,2}$$

$$C_2 = Z_a$$

$$C_3 = (A_a/8)[1-2Z_a+Z_a^{\,2}+Z_b^{\,2}+2\alpha(2Z_a-3Z_a^{\,2}-2Z_b^{\,2})]$$

Roorda and Nemat-Nasser compute W^{NC} treating Ω, Z_a and Z_b as unknowns. They enforce not only the condition $W^{NC} = 0$, but also two other nonlinear equations

derived from Hamilton's principle. Their procedure is equivalent to conserving energy in the limit cycle (to obtain A) and requiring that the equations of motion be satisfied (to get Ω, Z_a, and Z_b).

The method of imposed disturbances requires only that the condition $W^{NC} = 0$ is satisfied where W^{NC} is a function of some appropriate response mode; i.e., imposed disturbance. Numerical values for this problem can be obtained if $B_1 << B_2 << 1$, products of B_1 and B_2 are small, and if $\beta \equiv B_1/B_2$ is given. For $\beta = 10$, Equation (4.50) is used to compute $F = F(A)$ where Ω, Z_a, Z_b are the linearized values obtained from Equations (4.47). The expression for $\alpha = 1/2$ is

$$F = 24.34/(11.67+88.61A^2) ,$$

and for $\alpha = 0$ it is

$$F = 24.34/(11.67-28.25A^2)$$

The results are shown in Figure 40 and compared to those of Reference 83. For $\alpha = 1/2$ the system has what was termed in Chapter 3 as "soft nonlinearity." A "hard nonlinearity" occurs when $\alpha = 0$. The results of both methods agree quite well especially below amplitudes of about 0.3.

4.5 HYPERSONIC PANEL FLUTTER STUDY

An elastic panel subjected to hypersonic airflow over one side can, under certain combinations of flow and structural parameters, undergo large, destabilizing

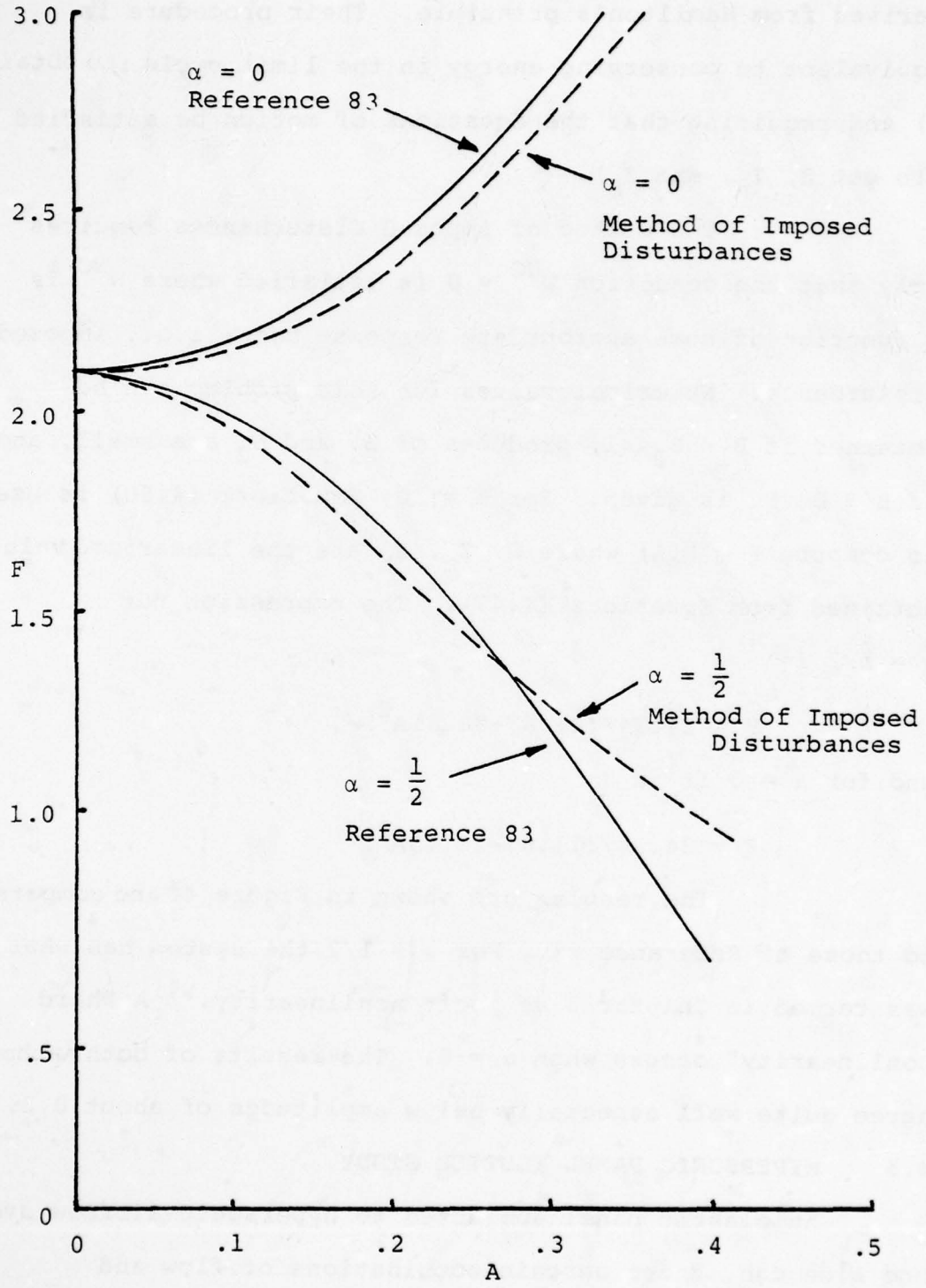

Figure 40. Load-Amplitude Relationship for Two-Degree-of-Freedom Follower Load Problem.

oscillations. In this section, an elastic panel of infinite span is studied in two-dimensional nonlinear hypersonic flow. The panel is mounted on a viscoelastic foundation. Boundary conditions are simple-suuports and an edge compression less than the static buckling load is allowed. Only aerodynamic nonlinearities are included. The Galerkin method is used to arrive at a system of ordinary nonlinear equations. A static subcase solution of the method of imposed disturbances is compared to numerical integration, and it is shown that both methods predict similar load-amplitude curves. It is then shown how the method of imposed disturbances can be used to perform parametric studies. The parameter selected is the foundation stiffness, and it is shown that great computational efficiency can be achieved using the method of imposed disturbances compared to multiple time history solutions.

4.5.1 Galerkin Solution of Panel Equation

The simply supported sandwich panel of length ℓ is shown in the sketch on the next page. A hypersonic air flow is loading the upper surface of the panel. A compressive force is applied to the ends and the lower surface is mounted on a viscoelastic foundation The structural properties of the panel are the bending stiffness, D, and the mass density, m. The book by Allen[94] gives expressions for D in terms of sandwich geometric and

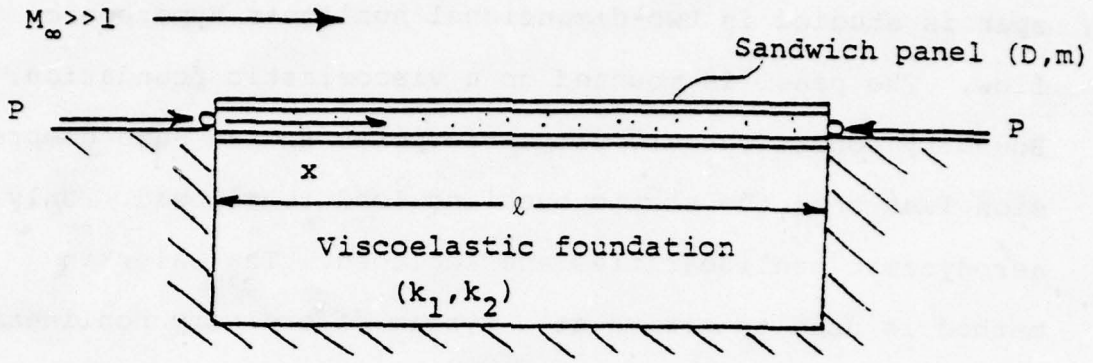

material properties. It will be sufficient for the purposes herein to state that a set of design variables such as face sheet thickness, core thickness, and elastic material constants can be used to define all the structural parameters. The results presented are for non-dimensional groupings of constants, and if needed, these terms can be expressed as functions of the basic sandwich panel properties. Such a procedure is necessary to solve a specific sandwich panel flutter problem, but it does not add further insight into the development of the method of imposed disturbances.

The governing nonlinear, partial differential equation for the panel is

$$Dw_{xxxx} + Pw_{xx} + mw_{tt} = -\frac{2q}{M_\infty}\left[w_x + \frac{1}{V_\infty} w_t + \frac{\kappa+1}{4} M_\infty \left(w_x^2 + \frac{2}{V_\infty} w_x w_t\right)\right] - k_1 w - k_2 w_t \tag{4.51}$$

where w is the transverse deflection of the panel, P is the compressive edge load, q is the dynamic pressure of the

airstream, M_∞ is the free-stream Mach number, V_∞ is the free-stream velocity, κ is the ratio of specific heats (1.4 for air), and k_1 and k_2 are the elastic and damping constants of the foundation. The subscripts x and t denote partial differentiation with respect to the streamwise coordinate and time, respectively. The left side of Equation (4.51) is derived from elementary beam theory, and the left side airloading terms come from a modified second order piston theory expansion[95] for the pressure. McIntosh[69] states that the nonlinear terms w_x^2 and $w_x w_t$ are the two most important for hypersonic flow.

It is convenient to introduce the following nondimensional variables

$$\xi = x/\ell$$

$$\tau = \sqrt{D/M_\infty \ell^4}\, t$$

$$\bar{w} = w/\ell$$

$$\bar{\mu} = \sqrt{\ell \rho_\infty / m M_\infty}$$

$$\bar{k}_1 = \ell^4 k_1 / D$$

$$\bar{k}_2 = \sqrt{\ell^4/mD}\; k_2$$

$$\bar{P} = \ell^2 P/D$$

$$\lambda = \sqrt{\ell^3 \rho_\infty V_\infty^2 / D M_\infty}$$

$$\bar{M} = (\kappa+1) M_\infty / 4$$

so Equation (4.51) becomes in nondimensional form

$$\bar{w}_{\xi\xi\xi\xi} + \bar{P}\,\bar{w}_{\xi\xi} + \bar{k}_1\bar{w} + \bar{k}_2\bar{w}_\tau + \bar{w}_{\tau\tau} \tag{4.52a}$$
$$= -\lambda^2(\bar{w}_\xi + \bar{M}\,\bar{w}_\xi^2) - \lambda\bar{\mu}(\bar{w}_\tau + 2\bar{M}\,\bar{w}_\xi\bar{w}_\tau)$$

on $0<\xi<1$. The boundary conditions for the simply supported condition are

$$\bar{w} = 0 \qquad \text{at } \xi = 0,1 \tag{4.52b}$$

$$\bar{w}_{\xi\xi} = 0 \tag{4.52c}$$

The Galerkin solution (see Chapter 6 of Reference 93, for example) has the form

$$\bar{w}(\xi,\tau) = \sum_{j=1}^{N} q_j(\tau)\sin j\pi\xi \tag{4.53}$$

where q_j are as yet undetermined functions. The terms $\sin j\pi\xi$ are seen to satisfy all the boundary conditions for the problem. Equation (4.53) is substituted into Equation (4.52a), the result is premultiplied by $\sin i\pi\xi$, and an integration on ξ from 0 to 1 is performed. The resulting N equations are

$$\sum_{j=1}^{N} (j^4\pi^4 - \bar{P}\, j^2\pi^2 + \bar{k}_1)\, I_{ij}^{(1)} q_j + \sum_{j=1}^{N} \bar{k}_2\, I_{ij}^{(1)} \dot{q}_j$$

$$+ \sum_{j=1}^{N} I_{ij}^{(1)} \ddot{q}_j = \sum_{j=1}^{N} (-\lambda^2 j\pi) I_{ij}^{(2)} q_j + \sum_{j=1}^{N} (-\lambda\bar{\mu}) I_{ij}^{(1)} \dot{q}_j$$

(4.54)

$$+ \sum_{j=1}^{N} \sum_{k=1}^{N} (-\lambda^2 \bar{M}\, jk\pi^2)\, I_{ijk}^{(3)} q_j q_k$$

$$+ \sum_{j=1}^{N} \sum_{k=1}^{N} (-2\lambda\bar{\mu}\, \bar{M} j\pi)\, I_{ijk}^{(4)} q_j \dot{q}_k$$

The Galerkin integrals $I_{ij}^{(1)}$, $I_{ij}^{(2)}$, $I_{ijk}^{(3)}$, and $I_{ijk}^{(4)}$ are defined in Appendix B. It is shown that $I_{ij}^{(1)}$ is equal to $\frac{1}{2}\delta_{ij}$ where δ_{ij} is the Kronecker delta. This expression for $I_{ij}^{(1)}$ is incorporated into the first order equations which follow. Let

(4.55a) $$x_i = q_i$$

and

(4.55b) $$x_{i+N} = \dot{q}_i$$

so Equations (4.54) have the final form

$$\dot{x}_i = x_{i+N}$$

$$\dot{x}_{i+N} = -(k_2+\lambda\pi)\,x_{i+N} - (\pi^4 i^4 - \bar{r}\pi^2 i^2 + \bar{k}_1)\,x_i$$

$$-2\lambda^2\pi \sum_{j=1}^{N} j\, I^{(2)}_{ij}\, x_j$$

(4.56)

$$-2\lambda^2\bar{M}\pi^2 \sum_{j=1}^{N}\sum_{k=1}^{N} j\,k\, I^{(3)}_{ijk}\, x_j\, x_k$$

$$-4\lambda\overline{\mu M}\pi \sum_{j=1}^{N}\sum_{k=1}^{N} j\, I^{(4)}_{ijk}\, x_j\, x_{k+N}$$

Equations (4.56) total 2N in number and can be solved by numerical integration.

4.5.2 Calculations of Nonconservative Work

The total nonconservative work done on the panel by the hypersonic flow and the viscoelastic foundation during one period of steady-state motion is

$$W^{NC} = -\lambda^2 J^{(1)} - \lambda^2\bar{M}J^{(2)} - \lambda\bar{\mu}J^{(3)} - 2\lambda\overline{\mu M}J^{(4)} - \bar{k}_2 J^{(3)} \tag{4.57}$$

where

$$J^{(1)} = \int_0^T \int_0^1 \bar{w}_\xi \bar{w}_\tau \, d\xi d\tau \tag{4.58a}$$

$$J^{(2)} = \int_0^T \int_0^1 \bar{w}_\xi^2 \, \bar{w}_\tau \, d\xi d\tau \tag{4.58b}$$

$$J^{(3)} = \int_0^T \int_0^1 \bar{w}_\tau^2 \, d\xi d\tau \tag{4.58c}$$

$$J^{(4)} = \int_0^T \int_0^1 \bar{w}_\xi \bar{w}_\tau^2 \, d\xi d\tau \tag{4.58d}$$

Using the Galerkin solution Equation (4.53), these integrals can be rewritten as

$$(4.59a) \qquad J^{(1)} = \pi \sum_{i=1}^{N} \sum_{j=1}^{N} j \, I_{ij}^{(2)} \, K_{ij}^{(1)}$$

$$(4.59b) \qquad J^{(2)} = \pi^2 \sum_{i=1}^{N} \sum_{j=1}^{N} \sum_{k=1}^{N} j \, k \, I_{ijk}^{(3)} \, K_{ijk}^{(2)}$$

$$(4.59c) \qquad J^{(3)} = \frac{1}{2} \sum_{i=1}^{N} K_i^{(3)}$$

$$(4.59d) \qquad J^{(4)} = \pi \sum_{i=1}^{N} \sum_{j=1}^{N} \sum_{k=1}^{N} j \, I_{ijk}^{(4)} \, K_{ijk}^{(4)}$$

where

$$(4.60a) \qquad K_{ij}^{(1)} = \int_0^T \dot{q}_i \, q_j \, d\tau$$

$$(4.60b) \qquad K_{ijk}^{(2)} = \int_0^T \dot{q}_i \, q_j \, q_k \, d\tau$$

$$(4.60c) \qquad K_i^{(3)} = \int_0^T \dot{q}_i^{\,2} \, d\tau$$

$$(4.60d) \qquad K_{ijk}^{(4)} = \int_0^T \dot{q}_i \, q_j \, \dot{q}_k \, d\tau$$

4.53 Application of the Method of Imposed Disturbances

Let the generalized coordinates, q_i, have the form

$$(4.61) \qquad q_i(\tau) = A\Psi_i(\tau)$$

where A is an undetermined amplitude parameter and Ψ is an appropriate imposed disturbance. Equation (4.57) can now be written

$$-W^{NC}/A^2 = T_1 A + T_2 \tag{4.61}$$

where

$$T_1 = \lambda^2 \bar{M}\, J^{(2)} + 2\lambda\bar{\mu}\, \bar{M}\, J^{(4)} \tag{4.62a}$$

$$T_2 = \lambda^2\, J^{(1)} + \lambda\bar{\mu}\, J^{(3)} + \bar{k}_2\, J^{(3)} \tag{4.62b}$$

and the J quantities are evaluated using the K integrals of Equations (4.60) which have the q's replaced by Ψ's.

At steady state motion, $W^{NC} = 0$, and $\lambda = \Lambda$ and so Equation (4.61) is solved to get A in terms of Λ and the system variables to get

$$A(\Lambda) = -T_2(\Lambda)/T_1(\Lambda) \tag{4.63}$$

To determine the function explicitly, it is now necessary to select an imposed disturbance, $\vec{\Psi}$. The components of the imposed disburbance are selected to be the steady-state solution

$$\Psi_i = a_i \sin\gamma \qquad i=1,N \tag{4.64}$$

where $\gamma = \omega\tau$. Substitution of these quantities into Equations (4.60) for the q terms gives

$$K_{ij}^{(1)} = 0 \tag{4.65a}$$

$$K_{ijk}^{(2)} = 0 \tag{4.65b}$$

$$K_i^{(3)} = \pi\omega a_i^2 \qquad i=1,N \tag{4.65c}$$

$$K_{ijk}^{(4)} = 0 \tag{4.65d}$$

and thus by Equations (4.52)

$$T_1 = 0 \tag{4.66a}$$

and

$$T_2 = (\pi\omega/2)(\lambda\bar{\mu}+\bar{k}_2)\sum_{i=1}^{N} a_i^2 \tag{4.66b}$$

Substitution of T_1 and T_2 into Equation (4.61) gives the result

$$W^{NC} = -(\pi\omega A^2/2)(\lambda\bar{\mu}+\bar{k}_2)\sum_{i=1}^{N} a_i^2 < 0 \tag{4.67}$$

This implies that there is no steady-state, limit cycle type instability based on the selected imposed disturbance, Equation (4.64). It will be shown in the next subsection that the static subcase of the method of imposed disturbances does lead to an amplitude dependent instability which occurs at zero frequency.

4.5.4 The Static Subcase of Nonlinear Panel Instability

The case of static instability is now checked. As the starting point, assume

$$\bar{w} = \bar{w}(\xi) = \sum_{j=1}^{N} q_j \sin j\pi\xi \tag{4.68}$$

where the q's are constants. Application of the Galerkin method as shown in Section 4.5.1 leads to the following system of nonlinear algebraic equations

$$\pi^4 \sum_{j=1}^{N} j^4 q_j I_{ij}^{(1)} - \bar{P}\pi^2 \sum_{j=1}^{N} j^2 q_j I_{ij}^{(1)}$$

$$+ \bar{k}_1 \sum_{j=1}^{N} q_j I_{ij}^{(1)} + \lambda^2 \pi \sum_{j=1}^{N} j q_i I_{ij}^{(2)} \tag{4.69}$$

$$+ \lambda^2 \bar{M} \pi^2 \sum_{j=1}^{N} \sum_{k=1}^{N} j k q_j q_k I_{ijk}^{(3)} = 0$$

For N=1, these nonlinear force balance equations reduce to

$$\Sigma F = -f_s + f_a = 0 \tag{4.70a}$$

where the restoring force, f_s, is

$$f_s = \frac{1}{2}(\pi^4 - \pi^2\bar{P} + \bar{k}_1)\, q_1 \tag{4.70b}$$

and the applied load due to the flow is

$$f_a = -\frac{2}{3} \lambda^2 \bar{M}\pi q_1^2 \tag{4.70c}$$

Solving equations (4.70) for q_1 gives

$$q_1 = -3(\pi^4 - \pi^2\bar{P} + \bar{k}_1)/4\lambda^2\bar{M}\,\pi \tag{4.71}$$

This last equation is an approximation to the required load-amplitude plot. It is seen that for $\bar{P}<\pi^2$ (the critical Euler buckling load), q_1 will be negative. Thus for any other q_1, e.g., q_1^* such that $q_1^*<q_1<0$, there will be a force imbalance in Equation (4.70a) and the panel will collapse inward. Such a failure mode is noted by McIntosh.[69]

4.5.5 Numerical Results

The results of a computer analysis of the hypersonic panel are now presented. The code performs a Kutta-Merson numerical integration of the equations of motion, Equations (4.56), and has the following graphical output displays available:

(1) Phase plane plots for any point on the panel ($\bar{w}_\tau$ vs. $\bar{w}$ at a specified point)

(2) Time history of displacement and velocity at a given point ($\bar{w}$, $\bar{w}_\tau$ vs. τ at a point)

(3) Mode shape plots at a given time ($\bar{w}$ vs. ξ at a given τ)

(4) Time history of the total work done by the external forces acting on the panel. This quantity, which is denoted by WTD on the plots, can be integrated over one cycle of motion to get the total nonconservative work, W^{NC}, given by Equation (4.57).

The code allows for up to 10 modes (N=10) in the Galerkin solution.

A separate code solves the nonlinear force balance equations (Equations 4.69)) by a standard Newton-Raphson method (see Ralston,[96] Chapter 8, for example) to get a set of q's. These particular q's are referred to as $Q_1, Q_2, \ldots, Q_N$ and can be written as

$$Q_i = A\Psi_i \tag{4.72}$$

where A is the maximum Q_i and Ψ_i are normalized constants. The Ψ's are input into the Kutta-Merson integration program as initial displacement conditions. By selecting various A values at the given λ values, a stability boundary can be determined which gives the $\lambda = \Lambda(A)$ curve. It is shown that the value of A predicted by the Newton-Raphson method agrees quite well with the one obtained parametrically in the Kutta-Merson code.

Figures 41 through 44 show typical stable panel motions (Case 1). Data for this case is given on the phase plane plot of Figure 41. In Figure 42, the time histories of w and w_τ are shown. The entire panel mode shape at $\tau = 0$ is given in Figure 43 which is followed by the work input time history. These plots, taken together, show that the panel is stable at an amplitude level of -.04.

Typical stable motion for N=2 is shown in Figures 45 and 46. At an amplitude level of -.04 the motion is stable as evidenced by the phase plane plot (Figure 43) and work input time history (Figure 46). By just changing the amplitude to -.0588, the unstable Case 3 phase plane plot is obtained in Figure 47. The work input is clearly shown to be increasing in the time history of Figure 48.

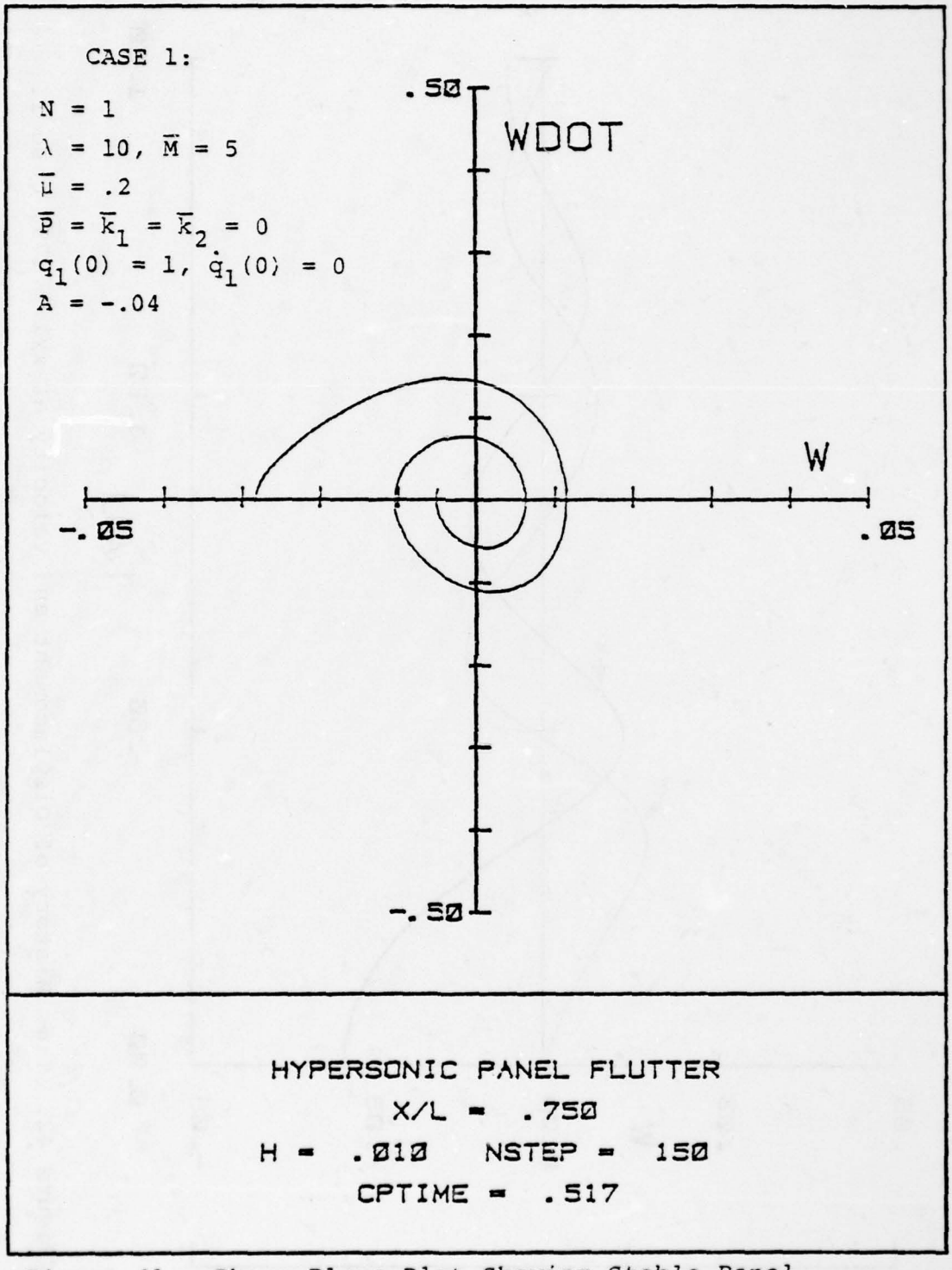

Figure 41. Phase Plane Plot Showing Stable Panel Motion, Case 1.

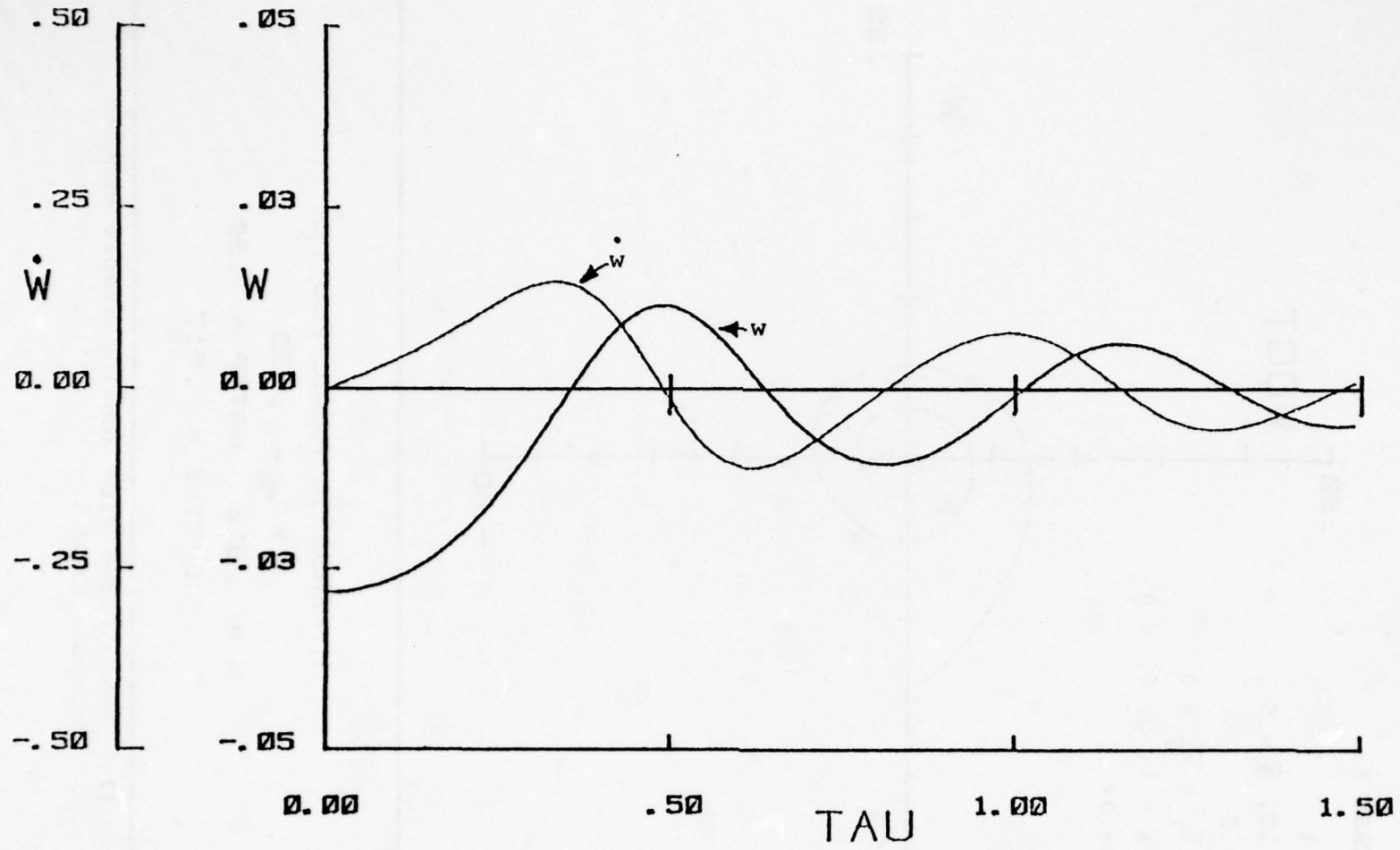

Figure 42. Time History of Displacement and Velocity at x/ℓ = .75, Case 1.

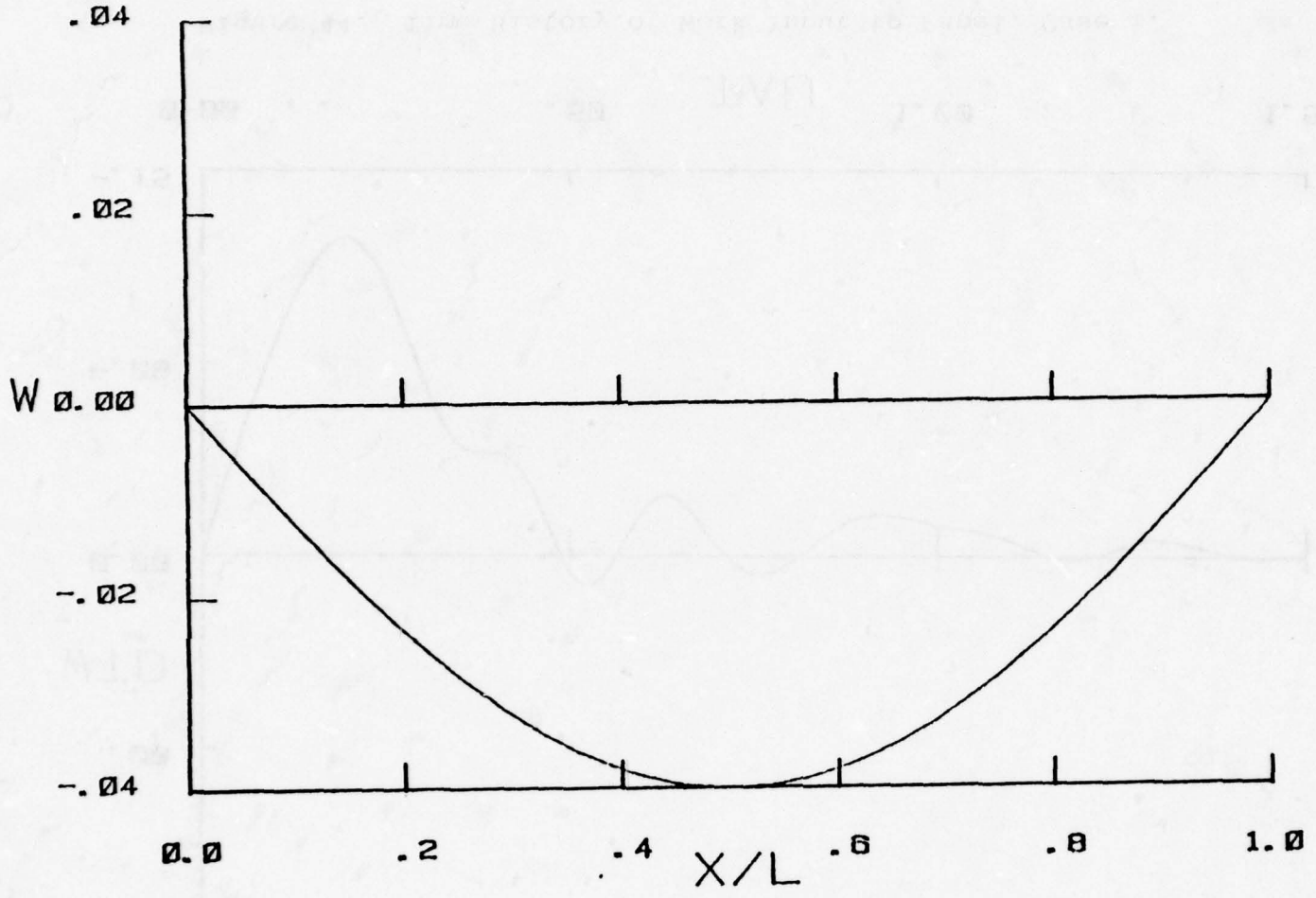

Figure 43. Panel Mode Shape at $\tau \approx 0$, Case 1.

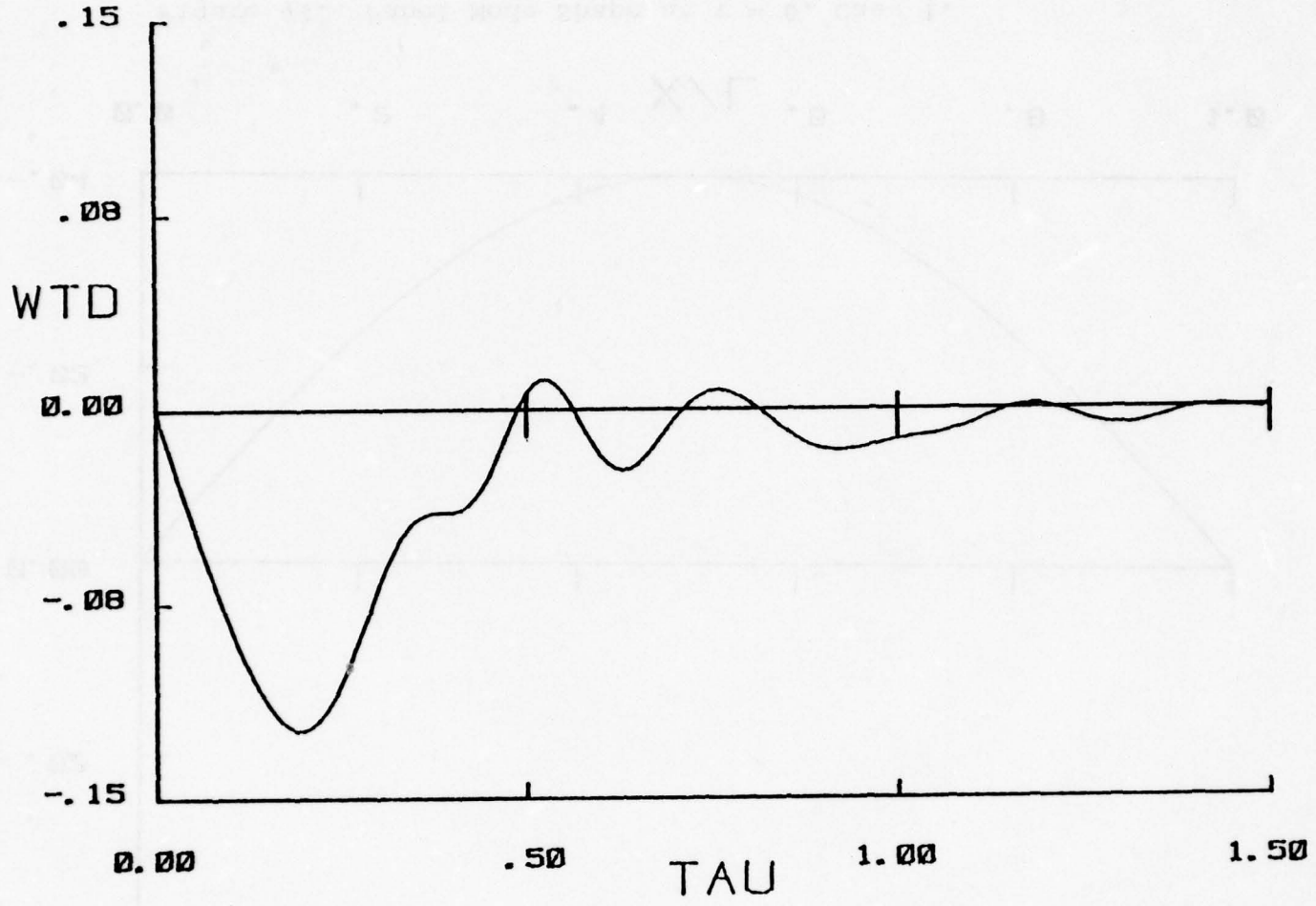

Figure 44. Time History of Work Input to Panel, Case 1.

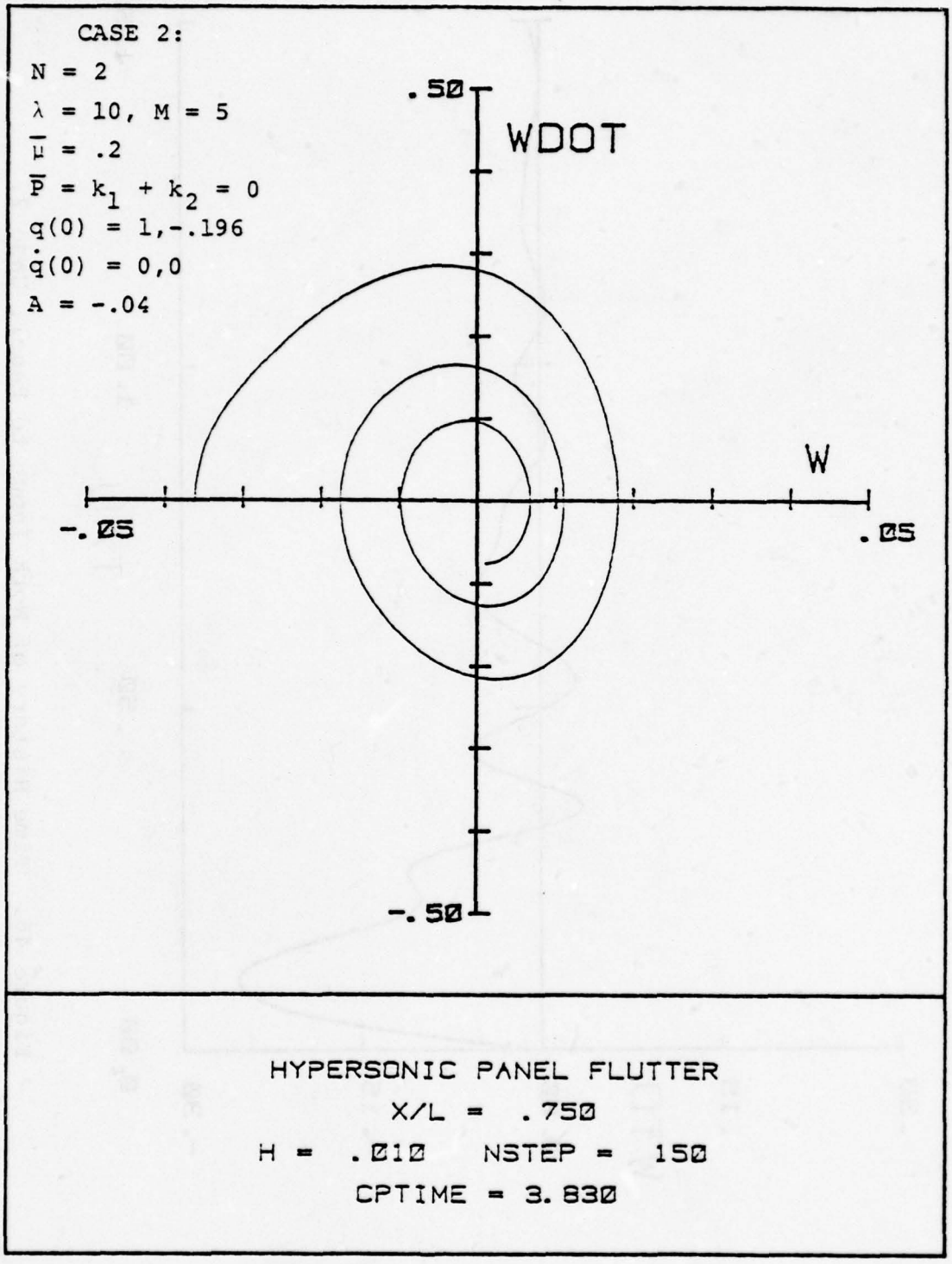

Figure 45. Phase Plane Plot Showing Stable Panel Motion, Case 2.

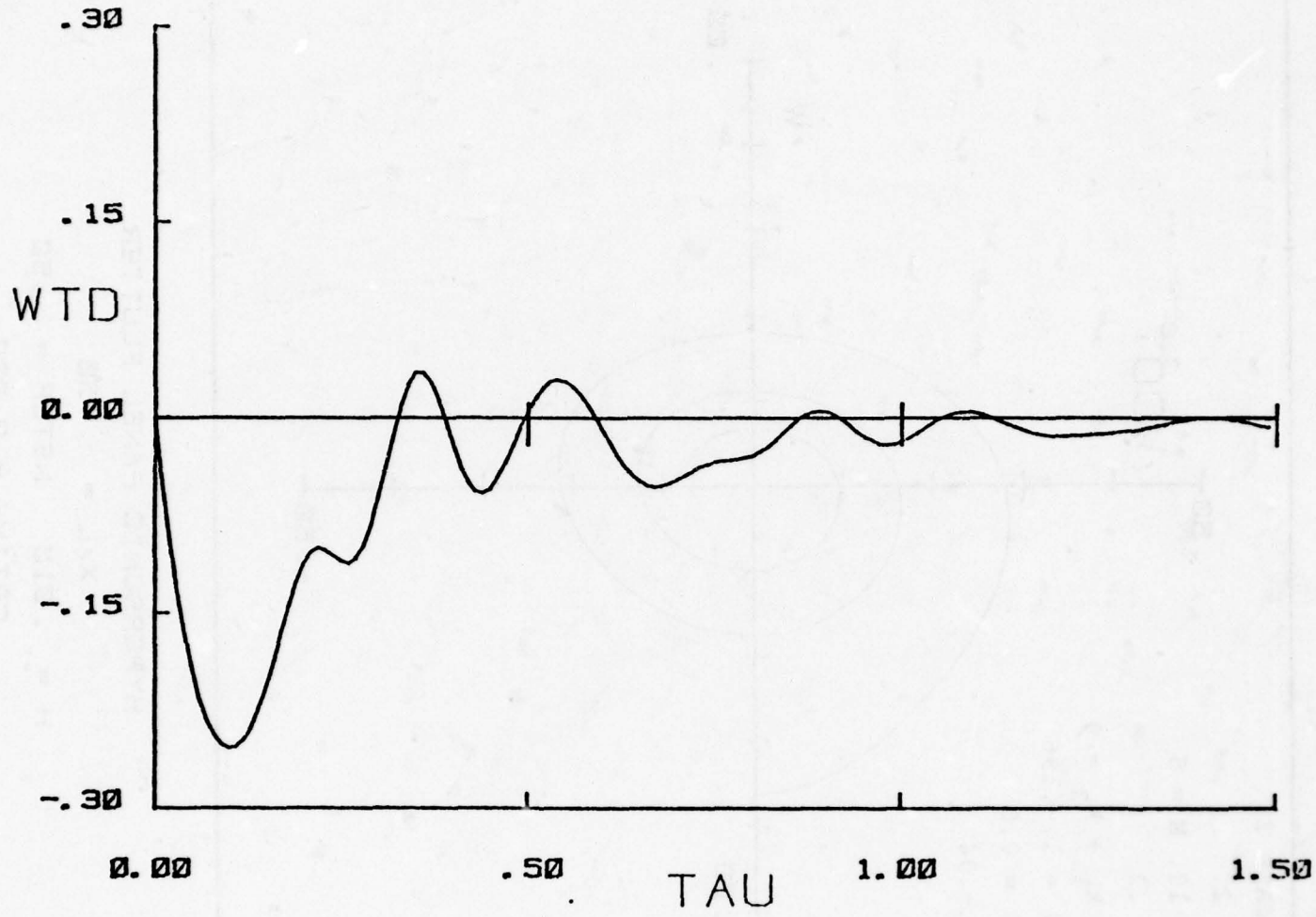

Figure 46. Time History of Work Input to Panel, Case 2.

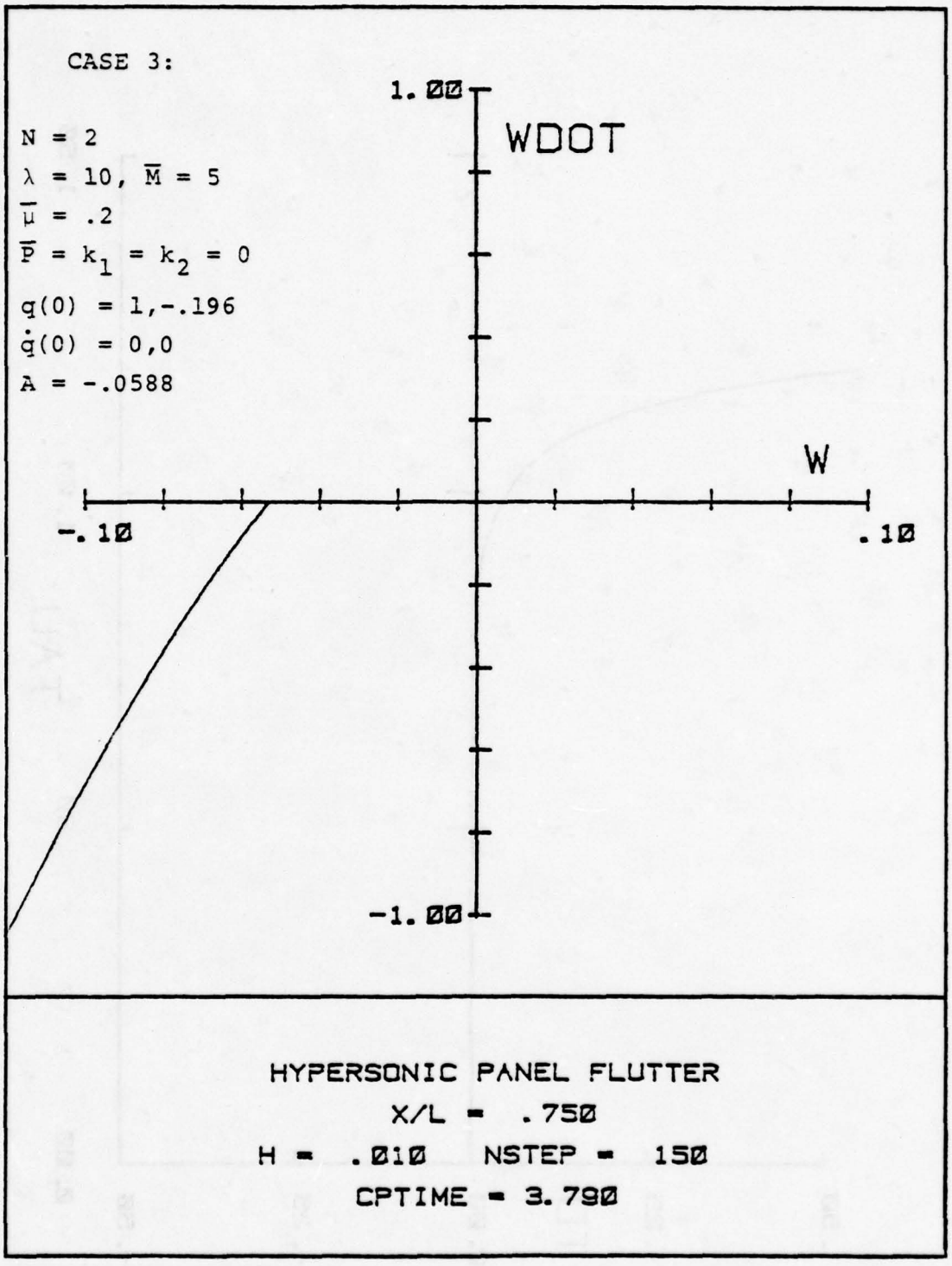

Figure 47. Phase Plane Plot Showing Unstable Panel Motion, Case 3.

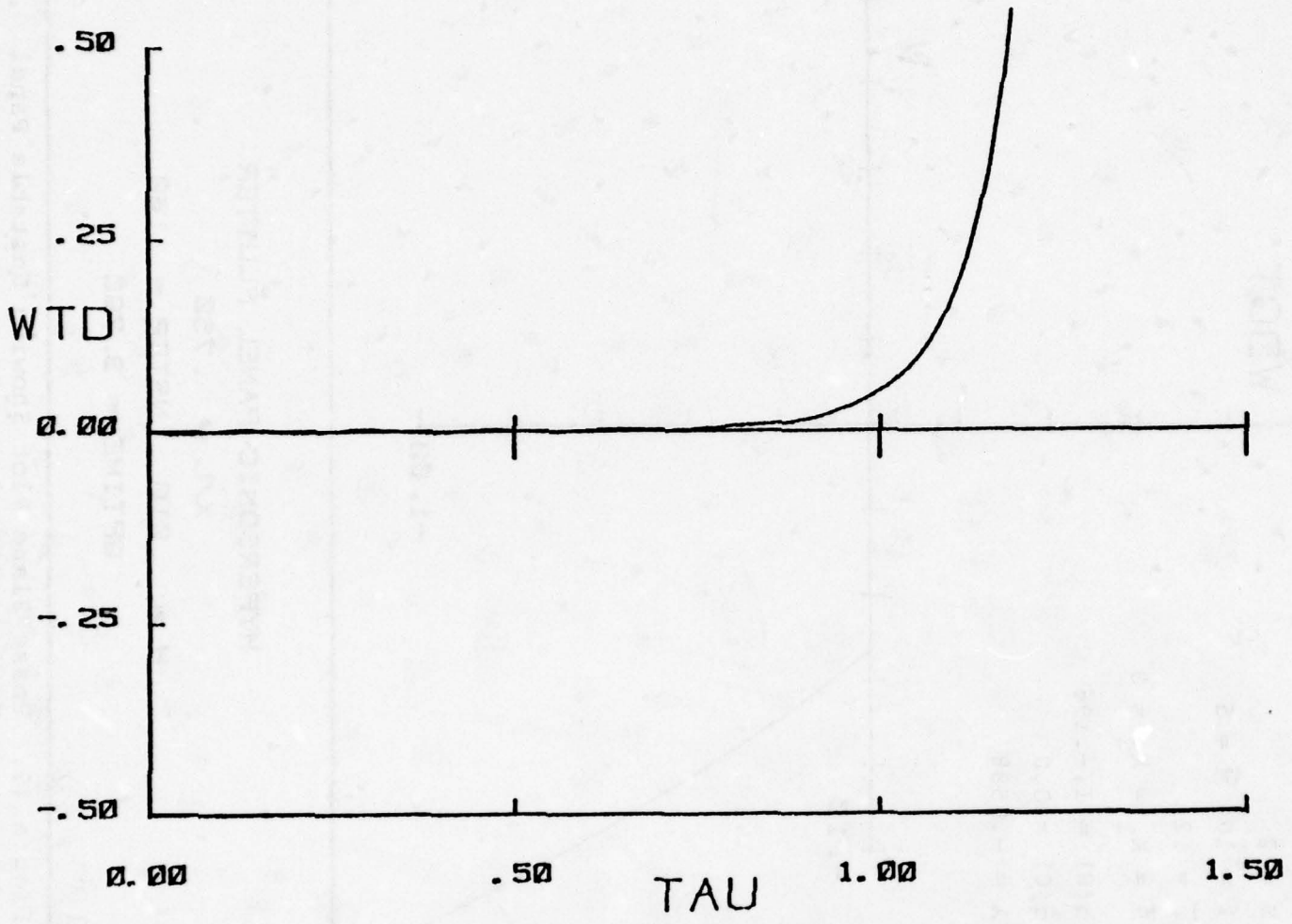

Figure 48. Time History of Work Input to Panel, Case 3.

Table 6 shows a systematic variation of all the parameters. The static subcase of the method of imposed disturbances is used to generate Ψ_1, Ψ_2, and the amplitude A_{ID}. The normalized terms Ψ_1, Ψ_2 are treated as imposed displacements in the time history solution. These conditions are then scaled until the motion is neutrally stable. The scale factor computed by Kutta-Merson integration is A_{KM} and is shown in the last column of Table 6. The effect of edge compression is seen to lower the amplitude at which the system first becomes unstable. On the other hand, increasing the stiffness of the foundation has the beneficial effect of increasing the amplitude. Foundation damping is shown to have little effect on amplitude. Increasing the Mach number parameter, $\overline{M}$, lowers the critical amplitude but the mass ratio, $\overline{\mu}$, variation has no effect. In all cases shown in Table 6, the method of improved disturbances and Kutta-Merson integration give very comparable results.

The relative computing efficiency of these methods is shown in Tables 7 and 8. Table 6 shows the normalized imposed disturbances, the amplitude parameter, and the computing time needed to solve the N=4 static equation by the Newton-Raphson procedure. Table 7 shows results for numerical integration using the predicted disturbances and two selected amplitudes, A_1 and A_2. The first is slightly lower than A_{ID} and the second slightly

TABLE 6

COMPARISON OF METHOD OF IMPOSED DISTURBANCES
AND KUTTA-MERSON INTEGRATION

$\lambda = 10$, $N = 2$

$\bar{M}$	$\bar{P}$	$\bar{k}_1$	$\bar{k}_2$	$\bar{\mu}$	Ψ_1	Ψ_2	A_{ID}	A_{KM}
4	0	0	0	.2	1	-.196	-.0735	-.074
5	0	0	0	.2	1	-.196	-.0588	-.059
6	0	0	0	.2	1	-.196	-.0490	-.050
7	0	0	0	.2	1	-.196	-.0420	-.043
5	2	0	0	.2	1	-.204	-.0511	-.052
5	4	0	0	.2	1	-.213	-.0437	-.044
5	6	0	0	.2	1	-.222	-.0365	-.037
5	8	0	0	.2	1	-.233	-.0295	-.030
5	0	20	0	.2	1	-.196	-.0667	-.067
5	0	40	0	.2	1	-.197	-.0745	-.075
5	0	60	0	.2	1	-.198	-.0823	-.083
5	0	80	0	.2	1	-.200	-.0900	-.091
5	0	0	.25	.2	1	-.196	-.0588	-.059
5	0	0	.50	.2	1	-.196	-.0588	-.059
5	0	0	.75	.2	1	-.196	-.0588	-.059
5	0	0	1.00	.2	1	-.196	-.0588	-.059
5	0	0	0	.05	1	-.196	-.0588	-.059
5	0	0	0	.10	1	-.196	-.0588	-.059
5	0	0	0	.30	1	-.196	-.0588	-.059

TABLE 7

METHOD OF IMPOSED DISTURBANCES
FOUNDATION STIFFNESS STUDY
$N=4$, $\bar{M}=5$, $\bar{\mu}=.2$, $\bar{P}=\bar{k}_2=0$, $\bar{k}_1=40$

λ	Ψ_1	Ψ_2	Ψ_3	Ψ_4	A_{ID}	CP Time (sec)
5	1.0	-.04661	.02855	-.00275	-.29213	.039
6	1.0	-.06722	.03970	-.00401	-.20583	.043
8	1.0	-.12030	.03443	-.00748	-.12235	.045
10	1.0	-.19054	.04410	-.01274	-.08598	.042
12	1.0	-.28087	.06087	-.02072	-.06693	.058
14	1.0	-.39517	.08705	-.03233	-.05427	.050
16	1.0	-.53671	.12576	-.04821	-.04387	.048
18	1.0	-.70736	.18192	-.06919	-.03482	.042

TABLE 8

KUTTA-MERSON NUMERICAL INTEGRATION
FOUNDATION STIFFNESS STUDY
$N=4$, $\bar{M}=5$, $\bar{\mu}=.2$, $\bar{P}=\bar{k}_2=0$, $\bar{k}_1=40$

λ	A_1	A_2	Comment	CP Time (sec)
5	-.291	-.293	S/U	62.889
6	-.205	-.207	S/U	62.594
8	-.122	-.123	S/U	62.548
10	-.085	-.087	S/U	58.121
12	-.066	-.068	S/U	61.056
14	-.054	-.055	S/U	53.908
16	-.043	-.044	S/U	52.239
18	-.034	-.036	S/U	50.650

higher. The comment column of Table 8 shows that the lower A produces stable motion (S) and the higher gives unstable motion (U). Thus the instability is bracketed in amplitude. Comparing the computing times, it can be seen that for this problem the method of imposed disturbances is almost 2000 times faster than numerical integration and has equivalent accuracy in predicting load-amplitude behavior.

Figure 49 shows the load-amplitude plots N=1,2,3 and 4. In all cases the method of imposed disturbances and numerical integration give good agreement for amplitudes above .05. Below this amplitude, the method of imposed disturbances should be supplemented by a linear flutter analysis which predicts the N=2, low amplitude flutter very accurately.

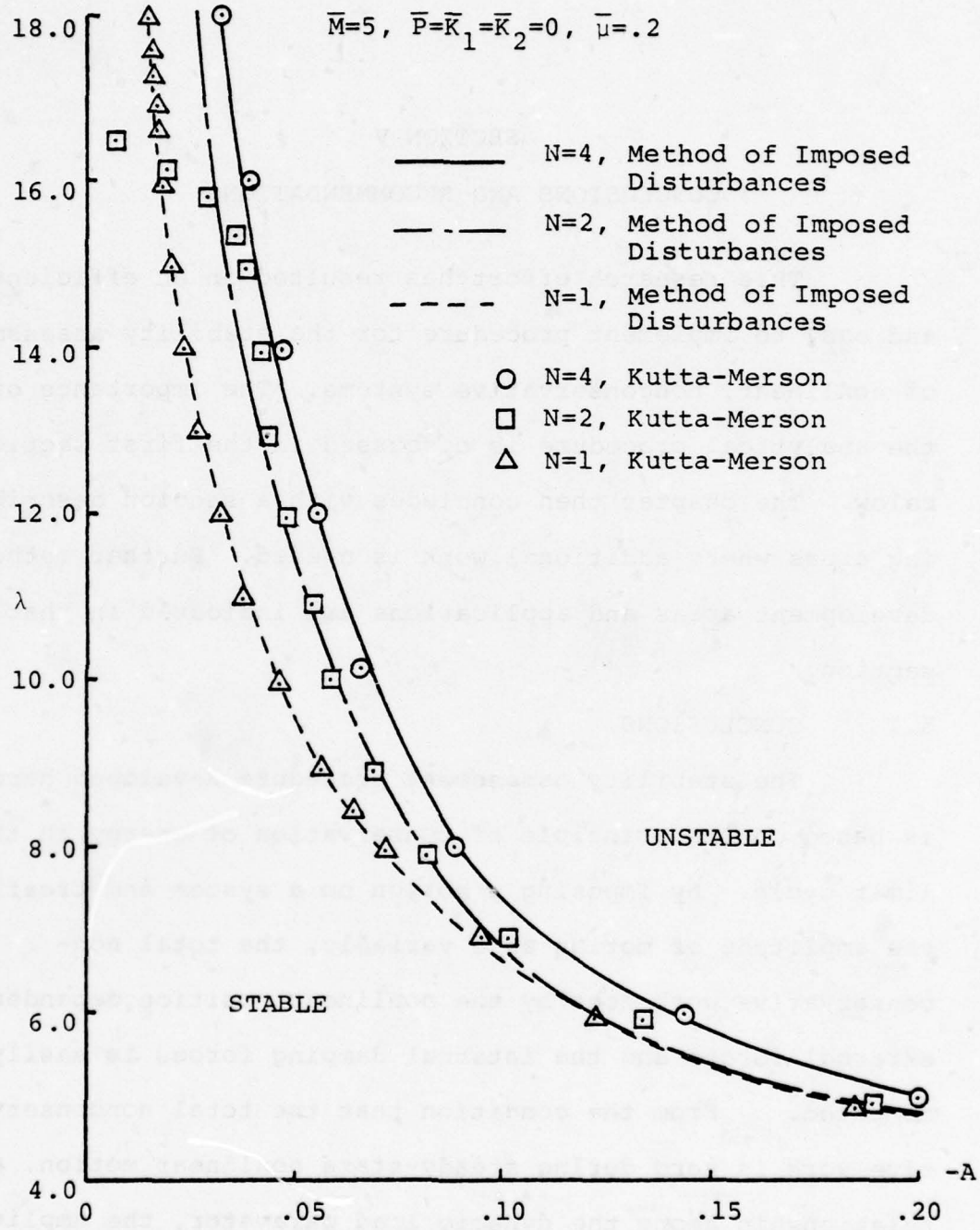

Figure 49. Load-Amplitude Plot for Hypersonic Panel.

SECTION V

CONCLUSIONS AND RECOMMENDATIONS

This research effort has resulted in an efficient and easy to implement procedure for the stability assessment of nonlinear, nonconservative systems. The importance of the analytical procedure is discussed in the first section below. The chapter then concludes with a section describing areas where additional work is needed. Further method development areas and applications are indicated in that section.

5.1 CONCLUSIONS

The stability assessment procedure developed herein is based on the principle of conservation of energy in the limit cycle. By imposing a motion on a system and treating the amplitude of motion as a variable, the total nonconservative work done by the nonlinear position dependent external forces and the internal damping forces is easily computed. From the condition that the total nonconservative work is zero during steady-state nonlinear motion, a relationship among the dynamic load parameter, the amplitude of motion, and the system variables can be established.

Such information is required in order to perform optimization studies on nonlinear systems.

The method of imposed disturbances has a clear advantage over current analytical methods for the following reasons:

- a definite answer to the stability question is obtained,
- numerical instability problems associated with time history solutions are avoided,
- an explicit analytical form for the external forces is not required,
- nonlinear transonic flutter studies can be performed without coupling the aerodynamic calculations to the structural equations,
- the method is applicable to nonlinear external loadings containing both circulatory and dissipative forces.

These positive aspects of the method plus its computational efficiency make it a prime candidate for inclusion in an automated design procedure where a structure or structural component is subjected to nonlinear, nonconservative forces. The procedure developed herein is a key analytic tool which makes the optimization of nonlinear systems feasible.

A static subcase of the method of imposed disturbances is applicable when the external forces contain terms

which are independent of velocity. By solving nonlinear static force balance equations, a relationship between the load parameter and the amplitude of the deformation can be established. The solution of the nonlinear static equations is much more economically obtained than the time history results when the prime mode of instability is static in nature.

5.2 RECOMMENDATIONS

Further work is needed to demonstrate the applicability of the method to lifting surface flutter problems. The method is shown herein to give good qualitative results for transonic pitch flutter, but applications are now needed for multiple degree-of-freedom airfoils in transonic flow. The effect of structural nonlinearities now needs also to be included in the analysis. Such applications present no conceptual difficulty for the method of imposed disturbances, and this work can be accomplished in a straightforward manner.

The hypersonic panel flutter application needs to be studied further. Alternate imposed disturbances should be used to calculate the nonconservative work to determine under what conditions oscillations with finite periods can be sustained. The effect of large panel deflections should also be included. In all cases presented the edge compression is kept below its Euler buckling value, and further

studies are now needed at higher edge loadings to determine the relationship between the static and dynamic instability phenomena.

The method needs further development to establish a relationship between the initial conditions and the critical amplitude of motion. In this way, critical initial velocities and displacements can be included in the design process. Such considerations are seen to be important in order to consider gust loadings and other transient aerodynamic phenomena.

Theoretical work is needed to develop criteria for the selection of imposed disturbances. In the problems reported herein, satisfactory results are obtained using solutions to the linearized system. The method can also be applied using steady-state solutions to the nonlinear problem. It appears feasible to develop an imposed disturbance method using multiple disturbances to define the load-amplitude plot in a piecewise manner. Time history solutions at selected amplitudes should be performed to aid in the selection of imposed disturbances.

From a design standpoint, the key results of this study are that the addition of system damping is more important than stiffness or mass changes in alleviating limit cycle instability. For systems which exhibit

nonlinear static instabilities, stiffness variables are of prime importance. These trends need to be verified further by additional applications to airfoil flutter and divergence problems.

LIST OF REFERENCES

1. Fung, Y. C. An Introduction to the Theory of Aeroelasticity. New York: Dover Publications, 1969.

2. Tijdeman, H. "Investigation of the Transonic Flow Around Oscillating Airfoils." Dissertation, Technological University Delft, The Netherlands, 1977.

3. Farmer, M. G., and Hanson, P. W. "Comparison of Supercritical and Conventional Wing Flutter Characteristics." Proceedings of AIAA/ASME/SAE 17th Structures, Structural Dynamics and Materials Conference, King of Prussia, PA, April 1976, pp. 608-611.

4. Stroud, W. J. "Automated Structural Design with Aeroelastic Constraints: A Review and Assessment of the State of the Art." Proceedings of ASME Symposium on Structural Optimization, New York, November 1974, pp. 77-97.

5. Taylor, R. F. "Aeroelastic Optimization of Plates: A Review and Research Prospectus," AFFDL-TM-78-118-FBR, November 1976.

6. Lansing, W., Lerner, E., and Taylor, R. F. "Applications of Structural Optimization for Strength and Aeroelastic Design Requirements," AGARD Report No. 664, September 1977.

7. Wasiutznski, Z., and Brandt, A. "The Present State of Knowledge in the Field of Optimum Design of Structures," Applied Mechanics Reviews, Vol. 16, No. 5, May 1963, pp. 341-348.

8. Sheu, C. V., and Prager, W. "Recent Developments in Optimal Structural Design," Applied Mechanics Reviews, Vol. 21, No. 10, October 1968, pp. 985-992.

9. Schmit, L. A. "Structural Synthesis from Abstract Concept to Practical Tool," Proceedings of AIAA/ ASME 18th Structures, Structural Dynamics and Materials Conference, San Diego, March 1977, pp. 1-8.

10. Venkayya, V. B. "Structural Optimization: A Review and Some Recommendations," International Journal for Numerical Methods in Engineering, Vol. 13, No. 2, 1978, pp. 203-228.

11. Turner, M. J. "Proportioning Members of a Structure for Maximum Stiffness with Given Weight," Vought Sikorsky Aircraft Corporation Report ANC-5, Hartford, January 1942.

12. MacDonough, E. P. "The Minimum Weight Design of Wings for Flutter Conditions," Journal of the Aeronautical Sciences, Vol. 20, No. 8, August 1953, pp. 573-574.

13. Head, A. L., Jr. "A Philosophy of Design for Flutter," Proceedings of AIAA National Specialists Meeting on Dynamics and Aeroelasticity, Ft. Worth, November 1958, pp. 59-65.

14. Ashley, H., and McIntosh, S. C., Jr. "Application of Aeroelastic Constraints in Structural Optimization," Proceedings of the 12th International Congress of Applied Mechanics, Stanford, August 1968, pp. 100-113.

15. Turner, M. J. "Optimization of Structures to Satisfy Flutter Requirements," AIAA Journal, Vol. 7, No. 5, May 1969, pp. 945-951.

16. Weisshaar, T. A. "An Application of Control Theory Methods to the Optimization of Structures Having Dynamic or Aeroelastic Constraints," Dissertation, Department of Aeronautics and Astronautics, Stanford University, October 1970.

17. Weisshaar, T. A. "Panel Flutter Optimization - A Refined Finite Element Approach," International Journal for Numerical Methods in Engineering, Vol. 10, No. 1, 1976, pp. 77-91.

18. McIntosh, S. C., Jr. "Structural Optimization via Optimal Control Techniques: A Review," Proceedings of ASME Symposium on Structural Optimization, New York, November 1974.

19. Rudisill, C. S., and Bhatia, K. G., "Optimization of Complex Structures to Satisfy Flutter Requirements," AIAA Journal, Vol. 9, No. 8, August 1971, pp. 1487-1491.

20. van de Vooren, A. I. "Theory and Practice of Flutter Calculations for Systems with Many Degrees of Freedom," Dissertation, Technical Institute of Delft, The Netherlands, published by Edward Ijdo N.V., Leyden, 1952.

21. Cross, A. K., and Albano, E. A., "Computer Techniques for the Rapid Flutter Clearance of Aircraft Carrying External Stores, Part I - Perturbation Theory and Application," AFFDL-TR-114, February 1973.

22. Fox, R. L., and Kapoor, M. P. "Rates of Change of Eigenvalues and Eigenvectors," AIAA Journal, Vol. 6, No. 12, December 1968, pp. 2426-2429.

23. Rogers, L. C. "Derivatives of Eigenvalues and Eigenvectors," AIAA Journal, No. 8, No. 5, May 1970, pp. 943-944.

24. Rudisill, C. S. "Derivatives of Eigenvalues and Eigenvectors for a General Matrix," AIAA Journal, Vol. 12, No. 5, May 1974, pp. 721-722.

25. Rudisill, C. S., and Chu, Yee-Yeen. "Numerical Methods for Evaluating the Derivatives of Eigenvalues and Eigenvectors," AIAA Journal, Vol. 13, No. 6, June 1975, pp. 834-836.

26. Simpson, A. "On the Rates of Change of Sets of Equal Eigenvalues," Journal of Sound and Vibration, Vol. 44, No. 1, 1976, pp. 83-102.

27. Stroud, W. J., Dexter, C. B., and Stein, M. "Automated Preliminary Design of Simplified Wing Structures to Satisfy Strength and Flutter Requirements," NASA TN D-6534, December 1971.

28. Fox, R. L., Muira, H., and Rao, S. S., "Automated Design Optimization of Supersonic Wing Structures Under Dynamic Constraints," Proceedings of AIAA/ASME/SAE 13th Structures, Structural Dynamics, and Materials Conference, San Antonio, April 1972.

29. Gwin, L. B. "Optimal Sizing of Complex Structural Systems for Flutter Requirements," Dissertation, Department of Aeronautics and Astronautics, Stanford University, May 1973.

30. Gwin, L. B., and Taylor, R. F. "A General Method of Flutter Optimization," AIAA Journal, Vol. 11, No. 12, December 1973, pp. 1613-1617.

31. Siegel, S. "A Flutter Optimization Program for Aircraft Structural Design," Proceedings of AIAA Fourth Aircraft Design, Flight Test, and Operations Meeting, Los Angeles, August 1972.

32. Bogner, F. K. "Modification of a Finite Element Computer Program and Evaluation of a Method of Flutter Optimization," University of Dayton Research Institute, UDRI-TR-74-12, February 1974.

33. Wilkinson, K., Markowitz, J. Lerner, E., Chipman, R., and George, D. "An Automated Procedure for Flutter and Strength Analysis and Optimization of Aeroelastic Vehicles," AFFDL-TR-75-137, December 1975.

34. Wilkinson, K., Lerner, E., and Taylor, R. F. "Practical Design of Minimum-Weight Aircraft Structures for Strength and Flutter Requirements," Journal of Aircraft, Vol. 13, No. 8, August 1976, pp. 614-624.

35. Prager, W., and Taylor, J. E. "Problems of Optimal Structural Design," Journal of Applied Mechanics, Vol. 35, Series E, March 1968, pp. 102-106.

36. Plaut, R. H. "Elastic Minimum-Weight Design for Specified Critical Load," SIAM Journal of Applied Mathematics, Vol. 25, No. 3, November 1973.

37. Segenreich, S. A., Johnson, E. H., and Rizzi, P. "Three Contributions to Minimum-Weight Structural Optimization with Dynamic and Aeroelastic Constraints," Department of Aeronautics and Astronautics, Stanford University, SUDAAR Report No. 501, August 1976.

38. McIntosh, S. C., Jr., and Ashley, H. "On the Optimization of Discrete Structures with Aeroelastic Constraints," Computers and Structures, Vol. 8, No. 3-4, May 1978, pp. 411-419.

39. Borland, C. J. "A Bibliography of Recent Developments in Unsteady Transonic Flow," AFFDL-TR-189, Volume 1, February 1979.

40. McCroskey, W. J. "Some Current Research in Unsteady Fluid Dynamics," The 1976 Freeman Scholar Lecture, Journal of Fluids Engineering, Vol. 99, March 1977, pp. 8-39.

41. Landahl, M. T. Unsteady Transonic Flow. New York: Pergamon Press, 1961.

42. Olsen, J. J. "Subsonic and Transonic Flow Over Sharp and Blunt Nosed Nonlifting Airfoils," Dissertation, Department of Aeronautical and Astronautical Engineering, The Ohio State University, June 1976.

43. Olsen, J. J. "Transonic Scaling for Three Dimensional Unsteady Flows," Unpublished notes, August 1976.

44. Ames, W. F. Numerical Methods for Partial Differential Equations. 2nd ed. New York: Academic Press, 1977.

45. Richtmyer, R. D. and Morton, K. W. Difference Methods for Initial-Value Problems. 2nd ed. New York: Interscience Publishers, 1976.

46. Ballhaus, W. F. and Goorjian, P. M. "Implicit Finite Difference Computations of Unsteady Transonic Flows about Airfoils," AIAA Journal, Vol. 15, No. 12, December 1977, pp. 1728-1735.

47. Ballhaus, W. F. and Goorjian, P. M. "Computation of Unsteady Transonic Flows by the Indical Method," AIAA Journal, Vol. 16, No. 2, February 1978, pp. 117-124.

48. Tijdeman, H. "On the Motion of Shock Waves on an Airfoil with Oscillating Flap," Symposium Transsonicum II. Berlin: Springer-Verlag, 1975, pp. 49-56.

49. Magnus, R. and Yoshihara, H. "The Transonic Oscillating Flap, AIAA Paper 76-327, July 1976.

50. Bisplinghoff, R. L. and Ashley, H. Principles of Aeroelasticity. New York: John Wiley and Sons, Inc., 1962.

51. Woolston, D. S., Runyan, H. L., and Andrews, R. E. "An Investigation of Effects of Certain Types of Structural Nonlinearities on Wing and Control Surface Flutter," Journal of the Aeronautical Sciences, Vol. 24, No. 1, January 1957, pp. 57-63.

52. Kryloff, N. and Bogoliuboff, N. Introduction to Nonlinear Mechanics. Translated by S. Lefschetz. Princeton: Princeton University Press, 1947.

53. Shen, S. F. and Hsu, C. C. "Analytical Results of Certain Nonlinear Flutter Problems," Journal of the Aeronautical Sciences, Vol. 25, No. 2, February 1958, pp. 136-137.

54. Shen, S. F. "An Approximate Analysis of Nonlinear Flutter Problems," Journal of the Aero/Space Sciences, Vol. 26, No. 1, 1959, pp. 25-45.

55. Woolston, D. S. and Andrews, R. E. "Remarks on 'Analytical Results of Certain Nonlinear Flutter Problems,'" Journal of the Aero/Space Sciences, Vol. 26, No. 1, January 1959, pp. 51-53.

56. Brunelle, E. J. "Transient and Nonlinear Effects on High Speed Vibratory, Thermoelastic Instability Phenomena," WADD TR-60-484, July 1960.

57. Dowell, E. H. Aeroelasticity of Plates and Shells. Leyden: Noordhoff International Publishing, 1975.

58. Dowell, E. H. "Nonlinear Oscillations of a Fluttering Plate I," AIAA Journal, Vol. 4, No. 7, July 1966, pp. 1267-1275.

59. Dowell, E. H. "Nonlinear Oscillations of a Fluttering Plate II," AIAA Journal, Vol. 5, No. 10, October 1967, pp. 1856-1862.

60. Kuo, C. C., Morino, L., and Dugundji, J. "Perturbation and Harmonic Balance Methods for Nonlinear Panel Flutter," AIAA Journal, Vol. 10, No. 11, November 1972, pp. 1479-1484.

61. LaSalle, J. and Lefschetz, S. Stability by Liapunov's Direct Method. New York: Academic Press, 1961.

62. Parks, P. C. "Some Applications of Liapunov Functionals." In Instability of Continuous Systems, pp. 125-131, Edited by H. Leipholz. Berlin: Springer-Verlag, 1971.

63. George, J. H. "Interpretation of Liapunov Stability Regions," AIAA Journal, Vol. 5, No. 5, May 1967, pp. 959-961.

64. Diamantha, P. C. and Roorda, J. "On the Domain of Asymptotic Stability of Nonlinear Nonconservative Systems," Applied Scientific Research, Vol. 20, March 1969, pp. 272-288.

65. Breitbach, E. "Effects of Structural Nonlinearities on Aircraft Vibration and Flutter," AGARD Report No. 665, January 1978.

66. Laurenson, R. M. and Trn, R. M. "Flutter Analysis of Missile Control Surfaces Containing Structural Nonlinearities," Proceedings of AIAA/ASME/ASCE/AHS 20th Structures, Structural Dynamics and Materials Conference, St. Louis, April 1979.

67. Sensburg, O. and Schoen, B. "Vibration and Flutter Investigations of Aircraft with Special Nonlinear Structural Properties," Zeitschrift fur Flugwissenschaften und Weltraumforschung, Vol. 2, Nov.-Dec. 1978, pp. 395-404.

68. Eastep, F. E. and McIntosh, S.C., Jr. "Analysis of Nonlinear Panel Flutter and Response under Random Excitation or Nonlinear Aerodynamic Loading," AIAA Journal, Vol. 9, No. 3, March 1971, pp. 411-418.

69. McIntosh, S. C., Jr. "The Effect of Hypersonic Nonlinear Aerodynamic Loading on Panel Flutter," Proceedings of AIAA/ASME/SAE 13th Structures, Structural Dynamics and Materials Conference, San Antonio, April 1972.

70. Hartlen, R. T. and Currie, I. G. "Lift-Oscillator Model of Vortex-Induced Vibration," Journal of the Engineering Mechanics Division, Proc. ASCE, Vol. 96, No. EM5, October 1970, pp. 577-591.

71. Minorsky, A. N., Introduction to Non-Linear Mechanics. Ann Arbor: J. W. Edwards, 1947.

72. Dugundji, J. and Chopra, I. "Further Studies of Stall Flutter and Nonlinear Divergence of Two-Dimensional Wings," NASA CR-144924, August 1975.

73. Smilg, B. "The Prevention of Aileron Oscillations at Transonic Speeds," AAF Technical Report No. 5530, December 1946.

74. Smilg, B. "The Instability of Pitching Oscillations of an Airfoil in Subsonic Incompressible Potential Airflow," Journal of the Aeronautical Sciences, Vol. 16, No. 11, November 1949, pp. 691-696.

75. Rizzetta, D. P. "Transonic Flutter Analysis of a Two-Dimensional Airfoil," AFFDL-TM-77-64-FBR, July 1977.

76. Rizzetta, D. P. "The Aeroelastic Analysis of a Two-Dimensional Airfoil in Transonic Flow," AFFDL-TR-77-126, December 1977.

77. Rizzetta, D. P. "Time-Dependent Response of a Two-Dimensional Airfoil in Transonic Flow." AIAA Journal, Vol. 17, No. 1, January 1979, pp. 26-32.

78. Isaacson, E. and Keller, H. B. Analysis of Numerical Methods. New York: Wiley, 1966, pp. 384-393.

79. Yang, T. Y., Striz, A. G., and Guruswamy, P. "Flutter Analysis of Two-Dimensional and Two-Degrees-of-Freedom Airfoils in Small-Disturbance Unsteady Transonic Flow," AFFDL-TR-78-202, December 1978.

80. Yang, T. Y., Guruswamy, P., and Striz, A. G. "Aeroelastic Response Analysis of Two-Dimensional Single and Two-Degree-of-Freedom Airfoils in Low-Frequency, Small-Disturbance Unsteady Transonic Flow," AFFDL-TR-79-3077, June 1979.

81. Farr, J. L., Traci, R. M., and Albano, E. D. "Computer Programs for Calculating Small Disturbance Transonic Flows About Oscillating Airfoils," AFFDL-TR-74-135, November 1974.

82. Ashley, H. "On the Role of Shocks in the 'Sub-Transonic' Flutter Phenomenon," Proceedings of the AIAA/ASME/AHS 20th Structures and Structural Dynamics and Materials Conference, St. Louis, April 1979.

83. Roorda, J. and Nemat-Nasser, S. "An Energy Method for Stability Analysis of Nonlinear, Nonconservative Systems," AIAA Journal, Vol. 5, No. 7, July 1967, pp. 1262-1268.

84. Minorsky, N. The Theory of Oscillations. New York: Wiley, 1958.

85. Cunningham, W. J. Introduction to Nonlinear Analysis. New York: McGraw-Hill, 1958.

86. Stoker, J. J. Nonlinear Vibrations in Mechanical and Electrical Systems. New York: Interscience, 1950.

87. Fox, L. Numerical Solution of Ordinary and Partial Differential Equations. Oxford: Pergamon Press, 1962.

88. Butenin, N. V. Elements of the Theory of Nonlinear Oscillations. New York: Blaisdell, 1965.

89. O'Connell, R. F., Hassig, H. J., and Radovcich, N. A., "Study of Flutter Related Computational Procedures for Minimum Weight Structural Sizing of Advanced Aircraft," NACA CR-2607, March 1976.

90. Knese, P. B. "A New Method for Analysis of Nonlinear Control Systems," Dissertation, Department of Aerospace Engineering, The University of Dayton, April 1978.

91. Personnal communication from P. M. Goorjian, March 1979.

92. Bolotin, V. V. Nonconservative Problems of the Theory of Elastic Stability. Translated by T. K. Lusher, edited by G. Herrmann. Oxford: Pergamon Press, 1963.

93. Meirovitch, L. Analytical Methods in Vibrations. New York: Macmillan Co., 1967.

94. Allen, H. G. Analysis and Design of Structural Sandwich Panels. Oxford: Pergamon Press, 1969.

95. Ashley, H. and Zartarian, G. "Piston Theory - A New Aerodynamic Tool for the Aeroelastician," Journal of the Aeronautical Sciences, Vol. 23, No. 12, December 1956, pp. 1109-1118.

96. Ralston, A. A First Course in Numerical Analysis. New York: McGraw-Hill, 1965.

APPENDIX A

TRANSONIC PITCH FLUTTER PHASE PLANE PLOTS

Additional phase plane plots are shown in the Figures 50 through 58. The point number given on each figure refers to the damping-amplitude plot of Figure 28. In most cases such as Figures 50, 52, 54, 55, 57, and 58, the phase plane trajectories are either converging toward the origin or diverging away from it. In these situations the points are not too closely situated to the stability boundary of Figure 28. In Figures 51, 53, and 57, the motions have a dual converging and diverging character. These points are generally close to the stability boundary.

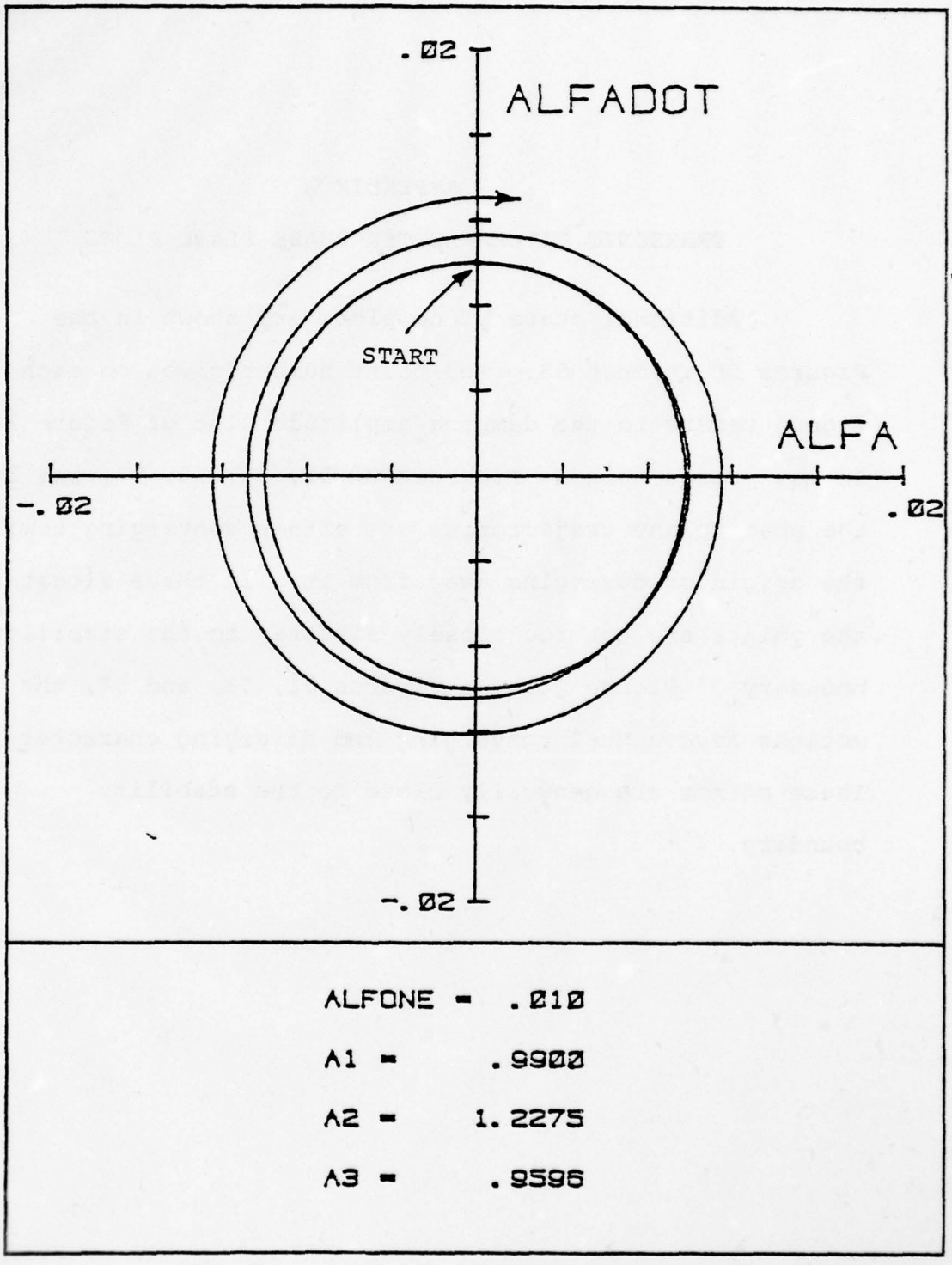

Figure 50. Phase Plane Plot for Point 1 on Damping-Amplitude Plot.

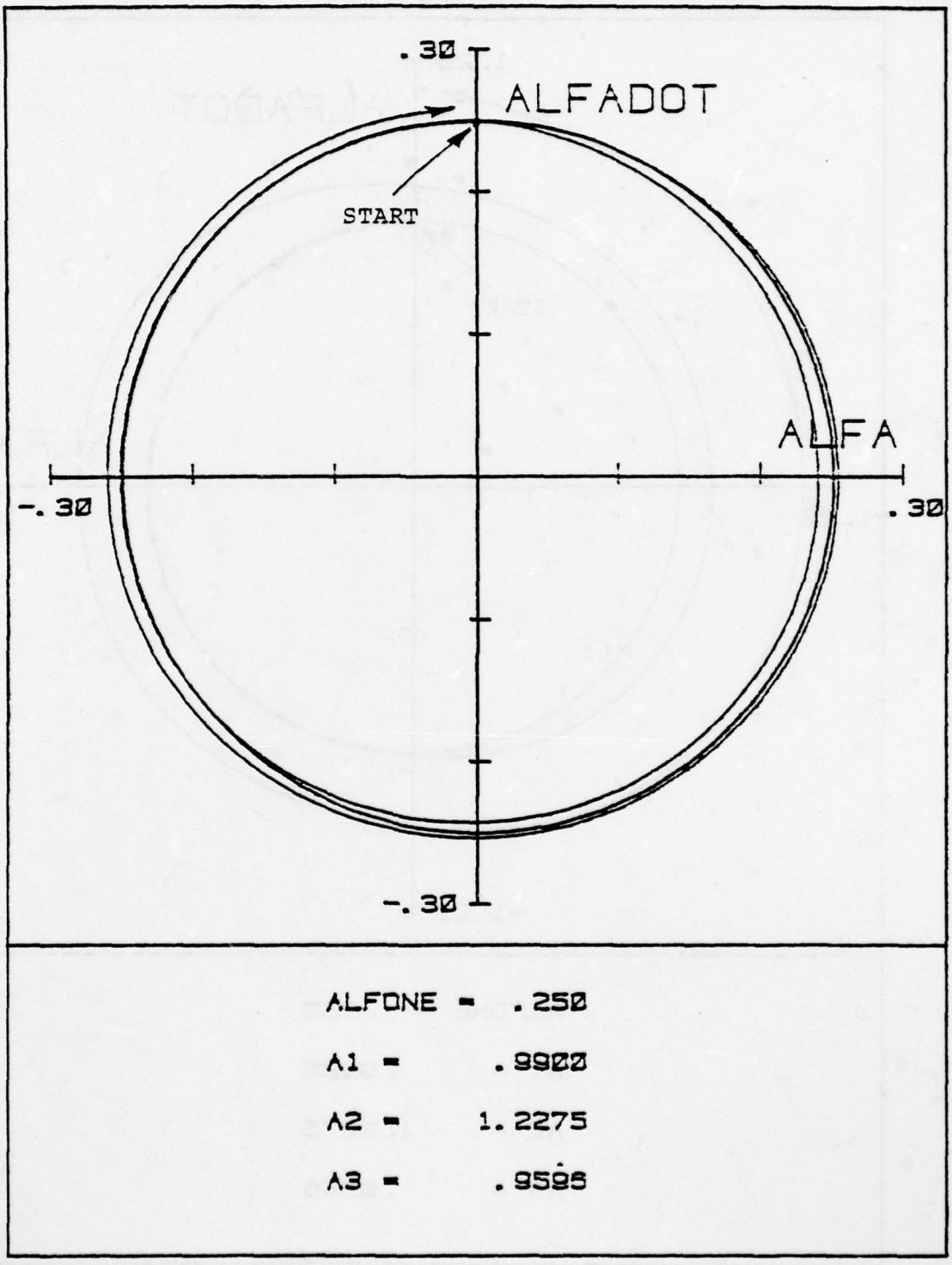

Figure 51. Phase Plane Plot for Point 2 on Damping-Amplitude Plot.

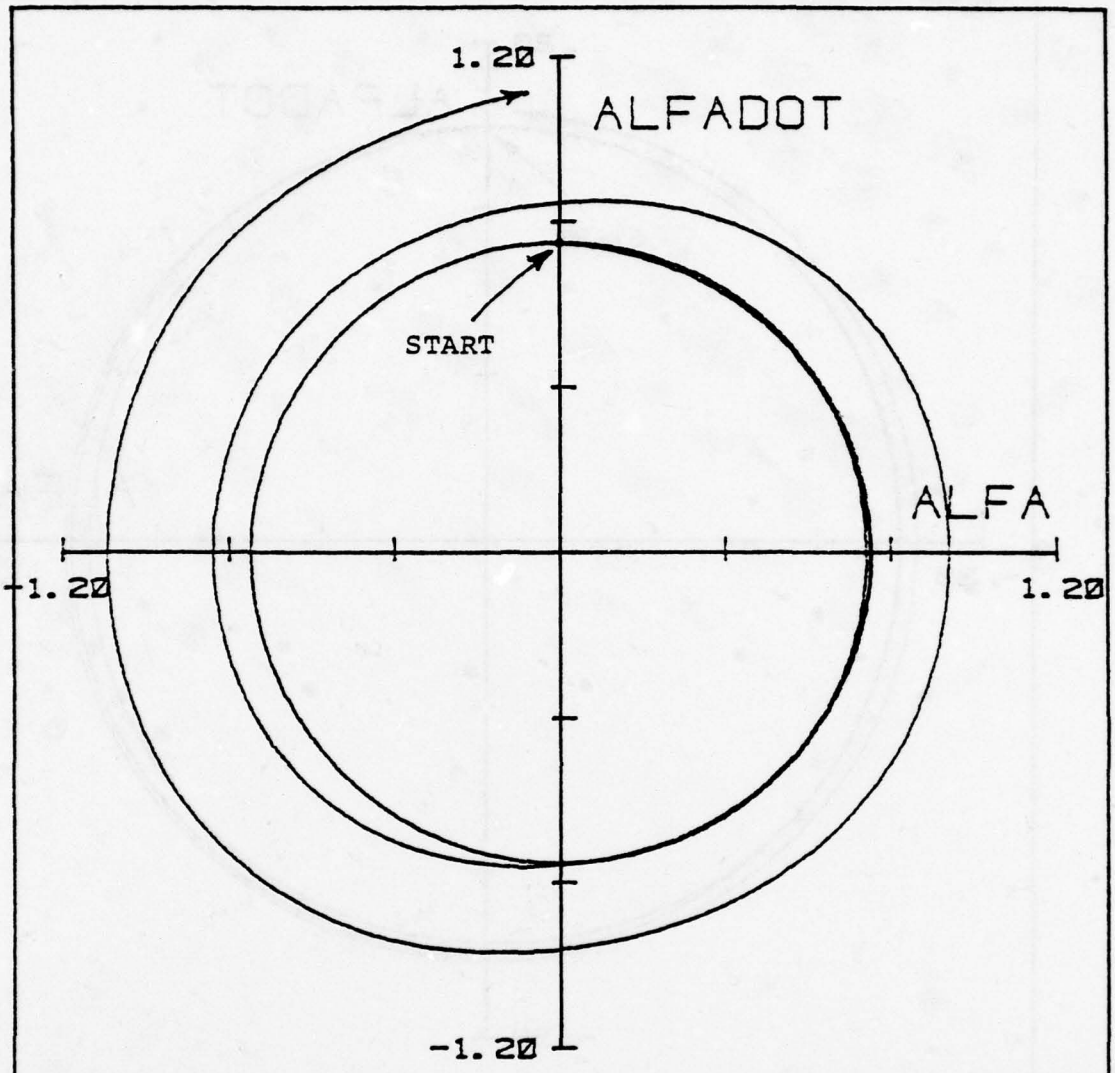

ALFONE = .750

A1 = .9900

A2 = 1.2275

A3 = .9596

Figure 52. Phase Plane Plot for Point 3 on Damping-Amplitude Plot.

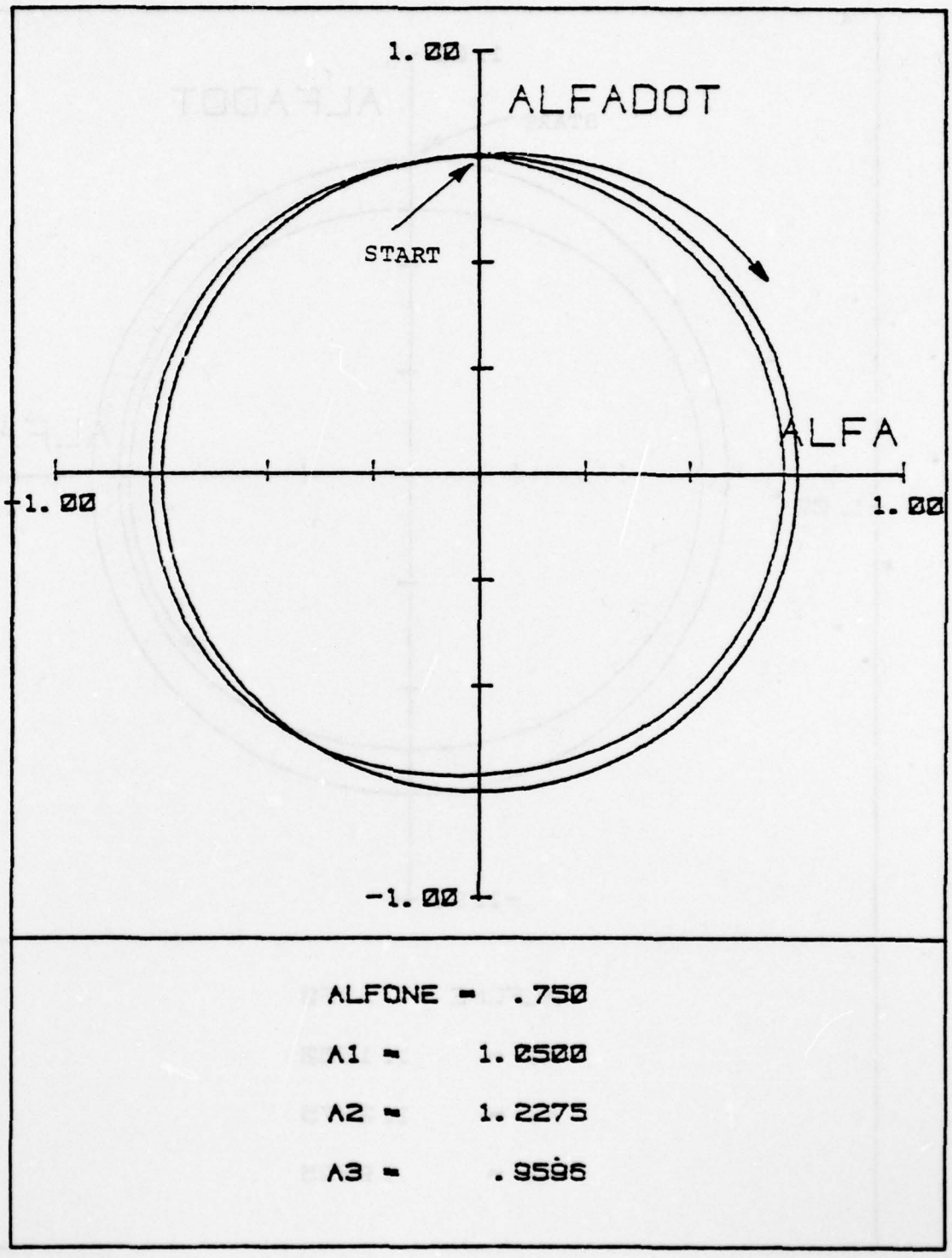

Figure 53. Phase Plane Plot for Point 5 on Damping-Amplitude Plot.

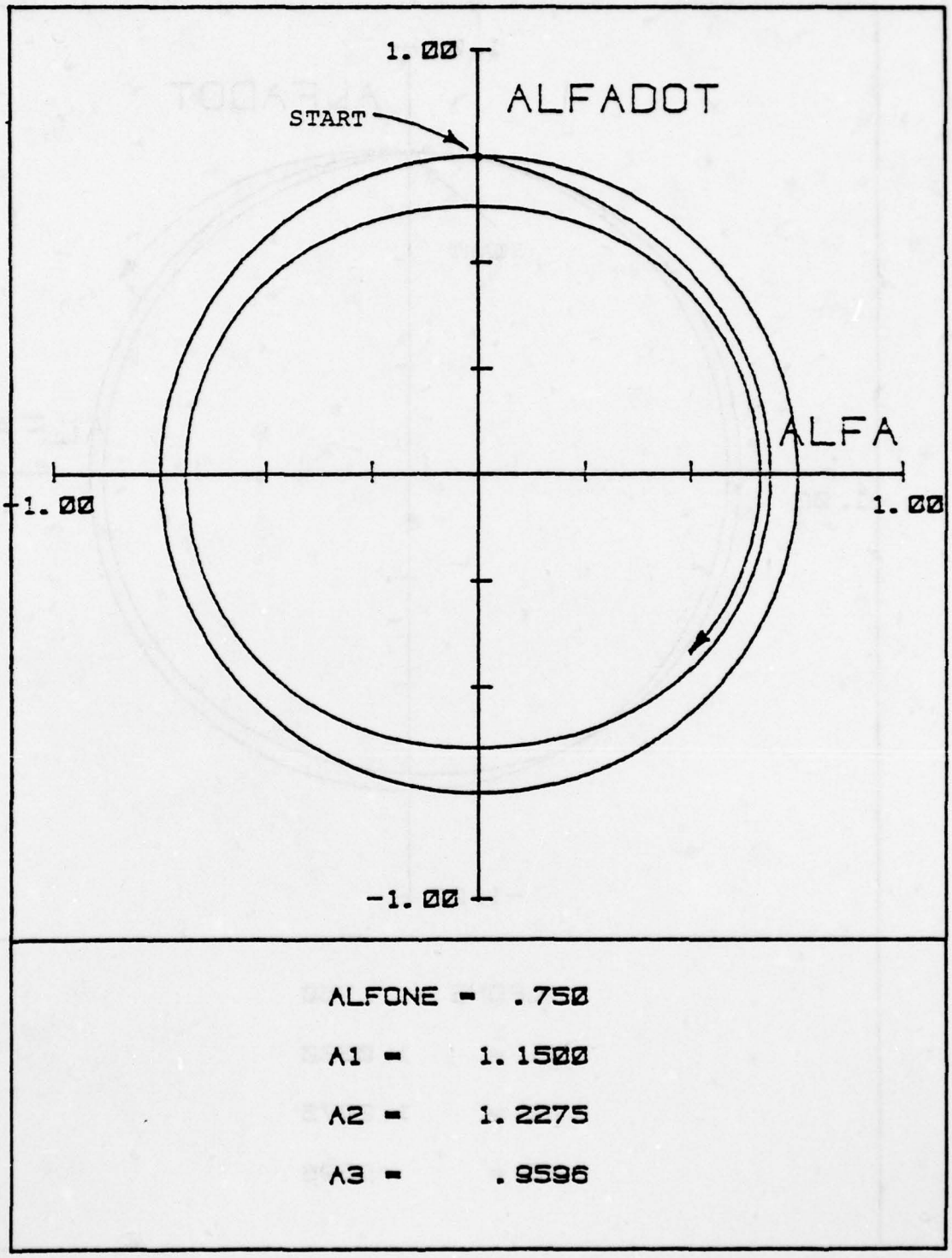

Figure 54. Phase Plane Plot for Point 7 on Damping-Amplitude Plot.

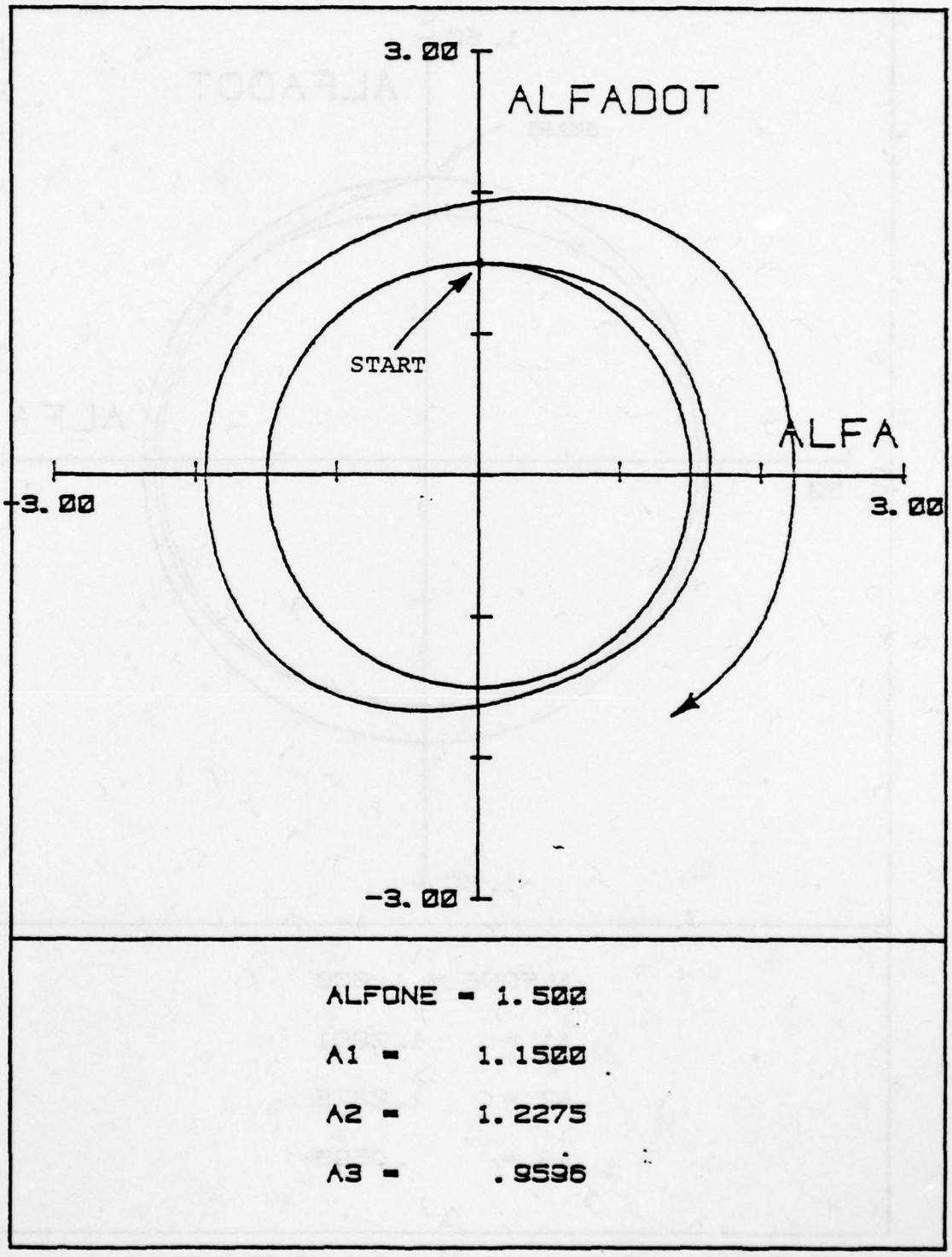

Figure 55. Phase Plane Plot for Point 8 on Damping-Amplitude Plot.

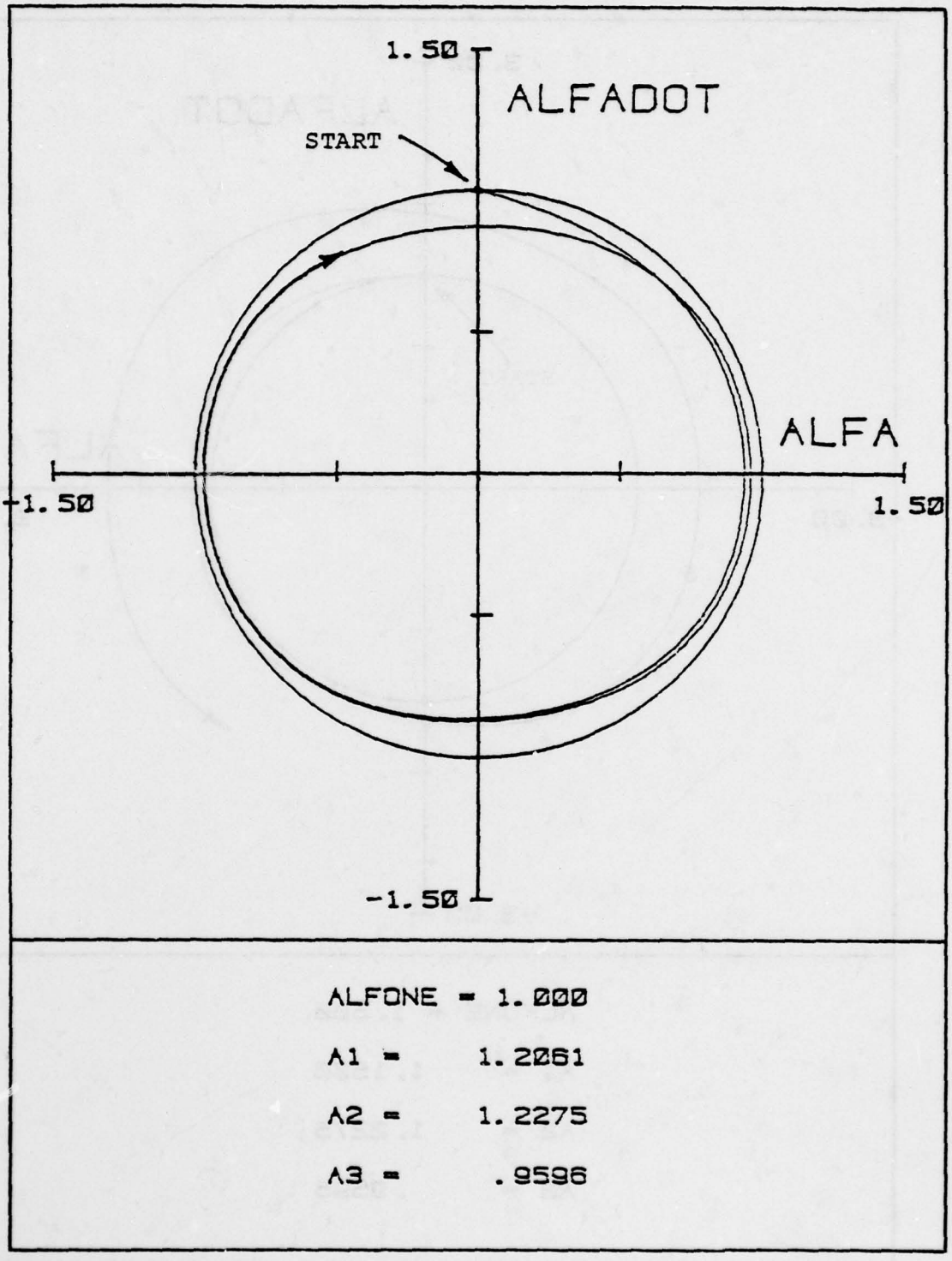

Figure 56. Phase Plane Plot for Point 9 on Damping-Amplitude Plot.

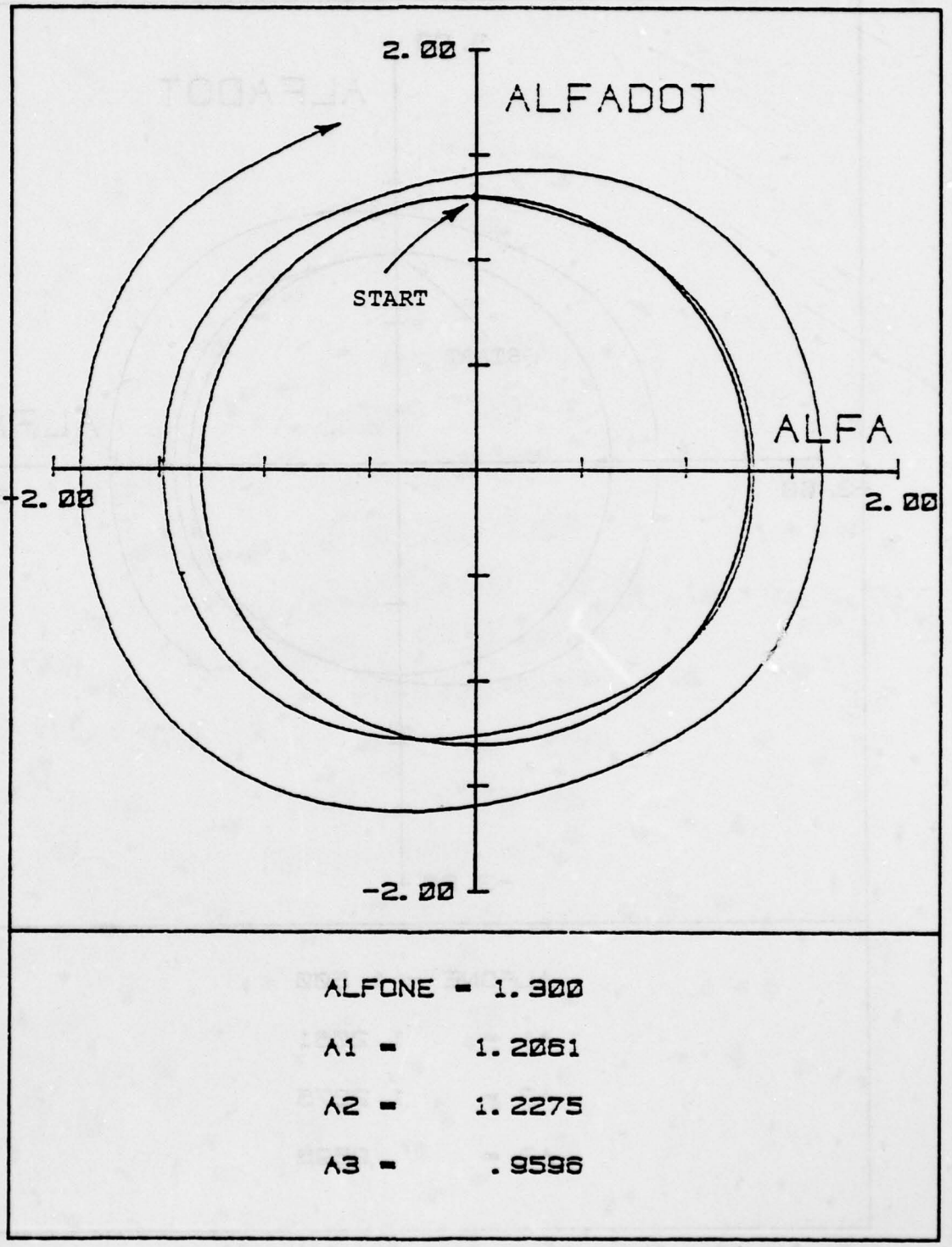

Figure 57. Phase Plane Plot for Point 10 on Damping-Amplitude Plot.

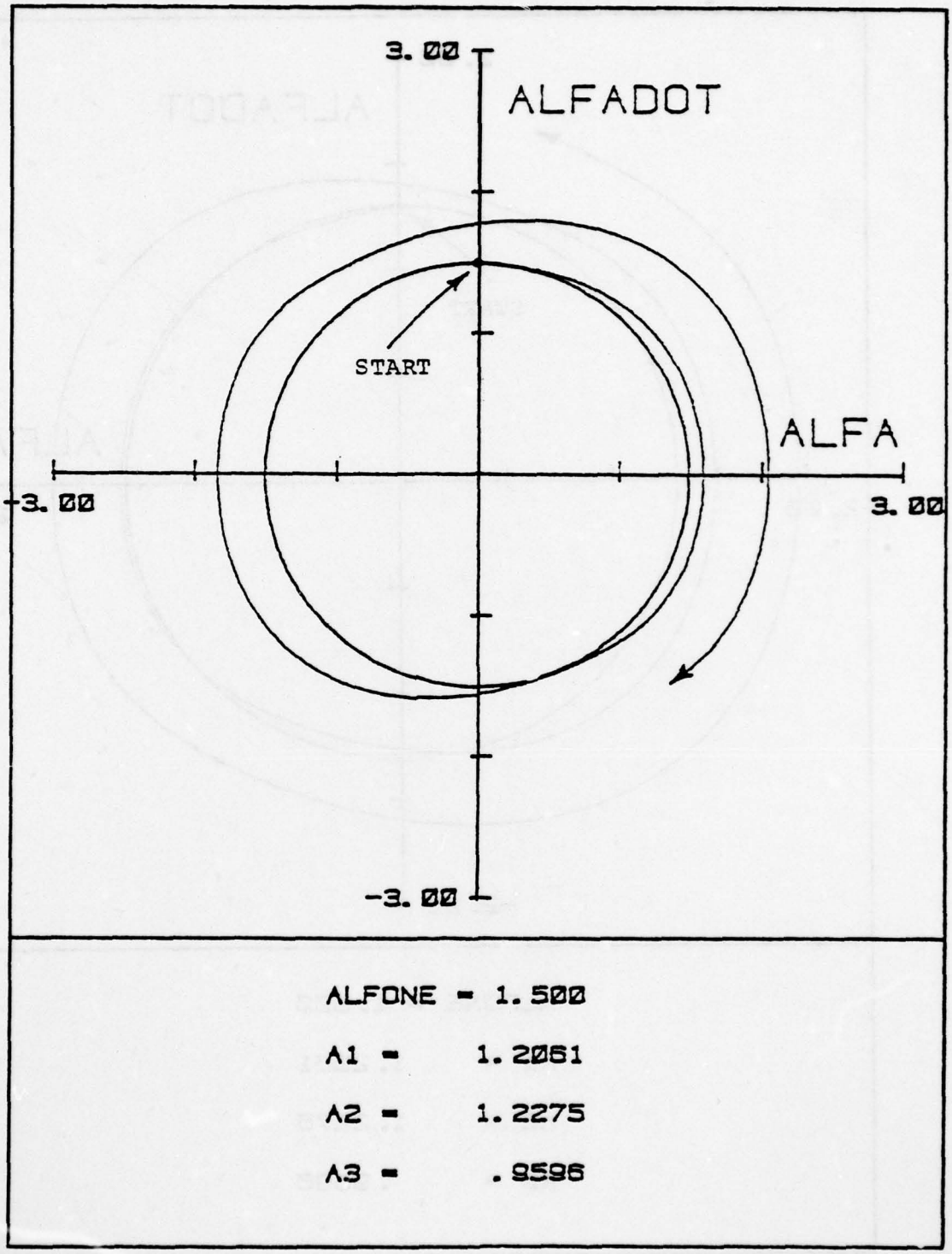

Figure 58. Phase Plane Plot for Point 11 on Damping-Amplitude Plot.

APPENDIX B

GALERKIN INTEGRALS FOR HYPERSONIC PANEL

The constants in Equations (4.54) which result from the integration of trigonometric functions are defined as follows.

$$(B.1) \quad I_{ij}^{(1)} = \int_0^1 \sin i\pi\xi \sin j\pi\xi \, d\xi$$

$$(B.2) \quad I_{ij}^{(2)} = \int_0^1 \sin i\pi\xi \cos j\pi\xi \, d\xi$$

$$(B.3) \quad I_{ijk}^{(3)} = \int_0^1 \sin i\pi\xi \cos j\pi\xi \cos k\pi\xi \, d\xi$$

$$(B.4) \quad I_{ijk}^{(4)} = \int_0^1 \sin i\pi\xi \cos j\pi\xi \sin k\pi\xi \, d\xi$$

By use of elementary trigonometric identities, these can be written as

$$(B.5) \quad I_{ij}^{(1)} = \begin{cases} \frac{1}{2} \text{ if } i = j \\ 0 \text{ if } i \neq j \end{cases}$$

$$(B.6) \quad I_{ij}^{(2)} = [S(i+j) + S(i-j)]/2\pi$$

$$(B.7) \quad I_{ijk}^{(3)} = [S(i+j+k) + S(i+j-k) + S(i-j+k) + S(i-j-k)]/4\pi$$

$$(B.8) \quad I_{ijk}^{(4)} = [S(i+j-k) - S(i+j+k) + S(i-j-k) - S(i-j+k)]/4\pi$$

The S and C functions have only integer arguments, and for any integer p they are defined as

$$S(p) = \begin{cases} 0 & \text{if } p = 0 \text{ or } p = \text{even} \\ 2/p & \text{if } p \neq 0 \text{ or } p = \text{odd} \end{cases} \tag{B.9}$$

$$C(p) = \begin{cases} 0 & \text{if } p \neq 0 \\ \pi & \text{if } p = 0 \end{cases} \tag{B.10}$$

☆U.S.Government Printing Office: 1979 — 657-084/258